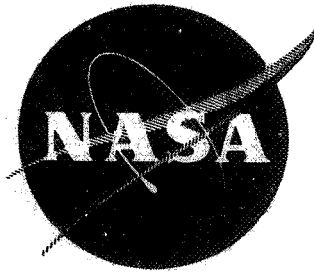GESP-578
NASA-CR-72845

EFFECTS OF VACUUM LEVEL ON SOLAR RECEIVER MATERIALS

FINAL REPORT

Prepared by

T. F. Lyon

Approved by

E. E. Hoffman

October 10, 1970

NUCLEAR SYSTEMS PROGRAMS
SPACE SYSTEMS
GENERAL ELECTRIC
CINCINNATI, OHIO 45215

EFFECTS OF VACUUM LEVEL ON SOLAR RECEIVER MATERIALS

FINAL REPORT

prepared by
T. F. Lyon

approved by
E. E. Hoffman

NUCLEAR SYSTEMS PROGRAMS
SPACE SYSTEMS
GENERAL ELECTRIC COMPANY
CINCINNATI, OHIO   45215

prepared for
NATIONAL AERONAUTICS AND SPACE ADMINISTRATION

CONTRACT NAS 3-11828

TABLE OF CONTENTS

TABLE OF CONTENTS (Continued)

LIST OF ILLUSTRATIONS

LIST OF TABLES

NOMENCLATURE

Symbol

A	Area	cm^2
i	Electron Emission Current	amperes
I (without subscript)	Strip Specimen Current	amperes
I (with subscript)	Positive Ion Current	amperes
m	Mass Incident Rate	$gm/cm^2 sec$
m_r	Reaction Rate	$gm/cm^2 sec$
M	Molecular Weight	gm/mole
P	Pressure	torr
Q	Gas Flow Rate	torr-liters/sec
R	Resistance	ohms
s	Gauge Sensitivity	$torr^{-1}$
S	Pumping Speed	liters/sec
t	Time	sec
T	Absolute Temperature	$^\circ K$
V	Volume	liters
α	Sticking Probability	dimensionless
ϵ	Total Hemispherical Emittance	dimensionless
σ	Stefan-Boltzmann Constant	$watts/cm^2 \, ^\circ K^4$

Subscripts

ig	Refers to Ionization Gauge
ms	Refers to Mass Spectrometer

FOREWORD

The work described herein was performed for the National Aeronautics and Space Administration under Contract NAS 3-11828. John A. Milko of Lewis Research Center was the NASA Technical Manager.

ABSTRACT

Resistively heated strip specimens of Cb-1Zr alloy were exposed at 1700°F (927°C) in a vacuum chamber at various levels of total pressure in the 10^{-6} torr range. Pressure levels were maintained by controlled in-leakage of air. Oxygen reacted rapidly with Cb-1Zr alloy under these conditions and final oxygen content of the specimens was between 4000 and 9000 ppm for exposure times between 200 and 500 hours. Oxygen sticking probabilities were found to depend on whether or not the specimens were annealed immediately before the test exposure. These results indicate that a normally undetectable oxide film exists on the Cb-1Zr surface as a result of oxidation by ambient air, and causes the sticking probability to be lower than on the clean metal surface. Sticking probabilities ranged from 0.65 on the clean surface to 0.16 on the surface with the oxide film. Mechanical tests of the contaminated material showed that Cb-1Zr alloy is considerably strengthened by homogeneous addition of oxygen to an oxygen level of about 6000 ppm, while still maintaining reasonably good room temperature ductility. At higher oxygen levels, the ductility decreased markedly with little additional increase in strength. Welded and annealed Cb-1Zr is considerably more sensitive to oxygen contamination. The weld metal is brittle after homogeneous addition of 4300 ppm oxygen.

I. INTRODUCTION

Refractory metal alloys are known to be reactive with atmospheric
constituents at elevated temperatures. In vacuum systems, even under
what is usually considered "high-vacuum conditions," residual gases tend
to react with these alloys. The contamination resulting from such
reactions can cause deleterious changes in the mechanical properties of
the alloy and, in the case of severe contamination, could cause premature
failure of a system or component under long-duration, high-temperature
test conditions. A knowledge of these reaction rates and the effects
on mechanical properties is thus required in order to establish the
environmental conditions necessary for long-term testing of refractory
alloy components or systems at elevated temperatures.

Tests of refractory alloy samples and small components are generally
performed in vacuum chambers of moderate size (up to about 1000 cubic
feet). Due to the necessity for minimizing contamination from residual
gases, these systems are usually getter-ion pumped and contain all-metal
seals. Such systems can maintain pressures of about 1×10^{-8} torr for
test durations of 10,000 hours or longer, with the test article at elevated
temperatures. Such total pressures have been shown to be adequate
in preventing appreciable contamination of refractory metals, even with
systems containing alkali metals. For testing full-scale systems, these
ultrahigh-vacuum techniques may be impractical, since the chamber volume
may be as large as one million cubic feet. In such test chambers, oil
diffusion pumps and elastomeric seals are used because of practical
considerations. Outgassing of materials of construction, in-leakage of
air, and backstreaming of oil from the diffusion pumps might limit the
vacuum to total pressures in the 10^{-6} torr range. Under these conditions,
excessive contamination of high-temperature, refractory alloy components
might be expected during long-duration testing.

The present program was formulated to determine the extent of con-
tamination of Cb-1Zr alloy when exposed to vacuum conditions simulating
those anticipated in a large, diffusion-pumped, elastomeric-sealed
system. In addition, the effects of such contamination on the mechanical

1

properties of the alloy were to be investigated. The results of this program were intended for application to the proposed testing of the Brayton Cycle Solar Heat Receiver in the Space Power Facility test chamber at Plum Brook Station, Ohio. In order to simulate the heat receiver conditions, a bellows capsule, filled with lithium fluoride, was intended to undergo cycling from 1500°F to 1700°F (816°C to 927°C) duplicating the cyclic heating conditions of the heat storage tubes in the heat receiver. In order to obtain specimens suitable for mechanical property testing, two resitively heated sheet specimens were to have been exposed simultaneously under isothermal conditions at 1700°F (927°C).

The test exposure conditions for the bellows capsule placed severe restrictions on the heating system for the capsule. Since the capsule had to be exposed to the chamber environment, no thermal shielding could be employed around the capsule, and the heat source had to be located some distance from the capsule. In addition, the test conditions required the use of materials in the heating system which would not react with the environmental gases within the chamber and thus modify the gas composition. A capsule heating system was designed and evaluated to meet these requirements. This system consisted of a cylindrical array of fifteen quartz lamps with aluminum reflectors. It was found that, even after several modifications to this heating system, the capsule heat flux requirements could not be met without applying excessive power to the lamps which resulted in premature lamp failure.

Because of these difficulties with the capsule heating system, and the change in NASA requirements, the contract was modified to exclude testing of the bellows capsules. This report describes the test exposures of the contaminated specimens. Four separate test exposures were conducted producing seven flat sheet specimens with various levels of oxygen contamination. The exposures were conducted at various vacuum chamber total pressures obtained by controlled in-leakage of air. From chamber partial pressure analyses performed with a mass spectrometer, oxygen reaction rates were calculated during the exposure. The overall effective oxygen reaction rate was obtained from posttest chemical analyses of the specimens. Evaluation includes chemical, metallographic, and X-ray diffraction

2

analyses, along with tensile, stress-rupture, and bend transition
temperature determination on selected samples of the contaminated
specimens.

A description of the design and performance of the capsule heating
system is given in an appendix.

II. TEST EQUIPMENT

A. Vacuum System

The strip test exposures were conducted in a vacuum chamber (shown in Figure 1) capable of operating in the 10^{-9} torr range. The chamber consists of a 48-inch-(1.22-meter) diameter by 96-inch-(2.44-meter) high movable bell jar with a fixed 30-inch-(0.76-meter) deep lower sump section. The chamber is constructed of Type 304 stainless steel. The bell jar and lower sump section are joined by a flange that incorporates two concentric butyl rubber O-rings with an evacuation groove between the O-rings to minimize in-leakage for ultrahigh-vacuum operation. All other flanges on the chamber are standard ultrahigh-vacuum type sealed with copper gaskets. The lower sump section contains the instrumentation and electrical power feedthroughs, a 10-inch-(25.4-cm) diameter pumping port, and several auxiliary flanged penetrations. The entire chamber is insulated and equipped with electrical heaters to bake out the chamber to 500°F (260°C). Water cooling coils are welded to the chamber wall and are capable of removing up to 100 kw of heat during test operations.

The vacuum chamber pumping system consists of a 10-inch oil diffusion pump (NRC model HS 10-4200) with rated pumping speed of 4200 liters per second with DC-705 silicone oil as the working fluid. Backstreaming of oil vapors from the diffusion pump is minimized by a liquid-nitrogen-cooled circular chevron cold trap (NRC type 0315-10). A second baffle (NRC type 0314-10) is water cooled and located directly above the diffusion pump. The diffusion pump is backed by a 46-cfm (22-liters-per-second) mechanical pump. A 15-cfm (7-liters-per-second) mechanical pump is used to evacuate the annular groove between the two O-rings in the main flange.

As required by the contract, this basic vacuum system was modified by addition of a calibrated ionization gauge (GE Model 22GT115), a mass spectrometer (GE Model 22PT180), a variable leak valve (Granville-Phillips No. 203-001-02-011-011), and a diffusion pump throttle mechanism to vary the effective pumping speed of the diffusion pump. This mechanism consists of a stainless steel disk attached to a shaft which is in turn attached

5
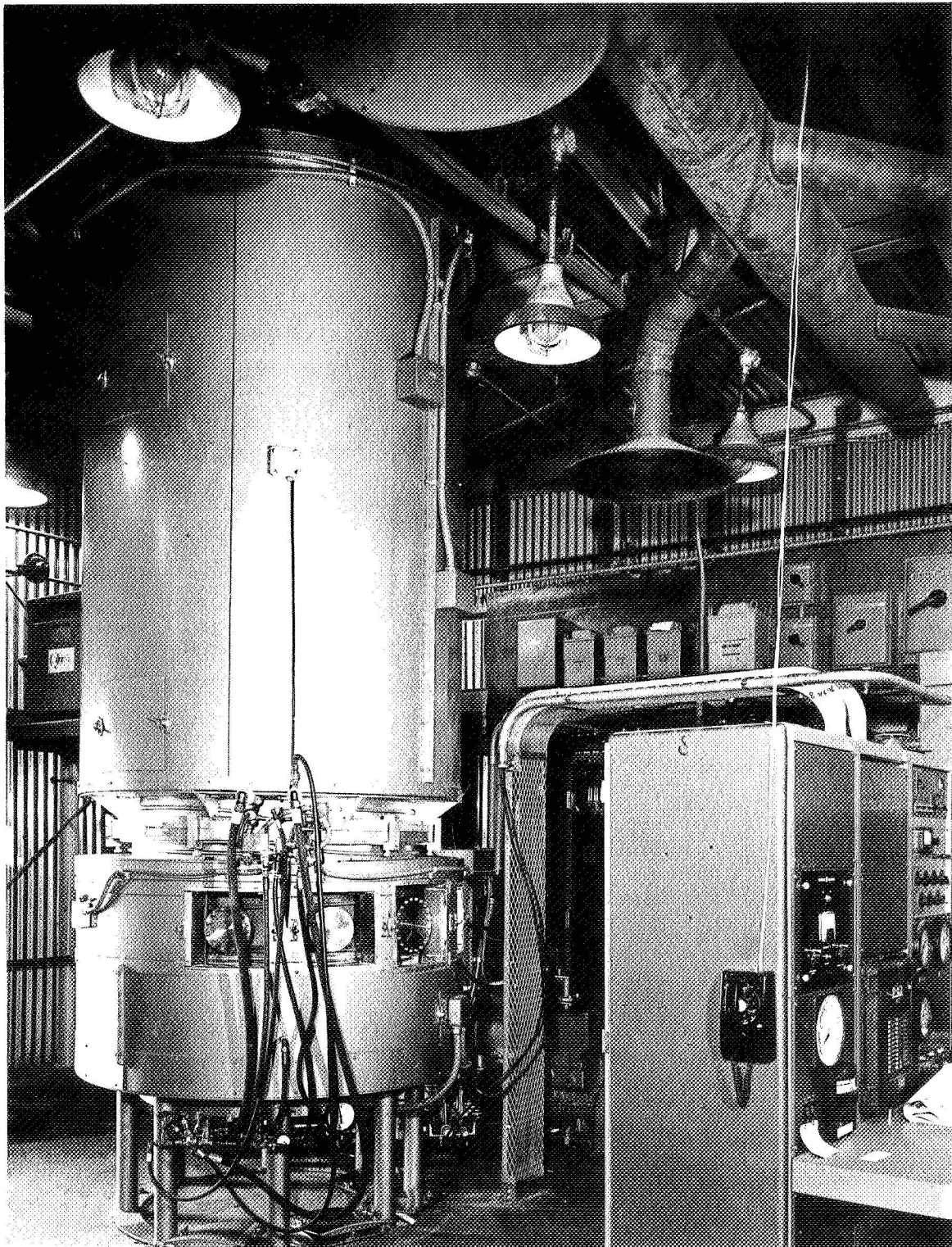
Figure 1. Vacuum System for Thermal Vacuum Tests. The Chamber is 4 Feet
in Diameter and 10 Feet High and is Evacuated by a 10-Inch Oil
Diffusion Pump with Liquid Nitrogen Trap. (C2012925)

to a magnetically operated, rotary feedthrough (Varian Model 954-5026).
The disk is so located in the diffusion pump duct that it effectively
blocks the duct when positioned perpendicular to the duct axis, and
allows full duct conductance when positioned parallel to the axis. The
purpose of this diffusion pump throttle was to permit changes in gas
composition within the chamber by varying the air in-leakage rate and
the effective pumping speed, while maintaining constant total pressure.
After construction and initial checkout of the throttle mechanism, it
was found that such manipulations added considerably to the complexity
of the tests, so that all test exposures were performed with the throttle
in the full open position giving maximum effective pumping speed. The
test exposures were thus conducted in an atmosphere of normal air com-
ponents (N_2, O_2, Ar) with less than 1 percent of the total pressure due
to other gases (H_2, H_2O, CO_2, etc.).

The chamber total pressure was adjusted by varying the air flow rate
into the chamber with the variable leak valve. In order to assure constant
inlet composition throughout the tests, the contaminating air was with-
drawn from a cylinder of dry air connected to the inlet of the variable
leak valve. Care was taken to prevent direct impingement of incoming
air on the test specimens. Uniform distribution of the air was obtained
by directing a portion of the air to the top of the chamber and the
remainder to the bottom.

B. Power Control and Instrumentation of Specimens

Power for each of two strip specimens was supplied by a stepless
controller which utilizes a silicon-controlled rectifier (SCR). The
basic components of the power circuit are shown in Figure 2. The output
voltage from each SCR unit (West Instrument Corporation Model PSCR-60-240)
is stepped down by a 10-kva transformer to provide approximately 10 volts
at 900 amperes.

The SCR units may be operated in either an automatic or manual mode
by means of a digital set point unit (West Instrument Corporation Model
JYSCR). In the automatic mode, a control current is generated which is
proportional to the difference between a preselected millivolt level and
the output from a strip-mounted thermocouple. This control current is

7
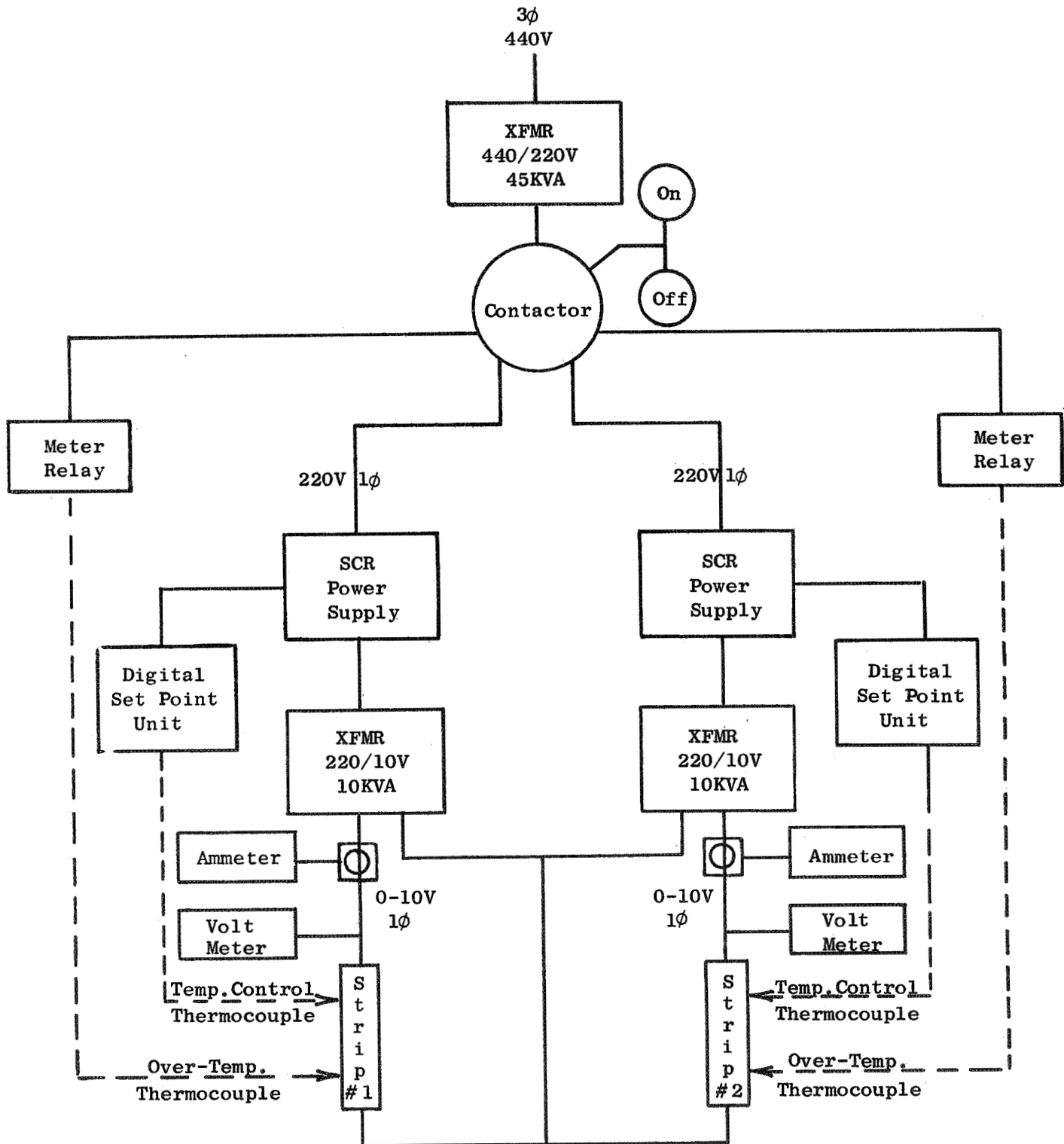
Figure 2. Strip Specimen Power and Control Circuit.

fed to the SCR unit and causes an appropriate increase or decrease in current to the strip specimen.

An automatic over-temperature trip circuit is provided to protect each of the strip specimens in case of control circuit malfunction. A separate strip-mounted thermocouple drives a meter relay with a high set point which may be adjusted to any desired value. The meter relay is connected to the contactor-holding coil and causes the contactor to open if tripped by an over-temperature indication from either strip. Current and voltage meters are provided to monitor strip power input.

Thermocouple circuits inside the vacuum chamber consist of W-3Re/W-25Re wires (0.005-inch-diameter) strung through 99.5 percent alumina insulators with junctions formed by spot welding the individual wires to the point at which temperature is to be measured. The alloy leads are joined to existing copper leads at terminal strips within the vacuum chamber, and the copper leads are connected to the readout instruments in the control room. Since the alloy wire-to-copper lead transition point is the reference junction, copper-constantan thermo-couples referenced to an ice bath are used to measure the internal terminal strip temperatures. Thermocouple EMF is measured by a precision millivolt indicator. In addition, thermocouple EMF was continuously monitored by strip chart recorders. The control console is shown in Figure 3.

The strip specimens were 26 inches (66 cm) long, 1 inch (2.5 cm) wide, and 0.030 inch (0.076 cm) thick. Electrodes of Cb-1Zr alloy, 6 inches long, 1 inch wide, and 0.25 inch thick were welded to each end of each specimen. Two strip specimens, mounted in the chamber, are shown in Figure 4 prior to strip test No. 4. The specimen on the left contains a full-length GTA weld at the mid-point of its width. Eight thermocouples are mounted at various positions along the length of each strip.

C. Ionization Gauge Calibration

The data analysis procedures (to be discussed in Section III of this report) required reliable information concerning ionization gauge
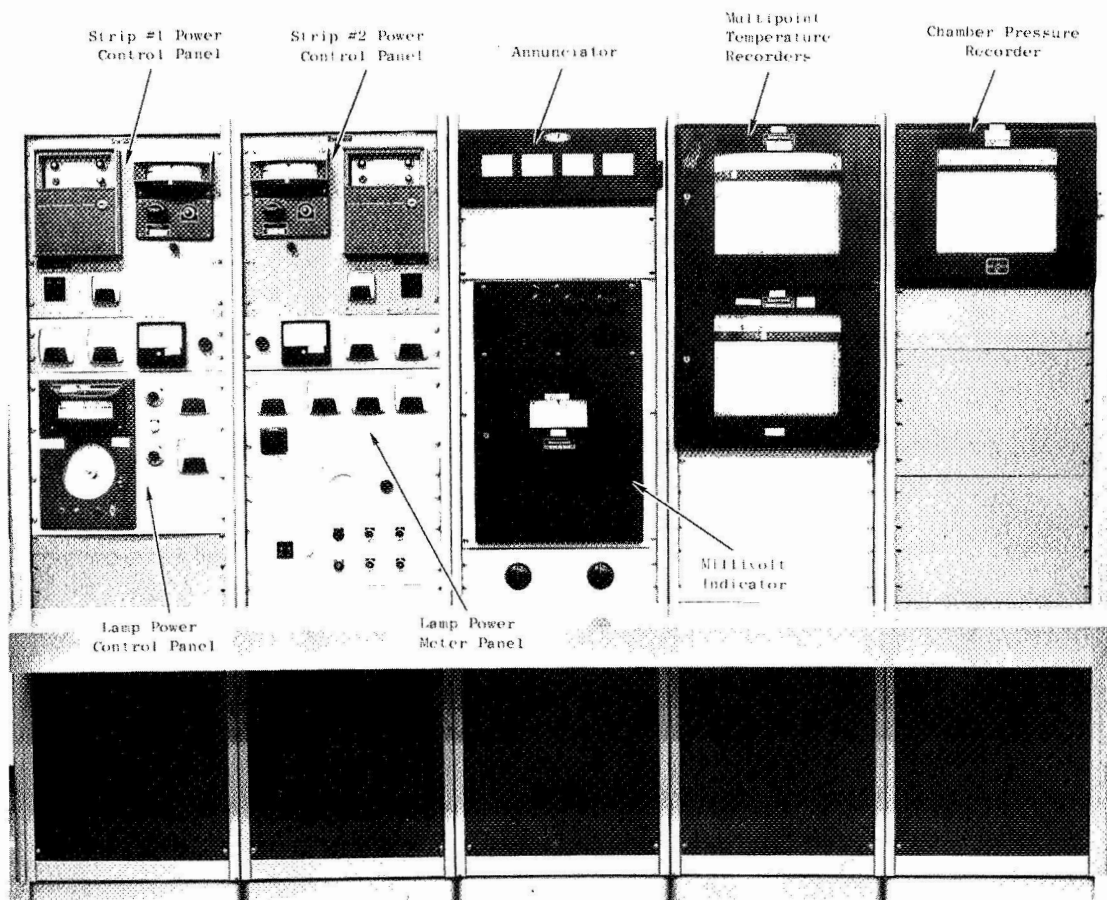
Figure 3. Control Console. (P68-11-33C)
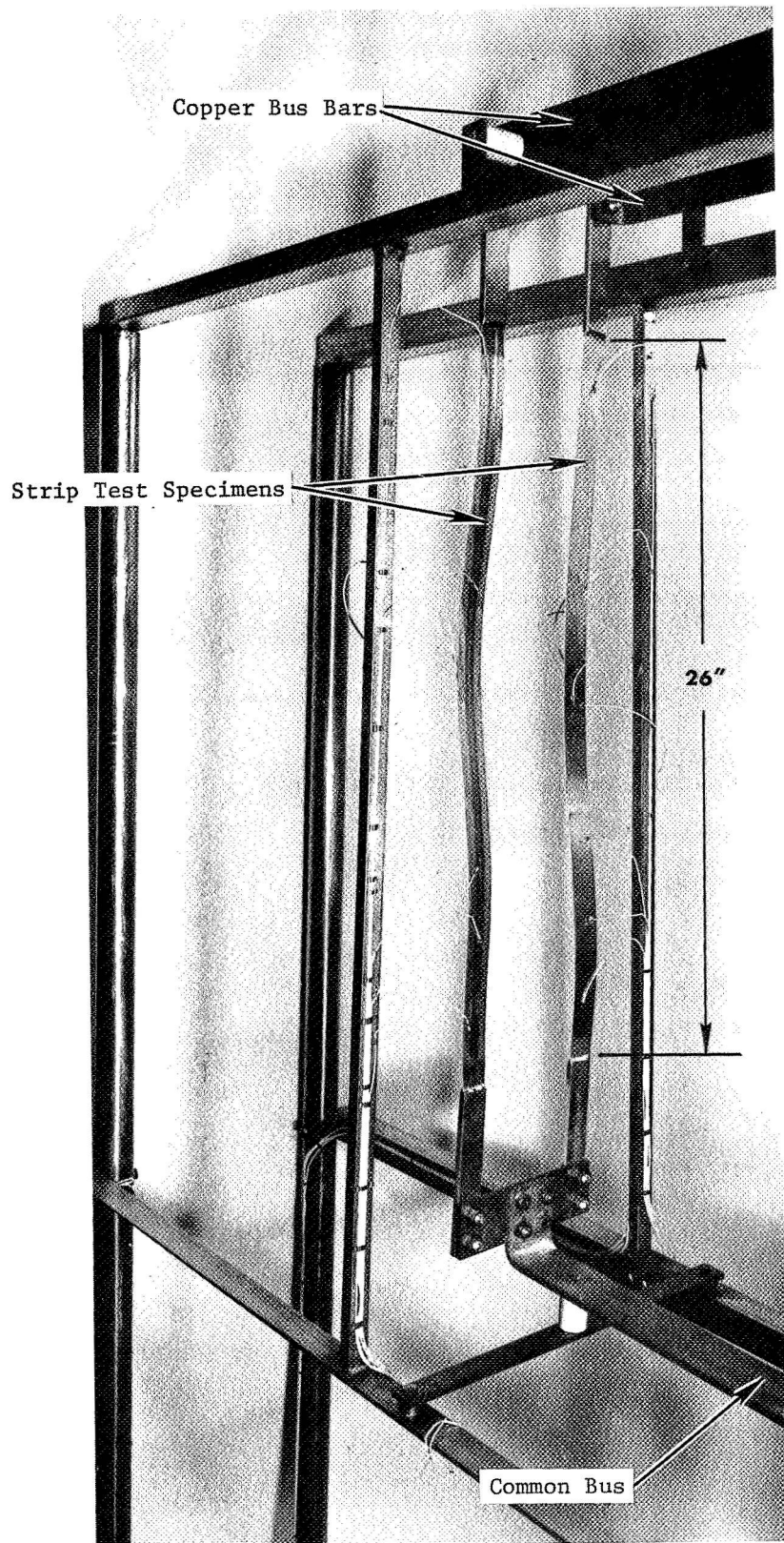
Figure 4. Two Strip Specimens Mounted in Chamber Prior to Strip Test
Exposure No. 4. Specimen on Left Contains a Full-Length
GTA Weld. (P70-2-1B)

11

sensitivity, since a primary test parameter is the oxygen partial pressure obtained from the ionization gauge reading and the mass spectral data. A number of inquiries sent to various vendors disclosed that few are willing and able to perform calibration of ionization gauges. Two ionization gauge tubes (GE Model 22GT 115) were originally purchased for use on this contract. Both these gauge tubes were calibrated by the vendor before delivery. Calibration was performed by comparison with a McLeod gauge in the range 10^{-5} torr for both oxygen and nitrogen. One of these gauge tubes (No. 3) was used for the first strip specimen test exposure. The other gauge tube (No. 2) was used for the final three strip specimen test exposures. Following the final test exposure, examination of the gauge tube elements revealed some discoloration. Gauge tube No. 2 was then recalibrated. This calibration was performed (by The Fredericks Company, Huntingdon Valley, Pennsylvania) for nitrogen and oxygen by comparison with a McLeod gauge in the range 10^{-6} to 10^{-5} torr. Total pressures for the final three test exposures were within this range.

The results of these calibrations are given in Table I where the ionization gauge sensitivity is given for each gauge tube and for each gas. The ionization gauge sensitivity, $s_{ig}(x)$, for a pure gas x is defined as

$$s_{ig}(x) = \frac{I_{ig}(x)}{i_{ig}P(x)} \tag{1}$$

where $I_{ig}(x)$ is the positive ion current obtained at a pressure $P(x)$ with electron emission current i_{ig}. In all tests and calibrations, the emission current was maintained at 1.0×10^{-3} amp using gauge filament No. 2 (thoria-coated iridium). The same control (GE Model 22GC101) was used for all tests and calibrations.

The agreement between the pretest and posttest calibration of gauge tube No. 2 indicates that no serious change in sensitivity occurred during the tests. ASTM Standard E297-66T, "Calibrating Ionization Vacuum Gauge

Tubes"[1] quotes an accuracy of ± 20 percent of reading from 10^{-4} to 10^{-8} torr using the standard technique.

Using the calibration results shown in Table I, the ionization gauge sensitivities required for calculation of partial pressures were obtained. These results are shown in Table II. For gauge tube No. 2, oxygen and nitrogen sensitivity listed in Table II are the average of the pretest and posttest values from Table I. Sensitivities for other gases were obtained from the nitrogen sensitivity and the sensitivity relative to nitrogen which was obtained from selected literature sources. It should be noted that calculated partial pressures depend mainly on the value of nitrogen sensitivity as will be seen in Section III of this report. This is due to the fact that, during the test exposures, the gas in the chamber was 90 to 95 percent nitrogen. Sensitivity values used for H_2, H_2O, and CO_2 had little effect on calculated partial pressures since their combined total was typically less than 1 percent of the total pressure.

D.   Pumping Speed Measurements

The vacuum system pumping speed is an important factor in the materials contamination tests, since, for a given total pressure, the partial pressure of "active" gas species will depend upon the rate of gas removal by the pumps relative to the rate of reaction of the "active" gases with the material surface. Thus for the present tests, in which air was admitted to the chamber, the oxygen reaction rate may be calculated from the gas composition within the chamber provided that the system pumping speed is known. This calculation is shown in Section III of this report.

The method initially used for the pumping speed determinations is based on a rate of pressure change measurement.[2]

The basic equation for the pressure in a vacuum system is

$$PS = -V\frac{dP}{dt} + Q + Q_o \qquad (2)$$

[1] 1968 Book of ASTM Standards, Part 30, General Testing Methods, American Society for Testing and Materials, Philadelphia (1968).

[2] Van Atta, C. M., Vacuum Science and Engineering, McGraw-Hill Book Company (1965).

TABLE I

RESULTS OF IONIZATION GAUGE CALIBRATION

Gauge Tube	Gas	Pretest Calibration s_{ig}(torr^{-1})	Posttest Calibration s_{ig}(torr^{-1})
No. 3	N_2	9.2	-
No. 3	O_2	8.4	-
No. 2	N_2	8.1	10.0
No. 2	O_2	7.7	9.0

TABLE II

IONIZATION GAUGE SENSITIVITY

	Gas	Sensitivity Relative to N_2 $s_{ig}(x)/s_{ig}(N_2)$	Sensitivity $s_{ig}(x)$(torr^{-1})
Gauge Tube No. 3	H_2	0.42	3.9
	H_2O	0.89	8.2
	N_2		9.2
	O_2		8.4
	Ar	1.56	14.4
	CO_2	1.37	12.6
Gauge Tube No. 2	H_2	0.42	3.8
	H_2O	0.89	8.1
	N_2		9.1
	O_2		8.4
	Ar	1.56	14.2
	CO_2	1.37	12.5

in which P is the pressure in the system, S is the pumping speed, V is the volume of the system, Q is the throughput of gas flowing into the system (from an external source), and Q_o is the gas flow due to interior surface outgassing. With no gas flowing into the system, the system eventually reaches a stable pressure referred to as the ultimate pressure, P_o, of the system. Thus if Q = 0 and $\frac{dP}{dt}$ = 0, equation (2) becomes

$$P_o S = Q_o \qquad . \qquad (3)$$

Now if the pressure in the system is greater than the ultimate pressure and no gas flows into the system, then combining equations (3) and (2) and setting Q = 0, we obtain

$$S = - \frac{V}{P - P_o} \frac{dP}{dt} \qquad . \qquad (4)$$

Thus if V and P_o are known, the pumping speed may be calculated from the pressure decrease as a function of time. A more convenient expression is obtained by integration of equation (4) to obtain

$$S = 2.30 \frac{V}{t_2 - t_1} \log_{10} \frac{P_1 - P_o}{P_2 - P_o} \qquad . \qquad (5)$$

The procedure used was to pump down and bake out the system to obtain a stable base pressure, P_o, of about 3×10^{-8} torr. Nitrogen was then admitted through the leak valve at such a rate as to bring the chamber pressure into the 10^{-6} torr range. The leak valve was then rapidly closed and pressure as a function of time was obtained by monitoring the ionization gauge pressure reading on a strip chart recorder.

Data from a typical run are shown in Figure 5 where $\log_{10} (P - P_o)$ is plotted against time. This particular run was made with the diffusion pump throttle closed giving minimum pumping speed. The calculated pumping speed is 209 liters per second.

Some data were also obtained with the diffusion pump throttle open giving maximum pumping speed. However, the rate of pressure change was too rapid to give a reliable pumping speed under these conditions. A second method, giving relative pumping speed, was then used to obtain

15
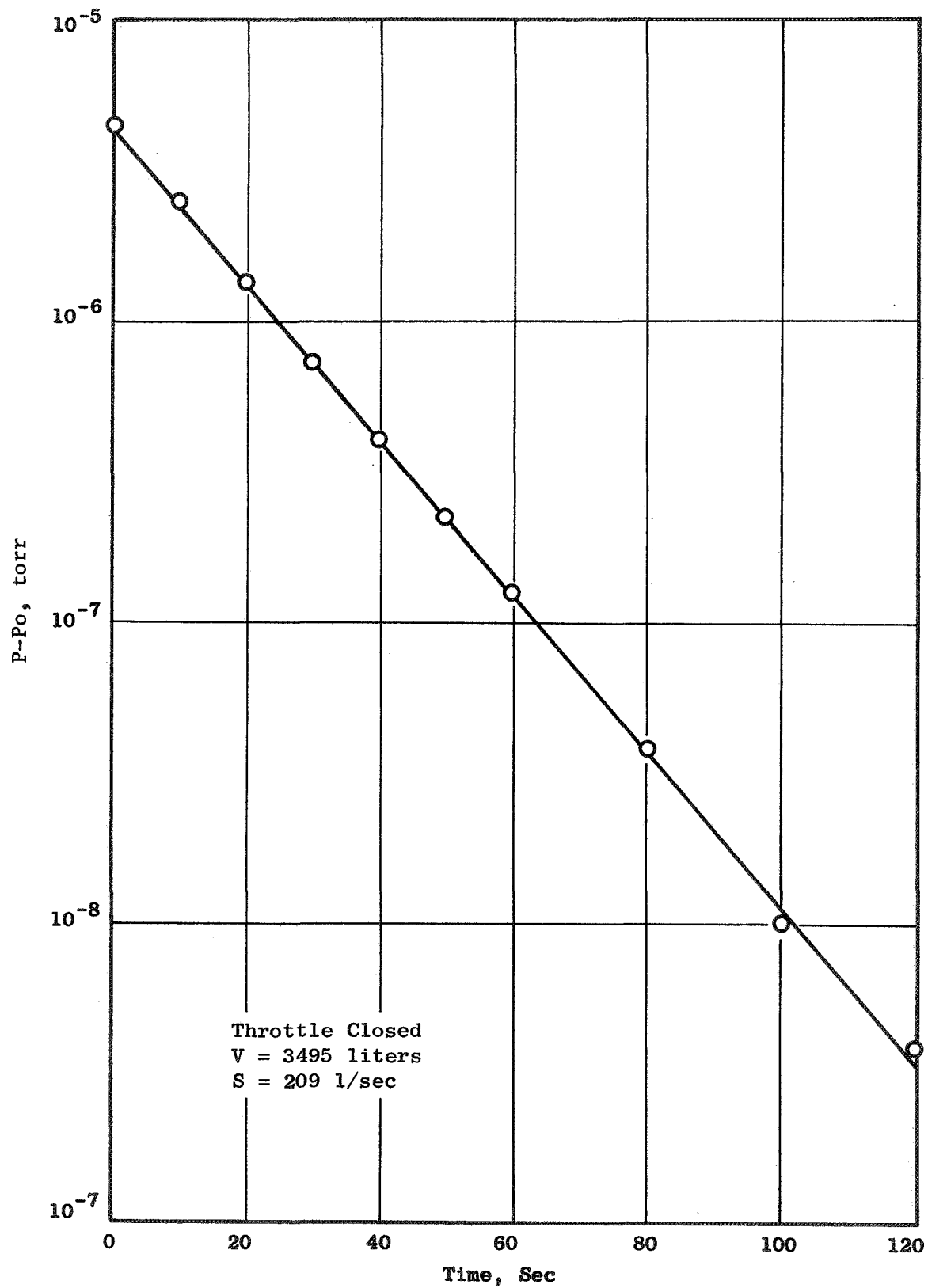
Figure 5. Typical Data for Pumping Speed Measurement by the Rate of
Pressure Change Method.

pumping speed at various orientations of the throttle plate. With the throttle closed, the pressure was stabilized in the 10^{-6} torr range by admission of nitrogen through the leak valve. Under these conditions, Q_o is negligible, and equation (2) becomes simply

$$P_1 S_1 = Q \qquad . \qquad (6)$$

If the throttle is then set at a different position while maintaining a constant flow, a second stable pressure, P_2, is obtained such that

$$P_1 S_1 = P_2 S_2 \qquad . \qquad (7)$$

Since S_1 had been found from the rate of pressure change method, S_2 is obtained from equation (7) by measurement of P_1 and P_2. The results of these initial pumping speed measurements are shown in Figure 6 where pumping speed is plotted against orientation of the throttle plate.

Following these measurements, for reasons mentioned previously, it was decided that the test exposures would be conducted with the pump throttle open. Under these conditions, it was found that the rate of pressure change was too rapid to be reliably measured by this technique A method utilizing measured gas flow rate into the chamber was then employed. Except for the method of gas admission into the chamber and the ionization gauge location, the method is essentially the same as that described in ASTM E-294-67T, "Effective Pumping Speed of Vacuum Chamber Systems."[2] The chamber was first pumped to the ultimate pressure P_o and then air was admitted at a measured flow rate, Q, resulting in a stable pressure, P. The pumping speed was then calculated from the equation

$$S = \frac{Q}{(P - P_o)} \qquad . \qquad (8)$$

For the air flow rate measurements, a simple constant pressure displacement meter was constructed using a 10-cc pipet inverted in a beaker of DC-704 diffusion pump fluid. This type of meter is described in ASTM E-295-67T.[2]
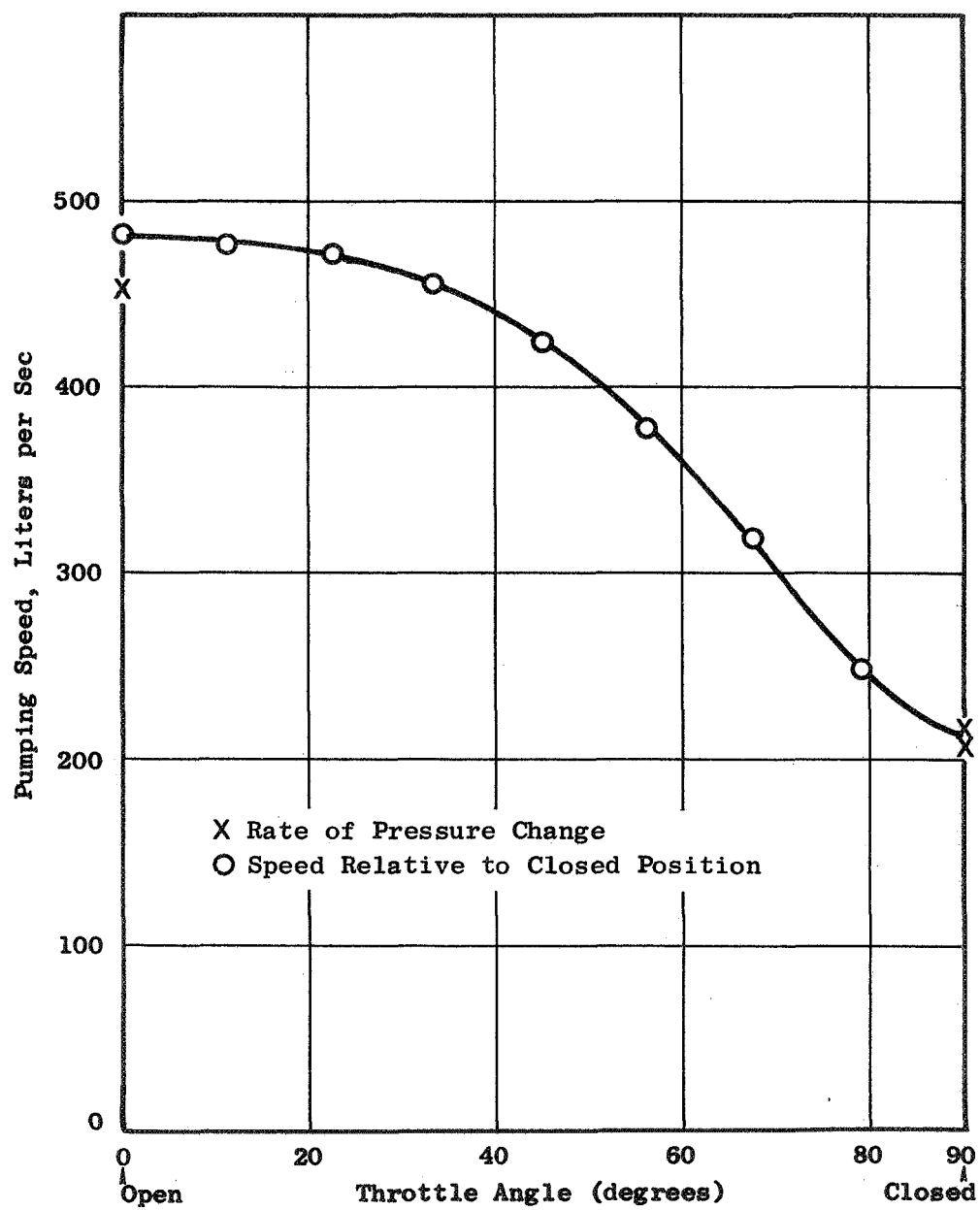
Figure 6. Pumping Speed (for Nitrogen) Versus Throttle Orientation.

18

Pumping speed was measured before and after each strip specimen test exposure. A summary of the results of all pumping speed measurements is given in Table III. The pretest value for test No. 1 is obtained from the rate of pressure change measurements shown in Figure 6. In test No. 4., the total air flow during the test was measured (as will be described later) and the pumping speed was obtained from the average nitrogen flow rate and average nitrogen partial pressure.

Values given in Table III show fairly consistent pumping speeds except for the first test in which the pumping speed was about one-half the value measured in the later tests. It should be noted that an interval of about 12 months elapsed between the conclusion of the first test and the start of the second test. During this period, evaluation of the lamp system performance was being made. No changes in the system can be definitely identified which would cause this large increase in pumping speed. However, it has been established that some changes were made in the cooling water system which could have affected the water flow to the diffusion pump. The higher values for pumping speed obtained for the last three tests are in good agreement with the system pumping speed calculated from the rated diffusion pump speed (4200 l/sec), the conductance of the cold trap (3000 l/sec) and the conductance of the water-cooled baffle (2100 l/sec). The net speed thus calculated is 955 l/sec.

TABLE III

SUMMARY OF PUMPING SPEED MEASUREMENTS

	P_0(torr)	P(torr)	Q(torr 1/sec)	S(1/sec)	
Before Test No. 1				481	See Note 1
After Test No. 1	2×10^{-8}	8.7×10^{-6}	3.00×10^{-3}	345	
Average				413	
Before Test No. 2	1.5×10^{-8}	5.0×10^{-6}	3.75×10^{-3}	753	
After Test No. 2	4×10^{-9}	5.33×10^{-6}	4.44×10^{-3}	833	
Average				793	
Before Test No. 3	4.2×10^{-8}	3.51×10^{-6}	3.32×10^{-3}	957	
After Test No. 3	1×10^{-8}	3.46×10^{-6}	2.88×10^{-3}	835	
Average				896	
Before Test No. 4	1×10^{-8}	3.30×10^{-6}	2.80×10^{-3}	851	
After Test No. 4	1×10^{-8}	2.79×10^{-6}	2.34×10^{-3}	841	See Note 2
Average				846	

Note 1: From Figure 6 throttle angle O degrees. All tests were made with throttle full open.

Note 2: Obtained from average N_2 partial pressure during test No. 4.

III. DATA ANALYSIS PROCEDURES

A. Partial Pressures from Mass Spectral Data

The mass spectrometer used in these tests was a General Electric Company Monopole 300 (Model 22PT180). On the recommendation of the manufacturer, the ion source, "Vee" block, and pole piece were gold-plated to minimize reaction with the relatively high oxygen partial pressures used in these tests. The output of the electron multiplier was read on a strip chart recorder through an electrometer (Keithley Model 416). As with other instruments utilizing electron multipliers, it was found that the electron multiplier gain will change with time and exposure conditions. Due to this effect, the mass spectrometer was used to obtain relative concentrations of the various gases within the chamber, with absolute partial pressures obtained from the ionization gauge reading, corrected for the relative concentrations.

A mass spectrum of the residual gases in the chamber at 5×10^{-8} torr is shown in Figure 7. The major constituents under these conditions are hydrogen (mass 2), water vapor (mass 18), and nitrogen (mass 28). Characteristic groups of peaks (mass 12 to 16, 24 to 30, 36 to 44, and 48 to 58) are indicative of hydrocarbons, probably from backstreaming oil vapor.

The method used for calibration of the mass spectrometer and subsequent partial pressure analyses involves the use of both the ionization gauge and the mass spectrometer in a procedure such that the total pressure is determined by the ionization gauge reading, corrected for relative concentrations of various gas species, with the relative concentrations being obtained from the mass spectrum. With this procedure, variations in electron multiplier gain do not affect the calculated partial pressures as long as the relative gain is constant.

The ionization gauge sensitivity was defined in equation (1). The mass spectrometer sensitivity, $s_{ms}(x)$, for any pure gas, x, is similarly defined:

$$s_{ms}(x) = \frac{I_{ms}(x)}{i_{ms} P(x)} \tag{8}$$
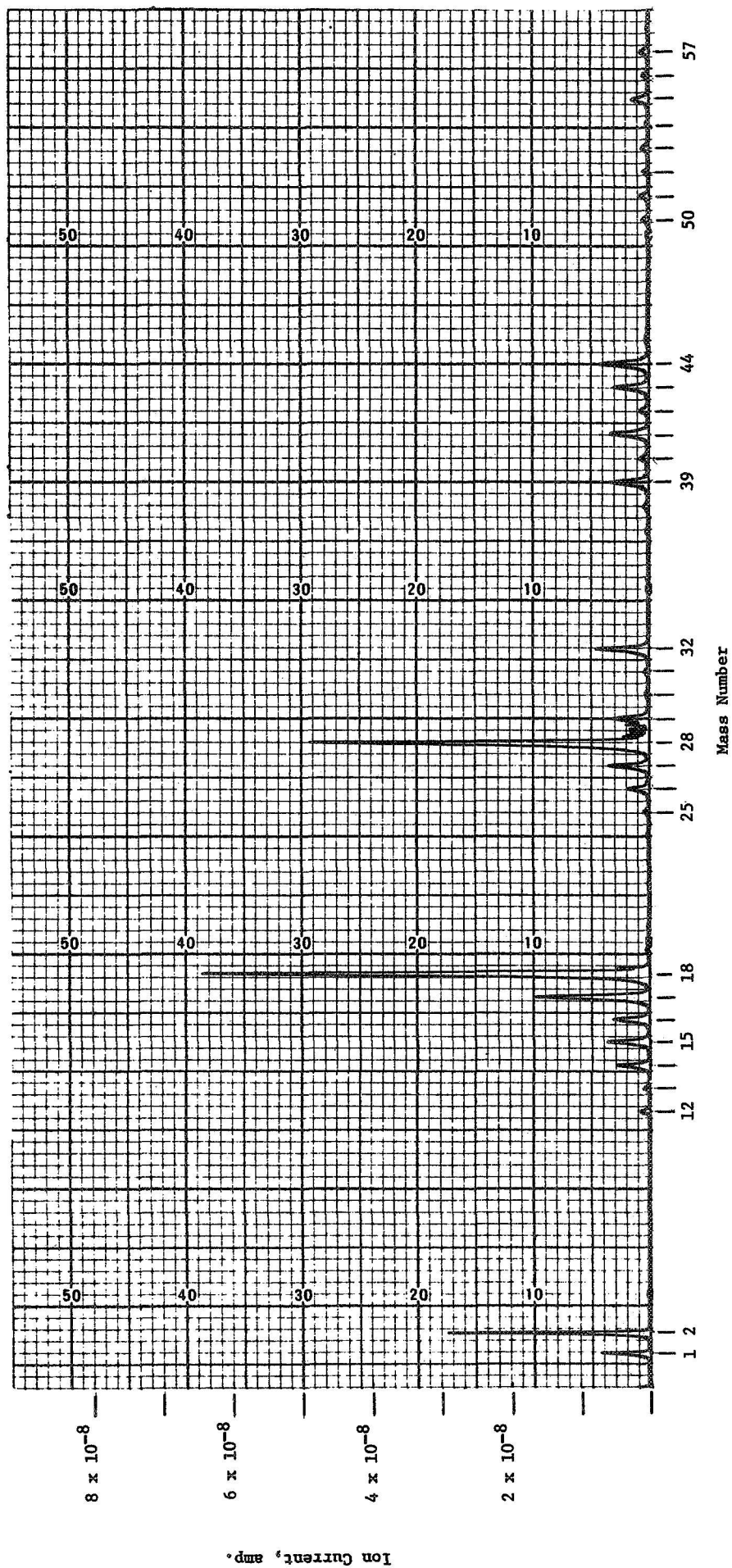
Figure 7. Mass Spectrum of Residual Gases in the Vacuum Chamber at 5×10^{-8} Torr.

where $I_{ms}(x)$ is the positive ion current of the mass spectrometer for a particular peak (usually the parent peak) in the pure gas mass spectrum, and i_{ms} is the electron emission current of the mass spectrometer. Now if a pure gas at pressure $P(x)$ is measured simultaneously with the ionization gauge and the mass spectrometer, then $P(x)$ can be eliminated with equations (1) and (8) to obtain

$$s_{ms}(s) = \frac{I_{ms}(x)}{i_{ms}} \frac{i_{ig} s_{ig}(x)}{I_{ig}(x)} \tag{9}$$

The mass spectrometer is thus calibrated to obtain $s_{ms}(x)$ for various pure gases using equation (9).

Now for any gas mixture, it is assumed that the total ionization gauge ion current is the sum of the ion currents due to each of the gases in the gas mixture. From equation (9) we thus obtain:

$$I_{ig}(T) = \sum_{x} I_{ig}(x) = \sum_{x} \frac{I_{ms}(x)}{i_{ms} s_{ms}(x)} i_{ig} s_{ig}(x) \tag{10}$$

where $I_{ig}(T)$ is the total ionization gauge ion current. But equation (10) involves the absolute mass spectrometer sensitivity rather than relative sensitivity, as desired. The right side of equation (10) is multiplied by $\dfrac{s_{ms}(N_2)}{s_{ms}(N_2)}$ to give

$$I_{ig}(T) = \frac{1}{s_{ms}(N_2)} \sum_{x} \frac{I_{ms}(x)}{\dfrac{i_{ms} s_{ms}(x)}{s_{ms}(N_2)}} i_{ig} s_{ig}(x) \tag{11}$$

Mass spectrometer sensitivity is taken, for the present purposes, relative to the nitrogen sensitivity, $s_{ms}(N_2)$, since nitrogen is the main residual gas in these tests. Actually, the term $\dfrac{1}{s_{ms}(N_2)}$ is simply a factor which, in effect, normalizes the sum of the partial pressures to be consistent with the ionization gauge reading.

Calculation of partial pressures and total pressure by this technique thus requires knowledge of the relative mass spectrometer sensitivities for each of the gases and the absolute sensitivities of the ionization gauge.

23

For a particular mass spectrum, the value $\dfrac{1}{s_{ms}(N_2)}$ is first calculated from equation (11). Having determined $\dfrac{1}{s_{ms}(N_2)}$, the absolute mass spectrometer sensitivities are calculated and the partial pressures are then obtained from equation (8).

Table IV shows relative sensitivity for the mass spectrometer. Sensitivity was measured for H_2, He, N_2, and Ar by admitting the pure gases into the vacuum chamber and calculating sensitivity from equation (9). Corresponding relative sensitivities were then obtained. Attempts to calibrate the analyzer for oxygen by this method were unsuccessful since exposure to oxygen pressures in the 10^{-6} torr range caused a large increase in sensitivity and thus consistent values could not be obtained. This effect is presumably due to "activation" of the electron multiplier detector in the mass spectrometer due to partial oxidation, and oxidation under more severe conditions has been used[3] to activate and stabilize the gain of such electron multipliers.

The oxygen sensitivity relative to nitrogen was obtained by admission of air to the chamber. Under such conditions, it can be shown from equation (8) that the relative sensitivity is related to the relative ion currents and relative partial pressures as follows.

$$\frac{s_{ms}(O_2)}{s_{ms}(N_2)} = \frac{I_{ms}(O_2)\ P(N_2)}{I_{ms}(N_2)\ P(O_2)} \quad . \tag{12}$$

The standard composition[4] (78.09 percent N_2 and 20.95 percent O_2) was taken for air and appropriate corrections for relative pumping speeds were made in calculating relative partial pressures. Calculation of relative mass spectrometer sensitivity for argon from the same mass spectra gave 0.81, in good agreement with 0.85 obtained from the pure gas calibration for argon.

The mass spectrometer sensitivity for H_2O and CO_2 is estimated to be the same as for N_2, as shown in Table IV.

[3] Beynon, J. H., _Mass Spectrometry and Its Applications to Organic Chemistry_, Elsevier Publishing Company, Amsterdam (1960).

[4] Grey, D. E., Ed., _American Institute of Physics Handbook_, McGraw-Hill Book Company, Inc., New York (1957).

TABLE IV

MASS SPECTROMETER RELATIVE SENSITIVITY

Gas	Major Peak	Sensitivity Relative to N_2 $\dfrac{s_{ms}(x)}{s_{ms}(N_2)}$	Source of Data
H_2	2	1.39	Separate Cal. for N_2 and H_2
He	4	0.50	Separate Cal. for N_2 and He
H_2O	18	1.00	Estimated Value
N_2	28	1.00	
O_2	32	1.03	Air Calibration
Ar	40	0.85	Separate Cal. for N_2 and Ar
CO_2	44	1.00	Estimated Value

B. Reaction Rate Calculations

From kinetic theory considerations, the mass incident rate, m, of a gas at a surface is

$$m = 5.833 \times 10^{-2} \ P\sqrt{\frac{M}{T}} \quad \frac{gm}{cm^2 \ sec} \tag{13}$$

where P is the gas pressure (torr), M the molecular weight, and T is the absolute temperature (°K). If a certain fraction, α, of the incident molecules are absorbed and react with the surface, the reaction rate is

$$m_r = 5.833 \times 10^{-2} \ \alpha P\sqrt{\frac{M}{T}} \quad \frac{gm}{cm^2 \ sec} \tag{14}$$

The parameter, α, is dimensionless and is the probability that an impinging gas molecule will react with the surface and hence is called the sticking probability or sticking factor for the gas under the particular conditions of surface exposure.

For the present tests, the main interest is in the oxygen reaction rate. If air flows into the chamber with the specimens at elevated temperature, a portion of the oxygen will react with the specimens according to equation (14) and the remainder will be pumped away. For calculation purposes, it is more convenient to express equation (14) in terms of oxygen flow rate (in $\frac{torr \ 1}{sec}$) to the specimens. Taking the appropriate gas temperature to be 20°C (293.15°K), the corresponding oxygen density is 1.752×10^{-3} gm/torr 1. With these values, equation (14) becomes

$$\text{oxygen reacting} = 11.00 \ \alpha A \ P(O_2) \ \frac{torr \ 1}{sec} \tag{15}$$

where A is the total reacting area (cm^2) of the specimens. Now the oxygen removed from the system by the pump is

$$\text{oxygen pumped} = P(O_2)S_{O_2} = 0.936 \ P(O_2)S \ \frac{torr \ 1}{sec} \ . \tag{16}$$

The oxygen pumping speed, $S_{O_2} = 0.936 \ S$ where S is the nitrogen (or air)

pumping speed as given in Table III. The factor 0.936 is obtained by assuming that the pumping system is conductance limited, a reasonable assumption since the measured pumping speed is less than 20 percent of the rated speed of the diffusion pump.

Now the air flowing into the chamber contains 0.934 percent argon. The argon is completely pumped away since argon does not react with the specimens. Thus

$$\text{argon pumped} = \text{total argon flow} = 0.838 \ P(Ar)S \ \frac{\text{torr l}}{\text{sec}} \qquad (17)$$

where the factor 0.838 is again obtained from the assumption of conductance limited pumping.

The total oxygen flow into the chamber is the sum of oxygen pumped and oxygen reacted. The ratio of total oxygen flow into the chamber to total argon flow is the standard air ratio. Thus

$$\frac{\text{total oxygen flow}}{\text{total argon flow}} = \frac{0.2095}{0.00934} = \frac{\text{oxygen pumped + oxygen reacted}}{\text{argon pumped}} =$$

$$\frac{0.936 \ P(O_2)S + 11.00 \ \alpha A P(O_2)}{0.838 \ P(Ar)S} \qquad (18)$$

This equation may be simplified to obtain

$$\frac{\alpha A}{S} = 1.708 \ \frac{P(Ar)}{P(O_2)} - 0.0851 \qquad (19)$$

This equation shows how the argon-to-oxygen pressure ratio varies with the ratio of oxygen reacted (proportional to αA) to system pumping speed. The minimum value of $\frac{P(Ar)}{P(O_2)}$ is obtained with no specimens in the chamber (or with $\alpha = 0$), and is the normal air ratio as modified by the conductance limitation. The ratio, $\frac{P(Ar)}{P(O_2)}$, becomes increasingly larger ($P(O_2)$ decreases) as the product, αA, increases with respect to S. This is shown in Figure 8 where $\frac{P(Ar)}{P(O_2)}$ is plotted against $\frac{\alpha A}{S}$. This demonstrates a very important consideration in the calculation of refractory metal contamination rate in a vacuum system under conditions of air in-leakage;
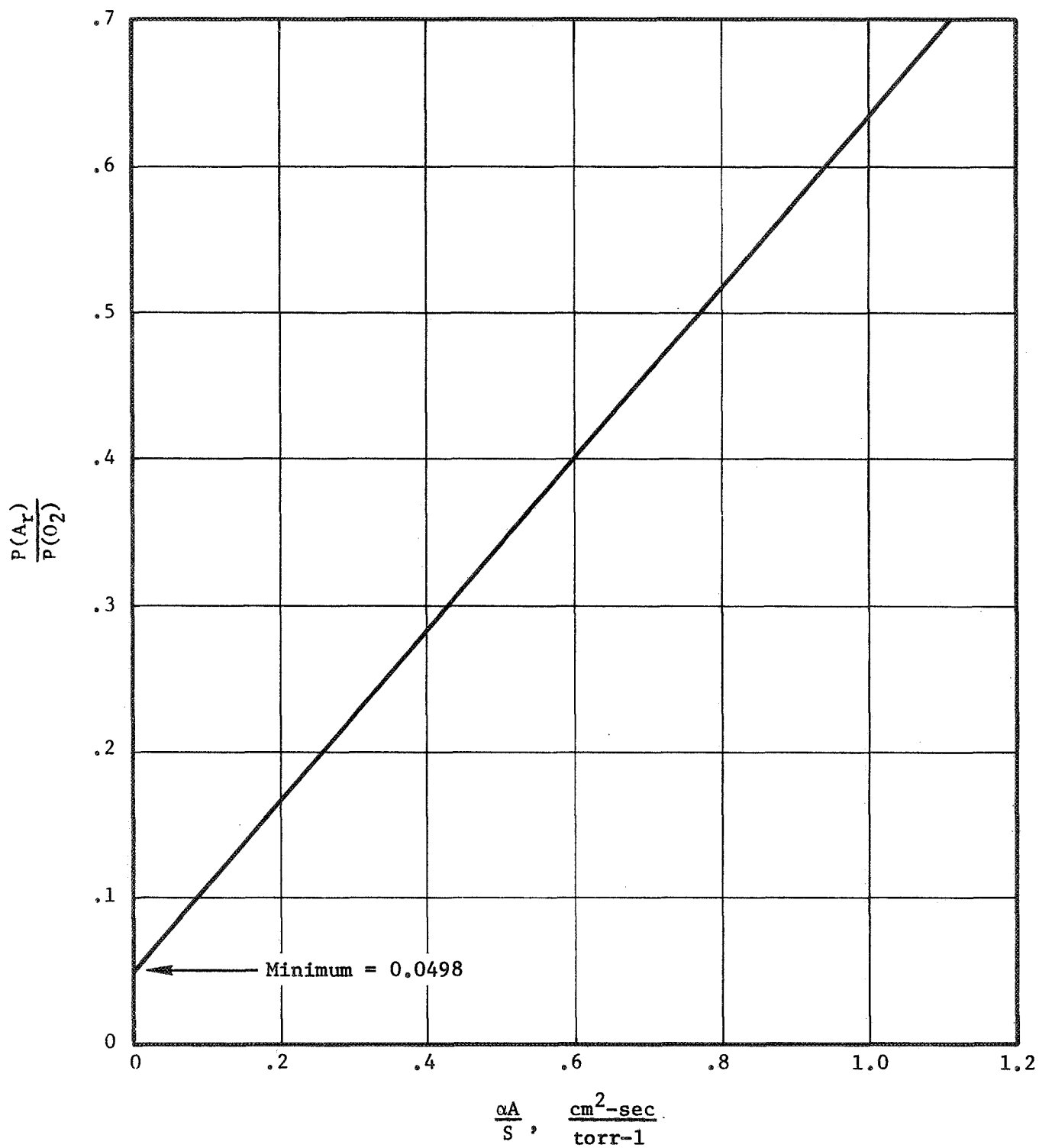
Figure 8. Change in Argon-to-Oxygen Pressure Ratio with the Factor $\frac{\alpha A}{S}$ for Air. (Ref. Equation 19)

that is, that the actual composition in the chamber will be considerably different from the nominal air composition if the ratio, $\frac{\alpha A}{S}$, is greater than about 0.05. Similar calculations could be performed to find the nitrogen-to-oxygen ratio.

In a particular test specimen exposure, the sticking probability can be calculated both from the gas analysis and system pumping speed (equation 19), and from the oxygen partial pressure and weight gain (equation 14). The agreement between these two essentially independent calculations is a measure of the overall consistency of the test data. The value of α calculated from equation (19) is the instantaneous value while that obtained from the total weight gain (equation 14) is the overall (or effective) value.

IV. STRIP TEST EXPOSURES

All strip specimens exposed in these tests were cut from the same sheet of Cb-1Zr, nominally 0.030-inch (0.076-cm) thick. The sheet was furnished by NASA, and the strip specimens were fabricated by GE-NSP. The strips were cleaned, prior to welding of the electrodes, according to specification 03-0010-00-D. This specification requires pickling in a solution of 20 percent nitric acid, 20 percent hydrofluoric acid, and 60 percent water. Other details pertaining to the preparation of the individual strip specimens are given below.

A. Test Exposure No. 1

The initial test exposure was made on a specimen consisting of a 17-inch length of material cut parallel to the rolling direction and a 9-inch length cut transverse to the rolling direction. The two sections were welded together by gas-tungsten arc (GTA) welding. The specimen was not annealed after welding. A summary of the test exposure conditions and results of test No. 1 are as follows:

Test Specimen — Cb-1Zr sheet, 26 inches (66.0 cm) long x 1.0 inch (2.54 cm) wide x 0.0316 inch (0.0802 cm) thick. Surface pickled. Longitudinal and transverse sections.

Exposure Time — 210 hours.

Specimen Temperature — 1700°F (927°C).

Vacuum System Pumping Speed — 413 1/sec.

Average Total Pressure — 8.57×10^{-6} torr.

Average Partial Pressure —

N_2 7.52×10^{-6} torr, 87.7%

O_2 8.76×10^{-7} torr, 10.2%

Ar 1.15×10^{-7} torr, 1.34%

H_2 3.01×10^{-8} torr, 0.35%

H_2O 2.55×10^{-8} torr, 0.29%

CO_2 4.9×10^{-9} torr, 0.05%

Specimen Analyses:

	(ppm) Oxygen	(ppm) Nitrogen	(ppm) Carbon
Posttest	5990	70	—
Pretest	44	22	342
Change	5950	48	—

Average Oxygen Reaction Rate $-$ m_r $=$ 2.71×10^{-9} $gm/cm^2 sec$
(Calculated from oxygen increase)

Sticking Probability: α $=$ 0.160 (Calculated from m_r, Ref. Equation 14)

α $=$ $0.183 \pm .039$ (Average of values calculated from Ar/O_2 ratio, Ref. Equation 19)

Total and partial pressures during the exposure are plotted against exposure time in Figure 9. The partial pressures are calculated as described in Section III of this report, and the total pressure is the sum of the partial pressures. The air constituents, O_2, N_2, and Ar account for more than 99 percent of the total pressure. CO, although probably present in small quantity, could not be detected due to interference from other species in the system. Small quantities of heavier hydrocarbons were detected with masses greater than 50 but quantitative analyses were not obtained. The most prominent of these hydrocarbons were in the C_4 group (masses 50 to 57) and benzene (masses 77, 78, 79).

The measured average argon-to-nitrogen partial pressure ratio is 0.0153 compared to 0.0142 calculated from the standard air composition and relative conductance limited pumping speed. The good agreement between these two values indicates a very low sticking probability for nitrogen. This conclusion is confirmed by the vacuum fusion analyses which show a nitrogen increase of only 48 ppm.

The sticking probability, calculated for each gas analysis from the argon-to-oxygen ratio (Equation 19), is shown in Figure 10. The line shown in the figure is calculated from a linear fit of the data by the method of least squares. This shows a slight tendency toward decreasing sticking probability with increasing exposure time.

The standard (RMS) deviation of the 20 data points in Figure 10 is ± 0.030 or about 21 percent of the average value of α. This variation is attributed to instabilities in the mass spectrometer and to changes in pumping speed throughout the test. The sticking probability calculated from the increase in oxygen content of the specimen is 0.160 in excellent agreement with $0.183 \pm .039$ calculated from the argon-to-oxygen partial pressure ratio.

During evaluation of the materials from the initial test exposure, it was found that the weld between the transverse and longitudinal
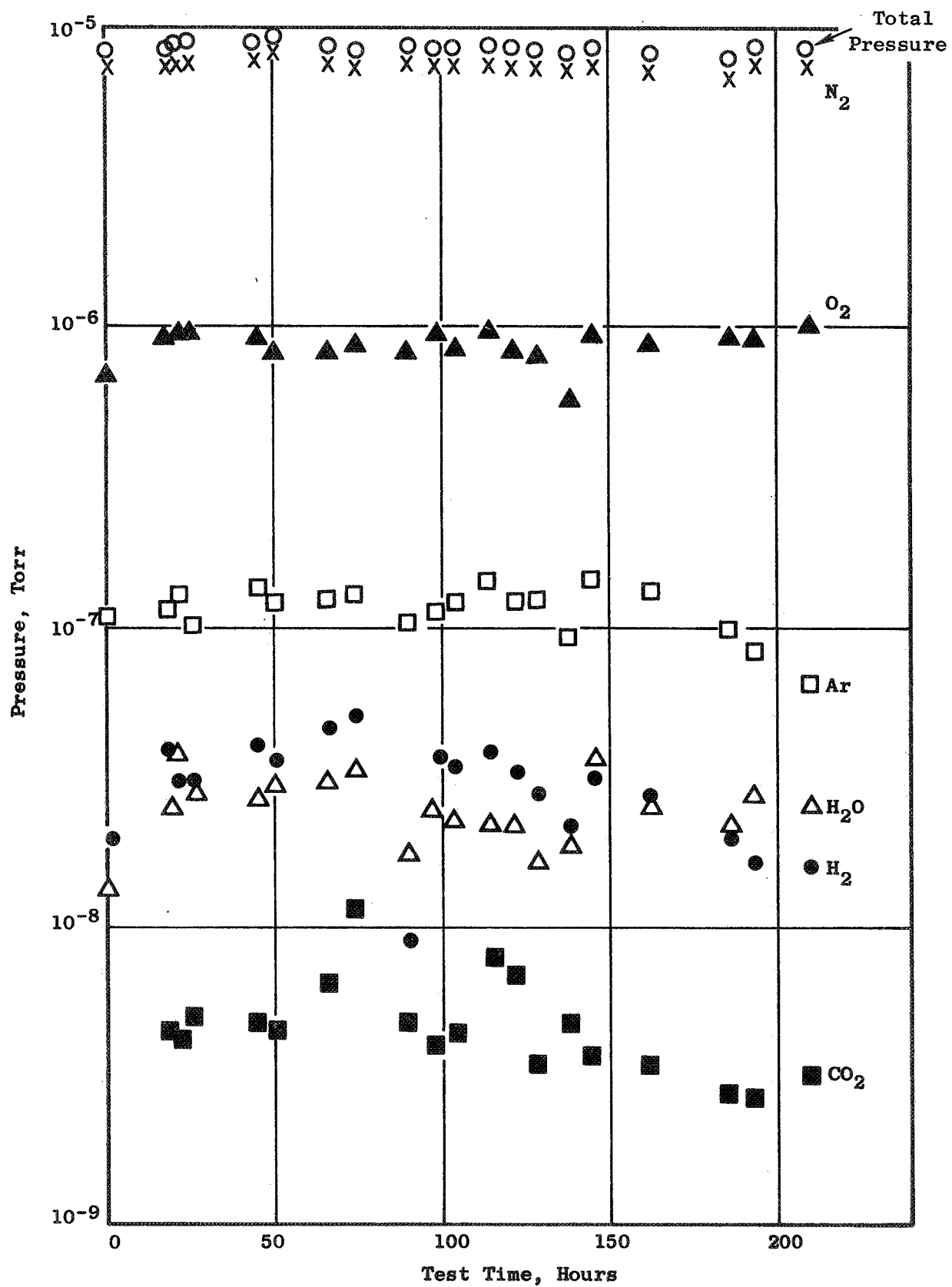
Figure 9. Total and Partial Pressures for Test Exposure No. 1, a Single Strip Specimen.
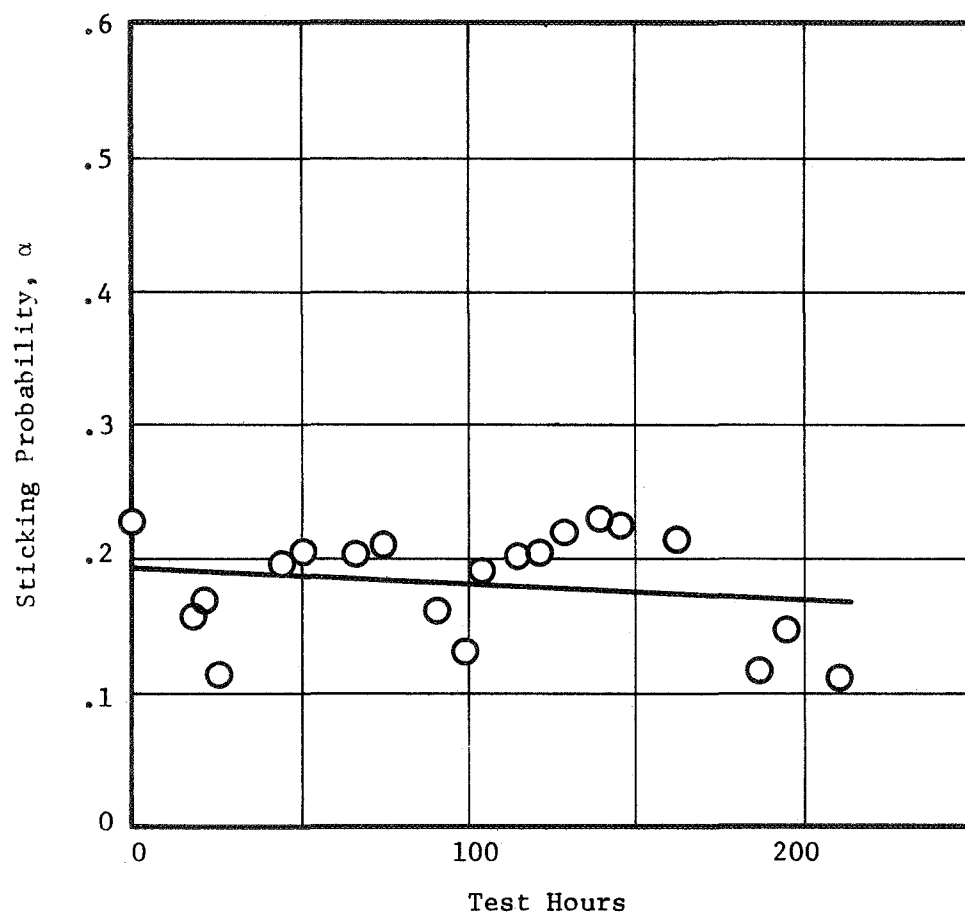
Figure 10. Sticking Probability Calculated From Argon-to-Oxygen
Ratio for Test Exposure No. 1, Single Strip Specimen.

sections was quite brittle. This effect will be discussed below in the evaluation section of this report.

B.   Test Exposure No. 2

In an attempt to minimize embrittlement of the weld metal on subsequent exposure, the specimens for test exposure No. 2 were vacuum annealed in the test chamber by heating to 2200°F for one hour. As events transpired, the specimens were exposed to ambient air for a period of several months following annealing and before the test exposure.

The two specimens exposed in this test were each 26 inches long, one inch wide, and 0.0316 inch thick and consisted of a 17-inch length cut parallel to the rolling direction and a 9-inch length cut transverse to the rolling direction. The two sections were welded together by gas-tungsten arc (GTA) welding. The surface of one specimen was roughened by grit-blasting all exposed surfaces with 60-grit alumina of 99.9 percent purity. All specimens were fabricated at GE-NSP and grit-blasting was performed at NASA-Lewis Research Center.

The duration of the second test exposure was 501.5 hours with a calculated average oxygen partial pressure of 2.2×10^{-7} torr. However, in performing the posttest chamber pumping speed measurements, it was found that unusually low pressures were obtained (indicating unreasonably high pumping speed). Investigation of this effect revealed that the ionization gauge had become contaminated during the test and was, in fact, reading too low during an unknown (but probably extensive) period during the test. Thus, no reliable pressure measurements were obtained for this test.

The probable cause of the deterioration of the ionization gauge readings during this test is the formation of an insulating deposit on the ion collector as a result of exposure to high concentrations of hydrocarbons during the test. These hydrocarbons were inadvertently evolved into the chamber on several occasions during the test due to failure of the automatic liquid nitrogen supply. The susceptibility of the Bayard-Alpert type of gauge to this hydrocarbon contamination is discussed in several references.[2,5] Careful outgassing of the gauge

[5] ASTM E296, "Ionization Gage Application to Space Simulators,"
     1968 Book of ASTM Standards, Part 30, General Testing Methods,
     Society for Testing and Materials. Philadelphia (1968).

following the test apparently restored the gauge to its normal operating characteristics. No instances of loss of liquid nitrogen were encountered in any test except exposure No. 2.

A summary of the test conditions and results is as follows:

Test Specimens - Cb-1Zr sheet, 26 inches (66.0 cm) long x 1.0 inch (2.54 cm) wide x 0.0316 inch (0.0802 cm) thick. Longitudinal and transverse sections. Specimens annealed but exposed to air for 3 months before test exposure.
Surface: Specimen A - cleaned and pickled
Specimen B - grit-blasted (60-grit alumina).

Exposure Time - 501.5 hours.

Specimen Temperature - 1700°F (927°C).

Vacuum System Pumping Speed - 793 1/sec.

Average Total Pressure - Not determined; ion gauge malfunction.

Average Partial Pressure - Not determined; ion gauge malfunction.

Specimen Analyses:

Specimen A - cleaned and pickled	(ppm) Oxygen	(ppm) Nitrogen	(ppm) Carbon
Posttest	8460	38	-
Pretest	44	22	342
Change	8420	16	-

Specimen B - grit-blasted	(ppm) Oxygen	(ppm) Nitrogen	(ppm) Carbon
Posttest	9670	39	730
Pretest	360	22	350
Change	9310	17	380

Average Oxygen Reaction Rate:

Specimen A - cleaned and pickled: m_r = 1.60 x 10^{-9} gm/cm^2sec.

Specimen B - grit-blasted: m_r = 1.77 x 10^{-9} gm/cm^2sec.

Sticking Probability: α = 0.274 ± 0.085 (Average value calculated from Ar/O_2 ratio, Equation 19).

The sticking probability, calculated for each gas analysis from the argon-to-oxygen ratio (Equation 19), is shown in Figure 11. It should be noted that, even though the absolute partial pressures were not obtained due to the ionization gauge malfunction, the relative partial pressures are still valid since the relative values are obtained solely from the mass spectrum. The line shown in the figure is calculated from a linear

36

Figure 11. Sticking Probability Calculated from Argon-to-Oxygen Ratio for Test No. 2.
Two Strip Specimens (One With Grit-Blasted Surface) Were Exposed for 501 Hours.

fit of the data by the method of least squares. This line shows a slight tendency toward decreasing sticking probability with increasing exposure time, as was observed in the first test. The standard deviation from the line is ± 0.035 (or ± 31 percent) indicating relatively poor precision in these measurements. The scatter in the data is due mainly to instabilities in the scanning circuit of the mass spectrometer during this particular test. This problem was corrected following this test.

The average of all sticking probabilities calculated from the argon-to-oxygen ratio (Figure 11) is 0.274 ± 0.035. This is higher than the average value of 0.183 ± 0.039 calculated for test exposre No. 1 but is still within the combined standard deviations of the measurements. Another factor to be considered is that the sticking probability, as indicated from the total oxygen increase, is about 10 percent higher for the grit-blasted strip than for the strip with bare surface. This indicates that the average sticking factor for the grit-blasted strip would be 0.287, and for the bare strip, 0.260 as calculated from the argon-to-oxygen pressure ratio and the relative oxygen increase.

The increase in carbon content of specimen B (grit-blasted) in this test was considerably larger (380 ppm) than for the other tests. This higher carbon pickup is apparently due to the malfunctions in the liquid nitrogen control during the test, and subsequent evolution of relatively large quantities of hydrocarbon vapor into the vacuum chamber.

C. Test Exposure No. 3

Simultaneous exposure of two strip specimens was performed for the third test. One strip contained a full-length GTA weld down its length at the mid-point of its width. The width of the fusion zone was about 0.25 inch (0.64 cm). The other strip contained transverse and longitudinal sections as described in the previous test. Both strips were annealed in the vacuum chamber immediately before the test exposure. The test setup was identical to that shown in Figure 4 for test No. 4.

A summary of the test conditions and results is as follows:

Test Specimens — Cb-1Zr sheet, 26 inches (66.0 cm) long x 1.0 inch (2.54 cm) wide x 0.0316 inch (0.0802 cm) thick. Annealed immediately before test exposure. Specimen A: Longitudinal and transverse sections. Specimen B: Full-length GTA fusion weld.

38

Exposure time -- 438.3 hours.

Specimen Temperature -- 1700°F (927°C).

Vacuum System Pumping Speed -- 896 liters per second.

Average Total Pressure: 2.95×10^{-6} torr.

Average Partial Pressures:

Nitrogen	2.76×10^{-6} torr,	93.5%
Oxygen	1.33×10^{-7} torr,	4.52%
Argon	4.22×10^{-8} torr,	1.43%
Hydrogen	1.14×10^{-8} torr,	0.39%
Water Vapor	3.7×10^{-9} torr,	0.13%
Carbon Dioxide	1.2×10^{-9} torr,	0.04%

Specimen Analyses:

Specimen A

	(ppm) Oxygen	(ppm) Nitrogen	(ppm) Carbon
Posttest	8130	30	538
Pretest	144	22	342
Change	8090	8	196

Specimen B - Welded Strip
(Fusion zone analyses)

	(ppm) Oxygen	(ppm) Nitrogen	(ppm) Carbon
Posttest	7080	47	435
Pretest	21	26	285
Change	7060	21	150

Average Oxygen Reaction Rate (from oxygen increase):

Specimen A: $m_r = 1.75 \times 10^{-9}$ gm/cm^{2}sec.

Specimen B(welded): $m_r = 1.53 \times 10^{-9}$ gm/cm^{2}sec.

Sticking Probability: Specimen A: $\alpha = 0.679$ (calculated from m_r).

Specimen B: $\alpha = 0.594$ (calculated from m_r).

$\alpha = 0.623 \pm 0.038$ (calculated from Ar/O$_2$ ratio).

The sticking probability, calculated for each gas analysis from the argon-to-oxygen ratio (Equation 19) is shown in Figure 12. The least square linear fit of the data shows good precision ($\pm$ 0.038 or $\pm$ 6.1 percent) compared with previous measurements. The sticking factor calculated from the gas analyses is in excellent agreement with the average of values calculated from the oxygen increase of each specimen. The very surprising result is that calculated sticking factors are about three times greater than values obtained on the first two test exposures. This effect is
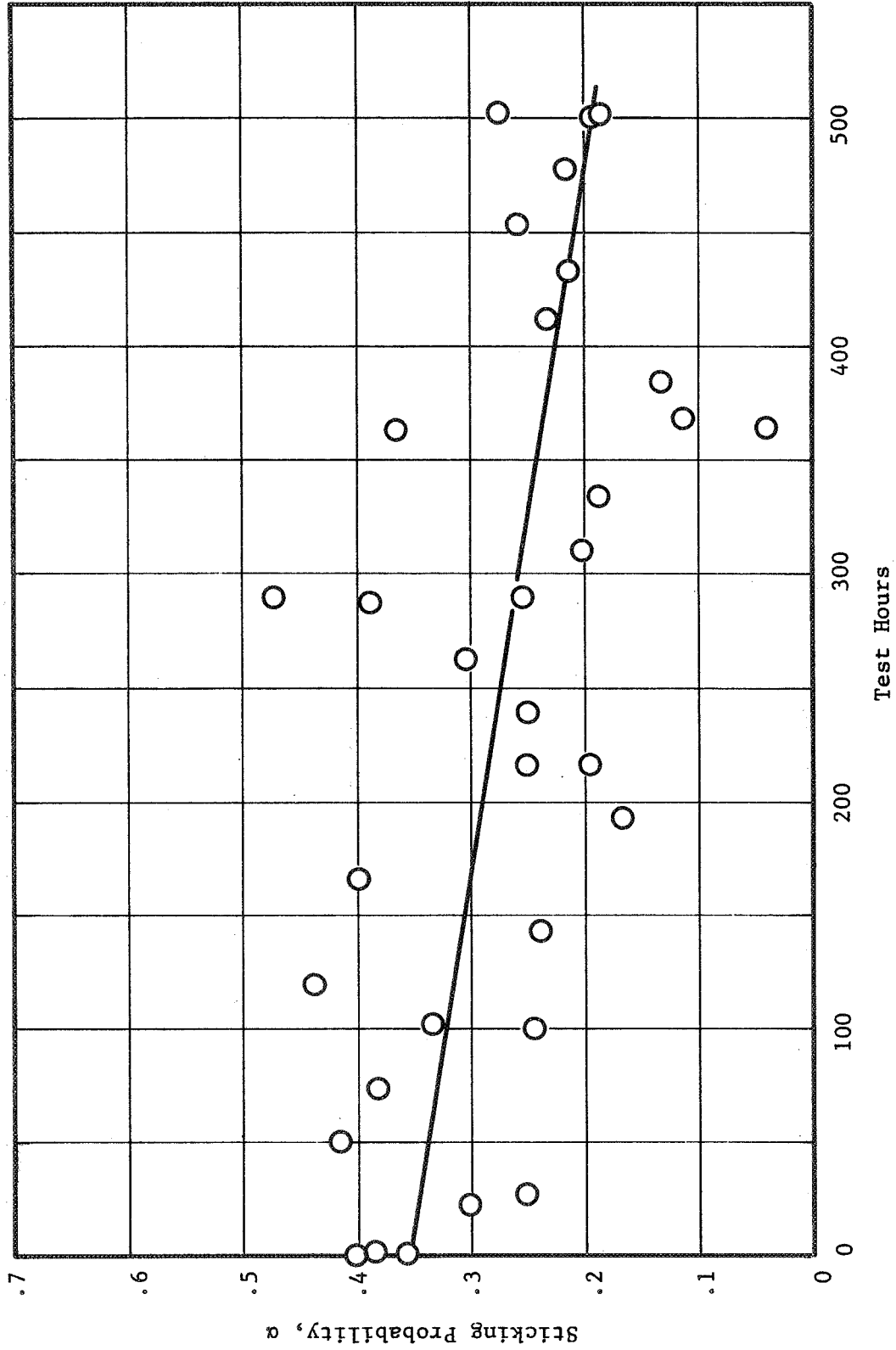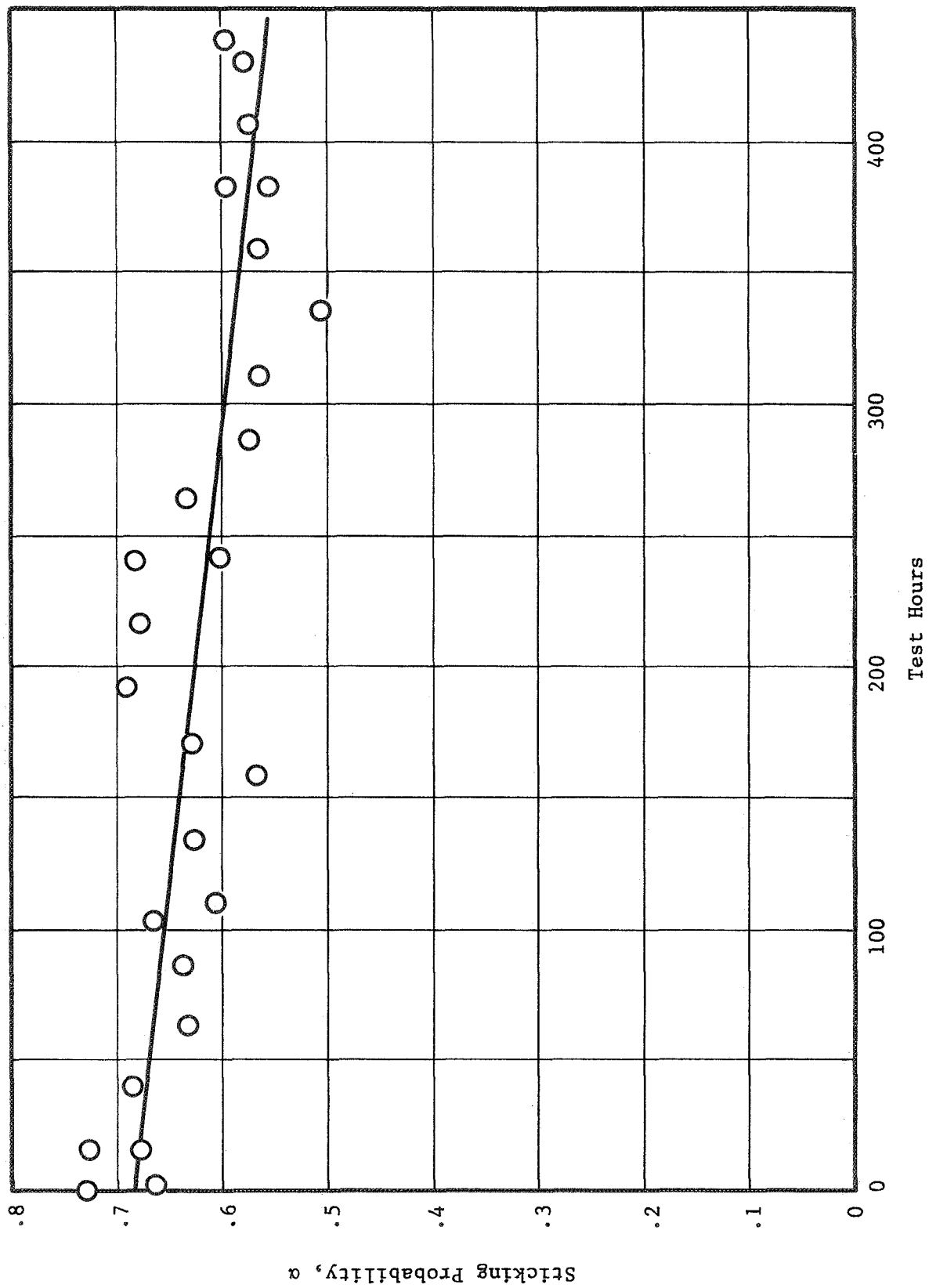
Figure 12. Sticking Probability Calculated from Argon-to-Oxygen Ratio for Test No. 3. Two Strip Specimens (One With Full-Length GTA Weld) Were Annealed Immediately Before the Test.

believed to be a result of annealing the specimens immediately before the test, as will be explained in a later section of this report. A significant difference exists between the oxygen increase of the non-welded material and that of the weld metal. This difference indicates that the sticking probability on the unwelded material is greater than on the weld metal by about 14 percent.

An increase in carbon content of both specimens was noted during the test, even though the liquid nitrogen trap was kept cold throughout the test and the mass spectrometer indicated low hydrocarbon content of the gas phase. The increase was, however, only about half the value obtained in test No. 2, when malfunctions in the liquid nitrogen supply were encountered. This observation indicates that the liquid nitrogen trap is only partially effective in preventing backstreaming of oil vapor from the diffusion pump and subsequent carbon contamination of the specimens.

D.   Test Exposure No. 4

Considerable difficulty had been encountered in the previous three tests in predicting the oxygen increase of the test specimen. There was, at this point, some doubt as to the stability of the system pumping speed and the accuracy of the measured values due to the unexplained differences in pumping speed between the first two tests. In addition, large and unexpected differences in sticking probability were encountered. Finally, the problems with the ionization gauge which occurred during the second test raised some doubt as to the accuracy of the pressure measurements until the final ionization gauge calibration was performed. In view of these uncertainties, a method was used for the final test which gave the desired increase in oxygen content even with large uncertainties in pumping speed, sticking factor, and pressure measurement.

This method is based on the measurement of total air flow into the chamber and on the fact that, with two strip specimens in the chamber, the majority of the air that enters the chamber reacts with the specimens. This can readily be seen by combining equations (15) and (16) to obtain

$$\frac{\text{Oxygen reacted}}{\text{Total oxygen}} = \frac{11.75 \frac{\alpha A}{S}}{11.75 \frac{\alpha A}{S} + 1} \tag{20}$$

It should be noted that the fraction of the total oxygen that reacts with the specimens is independent of the oxygen partial pressure. Inserting the measured values for α, A, and S from test No. 3 into equation (20), one finds that, for that test, 85 percent of the oxygen entering the chamber reacted with the specimens.

Equation (20) can be used to relate the total air flow (in torr-liters) to the oxygen increase of the specimens (ppm) using appropriate specimen geometrical factors and the standard air composition. Thus, it can be shown that

$$\text{Oxygen increase (ppm)} = \frac{1.25 \times 10^4 \frac{\alpha}{S}}{7.88 \times 10^3 \frac{\alpha}{S} + 1} \times \text{total air flow (torr-1).} \quad (21)$$

From equation (21) it can be seen that, for high values of $\frac{\alpha}{S}$, the oxygen increase is independent of $\frac{\alpha}{S}$ and is proportional to the total air flow. For very low values of $\frac{\alpha}{S}$, the oxygen increase is proportional to $\frac{\alpha}{S}$ and the total air flow, and only a small fraction of the inlet air reacts with the specimen.

The total air flow required for several values of oxygen increase is plotted against $\frac{\alpha}{S}$ in Figure 13. It is apparent from these curves that the oxygen increase is insensitive to $\frac{\alpha}{S}$ for $\frac{\alpha}{S}$ values greater than 1×10^{-3} sec per liter. Since the desired oxygen increase for this test was 4000 ppm, then with 3000 torr-1 total air flow, this target value ($\pm$ 500 ppm) would be obtained for any $\frac{\alpha}{S}$ between 0.35×10^{-3} and 2.3×10^{-3}. For test exposure No. 4, the primary controlling test parameter was thus the total air flow rather than oxygen partial pressure and time as in the previous tests.

In order to measure total air flow to the chamber, a stainless steel container of accurately measured volume (3.70 liters) was fabricated and connected to the inlet of the variable leak valve. The pressure in the container was measured throughout the test so that, with appropriate temperature corrections, the total air flow to the chamber could be determined.

The test specimens for test exposure No. 4 were identical to those of test No. 3. One strip contained a full-length GTA weld, and the other strip contained transverse and longitudinal sections. Both strips were

42
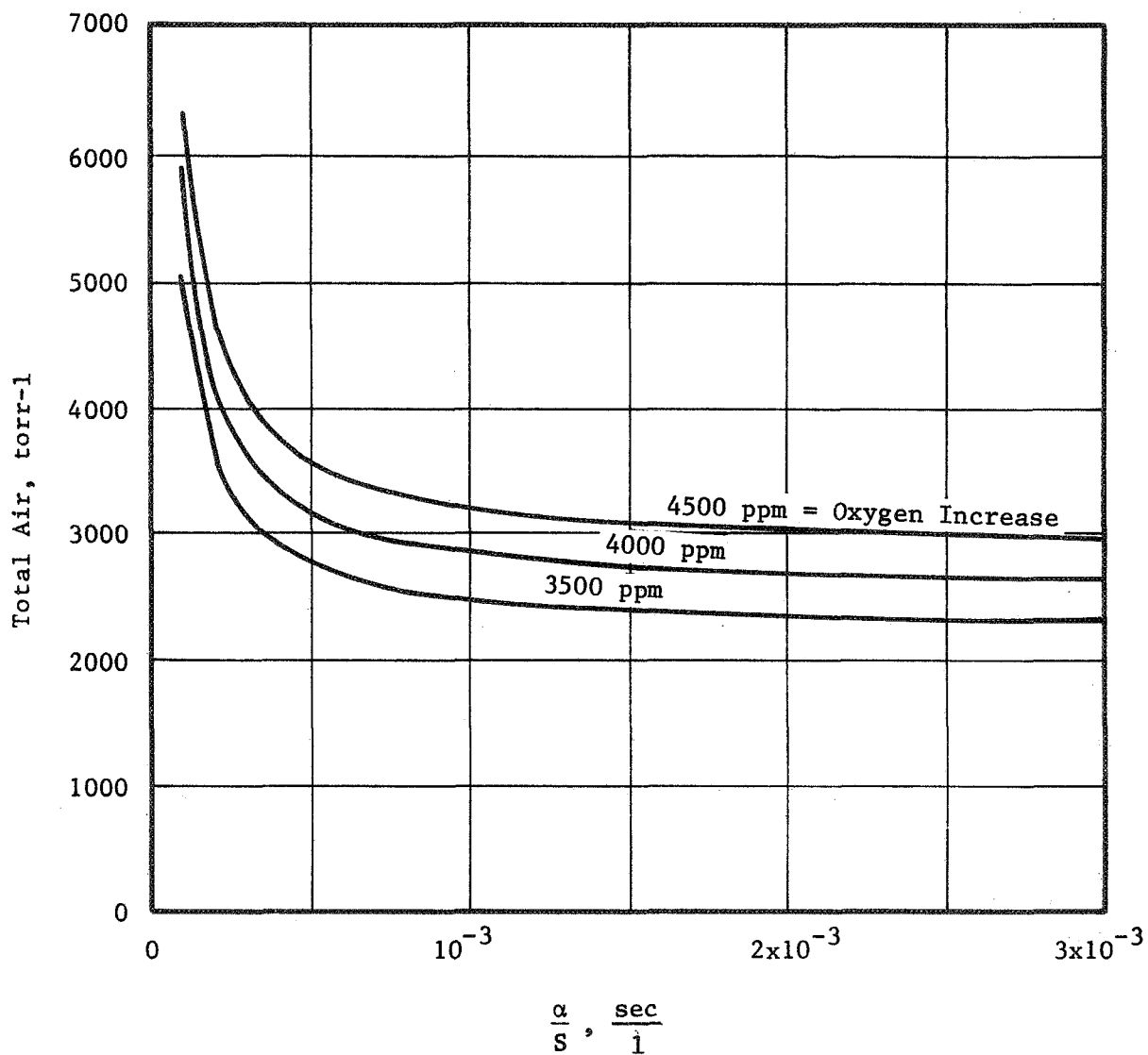
Figure 13. Calculated Total Air Required for Several Values
of Oxygen Increase Plotted Against $\frac{\alpha}{S}$.

annealed in vacuum for one hour at 2200°F immediately before the test exposure. The strip specimens mounted in the vacuum chamber are shown in Figure 4.

A summary of the test conditions and results for test No. 4 is as follows:

Test Specimens — Cb-1Zr sheet, 26 inches (66.0 cm) long x 1.0 inch (2.54 cm) wide x 0.0316 inch (0.0802 cm) thick. Annealed immediately before test.
Specimen A: Longitudinal and transverse sections.
Specimen B: Full-length GTA fusion weld.

Exposure Time — 274 hours.

Specimen Temperature — 1700°F (927°C).

Vacuum System Pumping Speed — 846 1/sec.

Total Air Flow to Chamber: 2948 torr-liters (20°C).

Average Total Pressure: 2.97×10^{-6} torr.

Average Partial Pressures:

Nitrogen	2.79×10^{-6} torr,	93.9%
Oxygen	1.27×10^{-7} torr,	4.28%
Argon	4.00×10^{-8} torr,	1.35%
Hydrogen	9.3×10^{-9} torr,	0.06%
Water Vapor	1.8×10^{-9} torr,	0.04%
Carbon Dioxide	1.1×10^{-9} torr,	0.04%

Specimen Analyses:

Specimen A

	(ppm) Oxygen	(ppm) Nitrogen	(ppm) Carbon
Posttest	4430	48	542
Pretest	44	22	342
Change	4390	26	200

Specimen B (welded strip)
Fusion Zone Analyses

	(ppm) Oxygen	(ppm) Nitrogen	(ppm) Carbon
Posttest	4210	50	483
Pretest	136	22	318
Change	4080	28	165

Average Oxygen Reaction Rate (from oxygen increase):

Specimen A: $m_r = 1.53 \times 10^{-9}$ gm/cm^2 sec.

Specimen B (welded): $m_r = 1.42 \times 10^{-9}$ gm/cm^2 sec.

Sticking Probability: $\alpha = 0.581 \pm 0.071$ (calculated from Ar/O$_2$ ratio).

Specimen A: $\alpha = 0.623$ (calculated from m_r).

Specimen B (welded): $\alpha = 0.578$ (calculated from m_r).

The sticking probability, calculated for each gas analysis from the argon-to-oxygen ratio (equation 19) is shown in Figure 14. The least square linear fit of the data shows a standard deviation of ± 0.071 (± 12 percent). As in all of the tests reported here, there is a slight tendency toward lower sticking factors with increasing test exposure time. The sticking probability calculated from the gas analyses is in good agreement with the average of the values calculated from the oxygen increase of the specimens.

As in the previous test, the sticking factors are much higher than obtained in the first two tests, where the strip specimens were not annealed immediately before the exposure.

E.   Strip Specimen Thermal Behavior

As shown in the preceding section of this report, large differences in oxygen sticking probability on Cb-1Zr were noted depending on whether or not the strip specimens were annealed immediately before the test exposure. The most logical explanation for this effect seemed to be that some change in the specimen surface occurred as a result of the annealing. If such surface change occurred, it might also cause a change in other surface properties, for example, the total hemispherical emittance. Although not specifically required by the contract, an investigation of the strip specimen thermal behavior was thus performed.

Thermocouples were attached to the strip specimens at six locations along the length of each strip. Temperatures were measured periodically throughout each test along with the current to each specimen. During the initial portion of each test, some variations were noted in both temperature profile along the strip and current required to maintain 1700°F. Figure 15 shows the temperature profile along the strip at various test times for a typical test exposure. This particular strip was specimen A of test No. 4 with surface pickled and annealed immediately before the test. These data show some variation in temperature along the strip during the initial 30 hours of the test after which time the temperature is quite uniform.

The current required to maintain the strips at 1700°F increased considerably during the initial portion of each test. This effect is apparently the result of an increase in total hemispherical emittance
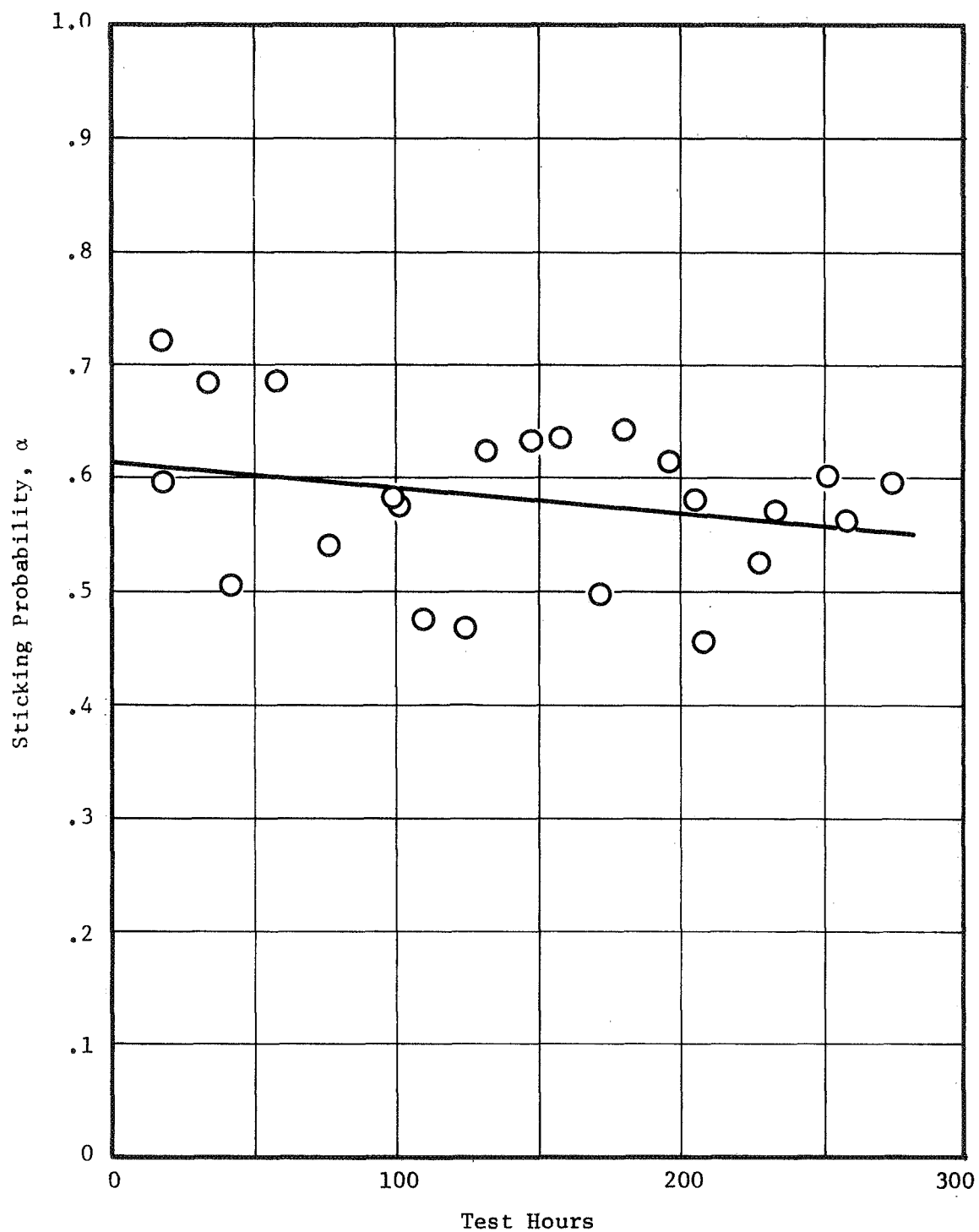
Figure 14. Sticking Probability Calculated From Argon-to-Oxygen Ratio for Test Exposure No. 4. Two Strip Specimens (One With Full-Length GTA Weld) Were Annealed Immediately Before Test.
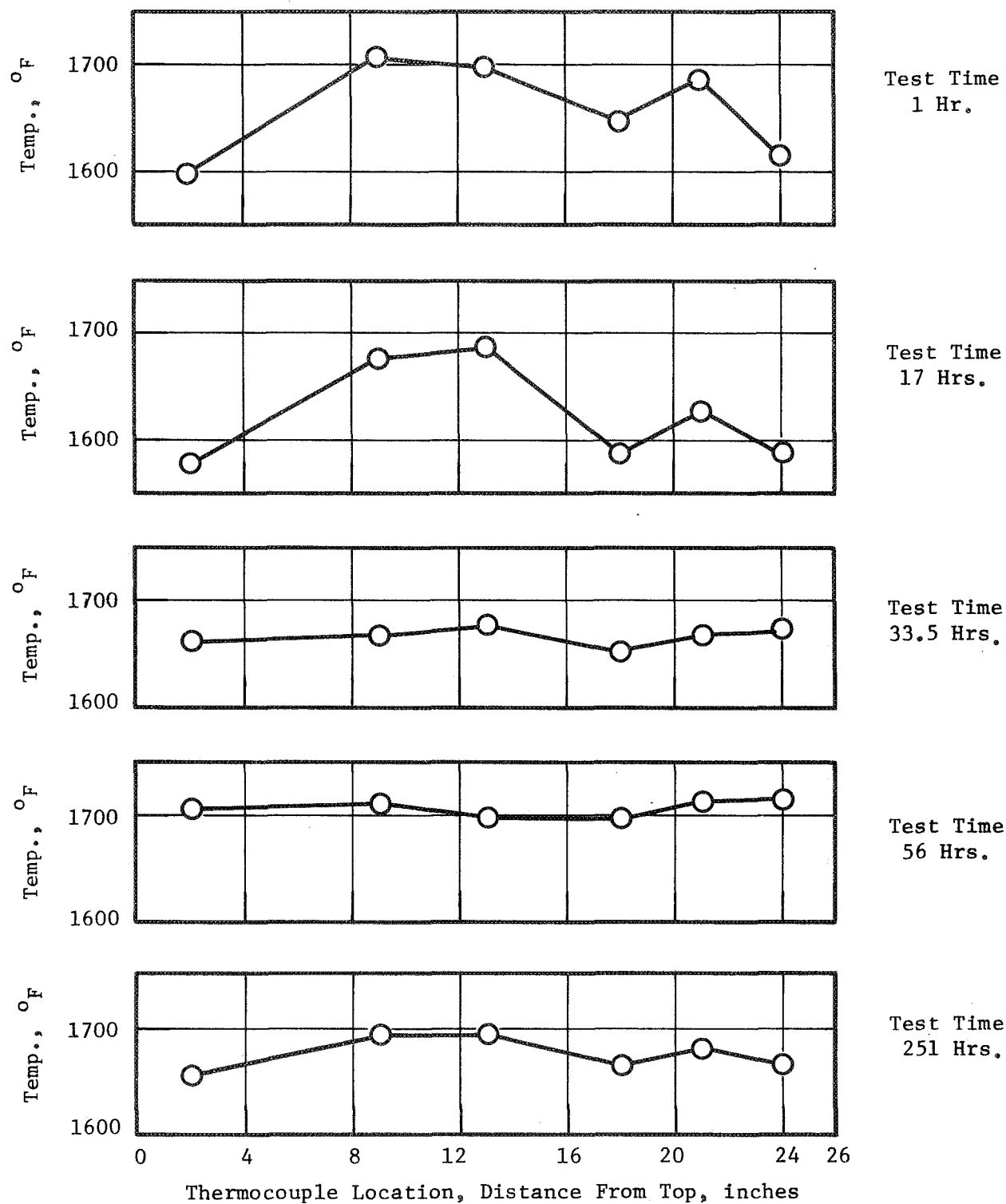
Figure 15. Temperature Profiles at Various Test Times For
Test Exposure No. 4, Specimen A.

of the specimen surface. In order to calculate the approximate emittance of the surface, it is assumed that the resistivity of the material is constant throughout the test. With this assumption, the electrical power dissipated is equated to the radiated power:

$$\text{Power radiated} = I^2 R = \epsilon \sigma T^4 \qquad (22)$$

where I is the current, R the resistance, ϵ the total hemispherical emittance, σ the Stefan-Boltzmann constant, and T is the absolute temperature. For a number of reasons, the voltage drop across the strip was not measured with sufficient accuracy to permit calculation of the emittance from the measurement.

In Figure 16, the specimen current, temperature, and calculated emittance are plotted against test time for specimen A of test No. 4. The specimen surface was pickled only and annealed immediately before the test. The total hemispherical emittance was obtained from equation 22 assuming a constant resistivity of 50×10^{-6} ohm-cm. This value has been reported[6] for Cb-1Zr containing about 500 ppm oxygen. The calculated emittance increased from 0.15 to 0.23 during the first 100 hours of the test and remained constant (0.23 to 0.24) until the test was concluded. The overall increase in oxygen content of this specimen was 4390 ppm. It should be noted that if the resistivity of the strip actually increased during the test, then (from equation 22) the change in emittance would have been even greater than shown in Figure 16.

It is of interest to compare the calculated emittance values for the four specimens with similar surface (that is, pickled only), one exposed in each of the four tests. These values are plotted in Figure 17. The initial emittance of all four specimens is about the same (0.15 to 0.17). An increase in emittance of all four specimens may be noted during the first 100 hours of exposure. However, the specimens that were not annealed immediately before the test exposure have a significantly higher maximum emittance (0.32 to 0.34) compared to the maximum of 0.23 to 0.24 for the specimens that were annealed immediately before the test. At

---

[6] Rigney, D. V., et al., "The Electrical Resistivity of Lithium and Columbium - 1 Zirconium Alloy to 1430°C," Pratt and Whitney Aircraft - CANEL, Report TIM-854 (August 1965).
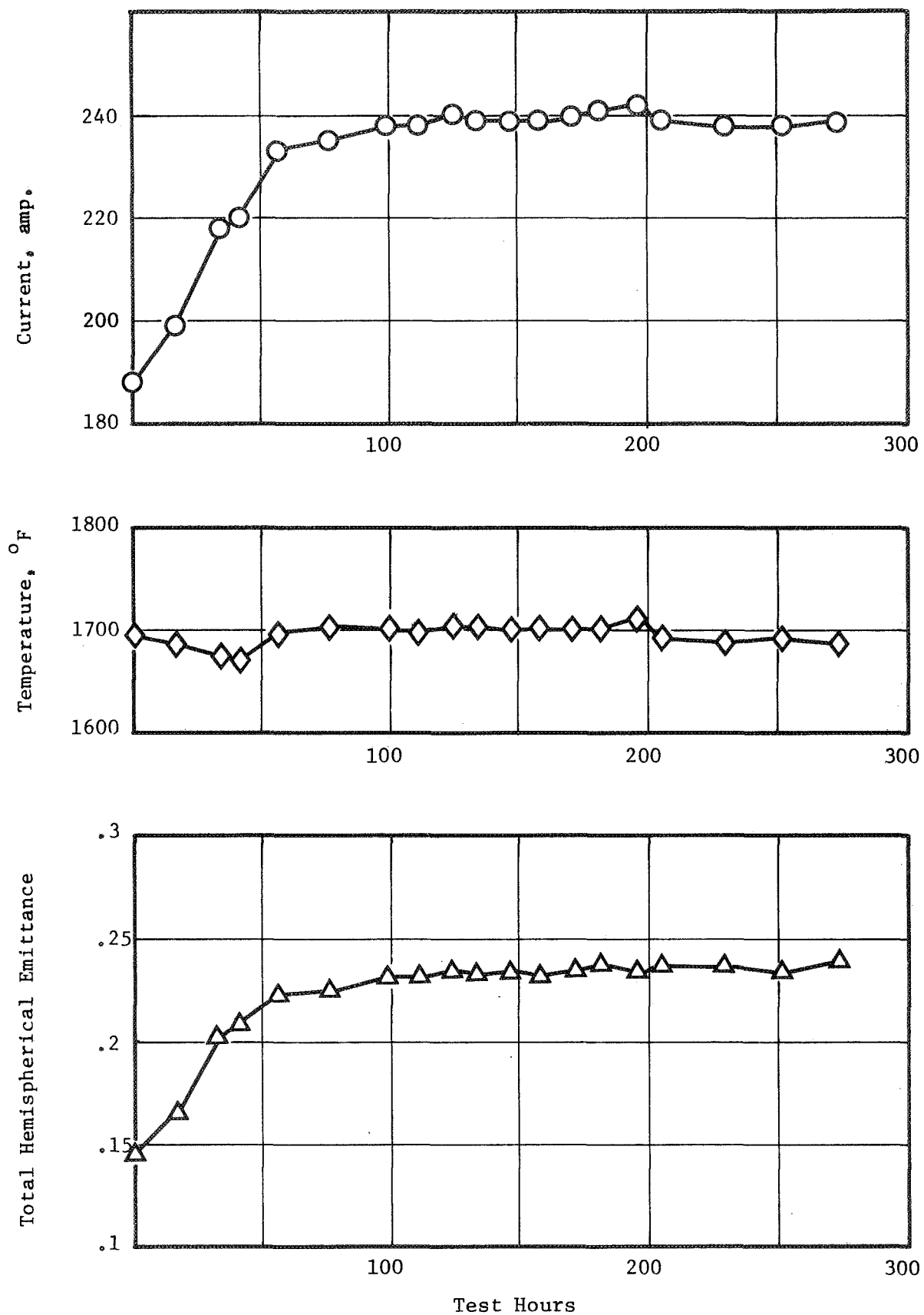
Figure 16. Specimen Current, Temperature, and Emittance Versus Test Time for Test Exposure No. 4, Specimen A. Emittance Calculated Assuming Constant Resistivity of 50 x 10^{-6} ohm-cm. Temperature at Midpoint of the Specimen.
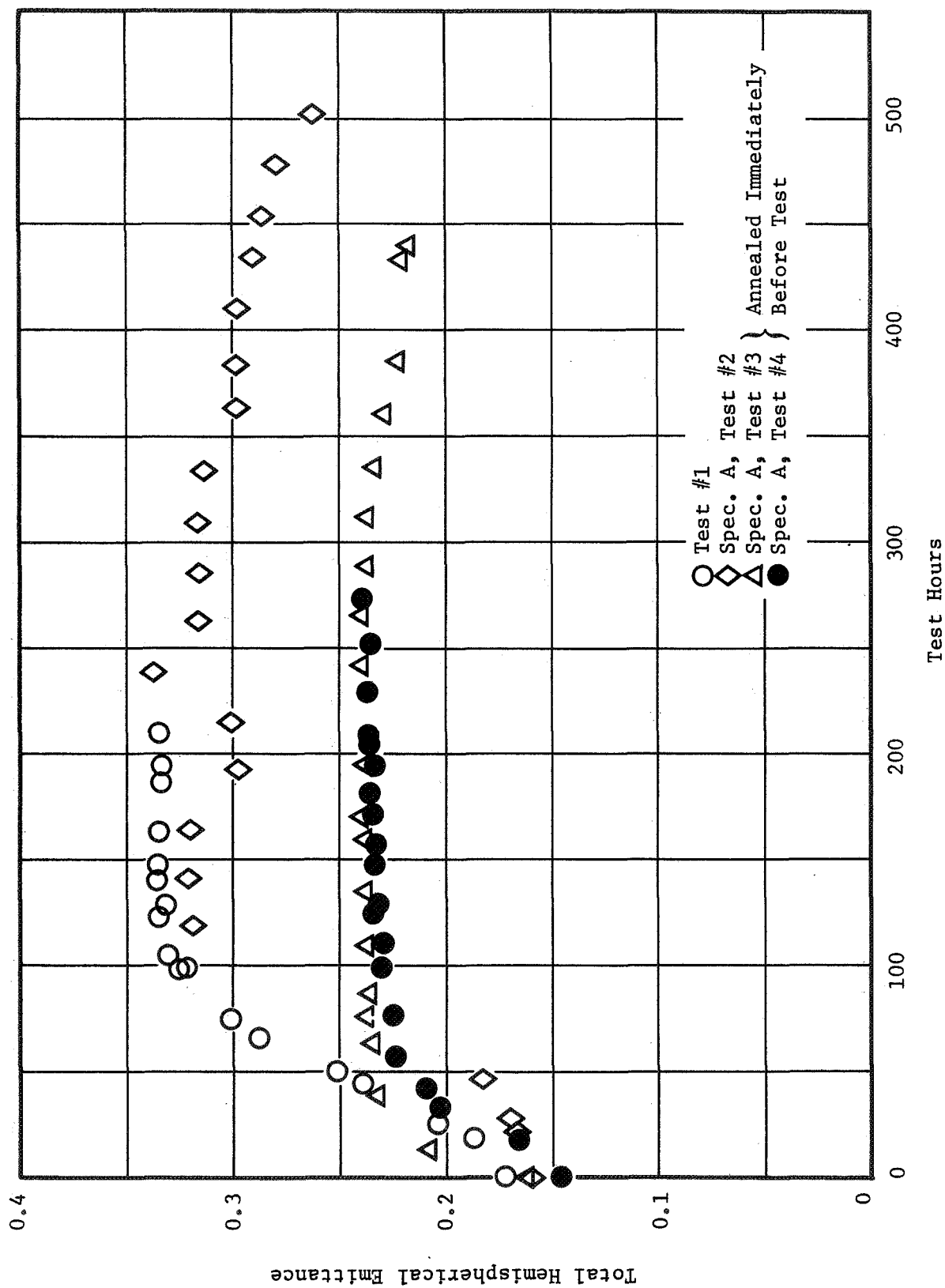
Figure 17. Comparison of Calculated Total Hemispherical Emittance for Specimens with Bare Surface. Specimens for Test No. 3 and Test No. 4 Were Annealed (1 Hour – 2200°F) Immediately Before the Exposure.

50

very high oxygen levels there is some tendency toward lower emittance, as indicated by the final emittance values on specimen A of test No. 2 (8460 ppm) and specimen A of test No. 3 (8090 ppm).

Since no attempt had been made to instrument the strip specimens for precise emittance measurements, there is considerable uncertainty (estimated ± 15 percent) in the calculated values. However, the relative values of calculated emittance should be much more reliable. There is thus a definite difference in the maximum stable emittance depending on whether or not the specimen is annealed immediately before the test exposure.

The calculated emittance of the grit-blasted strip (test No 2, specimen B) is considerably higher than strips with unprepared surface but showed the same general increase in emittance. The calculated total hemispherical emittance was 0.28 at the beginning of the test and increased to 0.48 after 100 hours. Thereafter the emittance decreased slowly and was 0.42 at the conclusion of the test (501 hours).

F.   Discussion of Oxidation Rate Measurements

Results of the oxidation rate measurements of oxygen with Cb-1Zr at 1700°F and oxygen partial pressures in the 10^{-7} torr range show a definite effect of pretest annealing. Specimens oxidized immediately following vacuum annealing for 1 hour at 2200°F had oxygen reaction rates corresponding to an average sticking probability of about 0.65. For the unannealed specimen, or for specimens annealed and subsequently exposed to ambient air, the rates were considerably lower, corresponding to a sticking factor of about 0.16.

A summary of the reaction rate measurements of oxygen with Cb-1Zr at 1700°F is given in Table V. Specimens for test No. 2 were annealed but were subsequently exposed to ambient air before the test exposure. The oxygen pressure for this test was not determined due to malfunction of the ionization gauge. The sticking probability for this test, as calculated from the gas analyses was slightly higher than that obtained in the first test in which the specimen was not annealed.

51

TABLE V

SUMMARY OF REACTION RATES OF OXYGEN WITH Cb-1Zr AT 1700°F

Test Exposure	Specimen	Test Time (Hours)	Oxygen Increase (ppm)	Avg. O_2 Pressure (torr)	Reaction Rate, m_r (gm/cm²sec)	α, Calc. from m_r	α, Calc. from Gas Analysis
No. 1	Pickled	210	5950	8.76×10^{-7}	2.71×10^{-9}	0.160	$0.183 \pm .039$
No. 2	A. Pickled	501.5	8420	--	1.60×10^{-9}	--	$0.274 \pm .085$
No. 2	B. Pickled Grit-blasted	501.5	9310	--	1.77×10^{-9}		
No. 3	A. Pickled Annealed	438.3	8080	1.33×10^{-7}	1.75×10^{-9}	0.679	$0.623 \pm .038$
No. 3	B. Pickled Long. Weld Annealed	438.3	7060	1.33×10^{-7}	1.53×10^{-9}	0.594	
No. 4	A. Pickled Annealed	274	4390	1.27×10^{-7}	1.53×10^{-9}	0.623	$0.581 \pm .071$
No. 4	B. Pickled Long. Weld Annealed	274	4080	1.27×10^{-7}	1.42×10^{-9}	0.578	

NOTE: Specimens for test No. 2 were annealed but subsequently exposed to air before the contamination tests. Specimens for test No. 3 and test No. 4 were annealed within the vacuum chamber just prior to the contamination test. Oxygen pressure not determined for test No. 2 due to ionization gauge malfunction.

A number of other investigations have been made of the low pressure oxidation rate of columbium and columbium alloys. The two studies most pertinent to the present investigation are those of Hogan, Limoncelli, and Cleary[7] and the recently published data of Barrett.[8] Other data will not be considered here since they were obtained either on pure columbium, in a furnace (hot wall) system, or at oxygen pressures so high (greater than 10^{-5} torr) that gross surface oxides could have formed. Measurements of Hogan, et al., were made in an induction heated system (cold wall), on 0.030-inch- (0.076-cm) thick material, and the material was cleaned and pickled before the test exposure. The data of Barrett include a number of variables; pressure, temperature, hot and cold wall tests, and zirconium content. Significance of these variables was determined by multiple linear regression analysis. One set of data, however, was obtained under conditions similar to those reported here; that is, an induction-heated (cold wall) test with Cb-.75Zr. The specimen (No. 88) was 0.050 inch (0.127 cm) thick and was cleaned and pickled before the test exposure. Test conditions and specimen preparation for these cited tests were thus very similar to those of the present tests.

Comparison of reaction rates, from the two studies cited above, with data from the present investigation is shown in Figure 18. The data at higher pressures (above 1 x 10^{-5} torr) from Reference 7 are not shown. The three data points from the present study are for test No. 1 (not annealed), test No. 3 specimen A, and test No. 4 specimen A (both annealed immediately before the test exposure). The striking feature of this comparison is that the sticking probability on the annealed specimens agrees well with the data of Reference 7 (2000°F) while the sticking probability on the unannealed specimen is in agreement with the data of Reference 8 (1796°F).

[7] Hogan, J. F., Limoncelli, E. A., and Cleary, R. E., "Reaction Rate of Columbium - 1 Zirconium Alloy with Oxygen at Low Pressures," Report TIM-901, Pratt and Whitney Aircraft (August 24, 1965).

[8] Barrett, C. A., "Absorption Rate Sticking Probabilities for Oxygen on Columbium and Dilute Columbium - Zirconium Alloys," NASA TN D-4885 (November 1968).
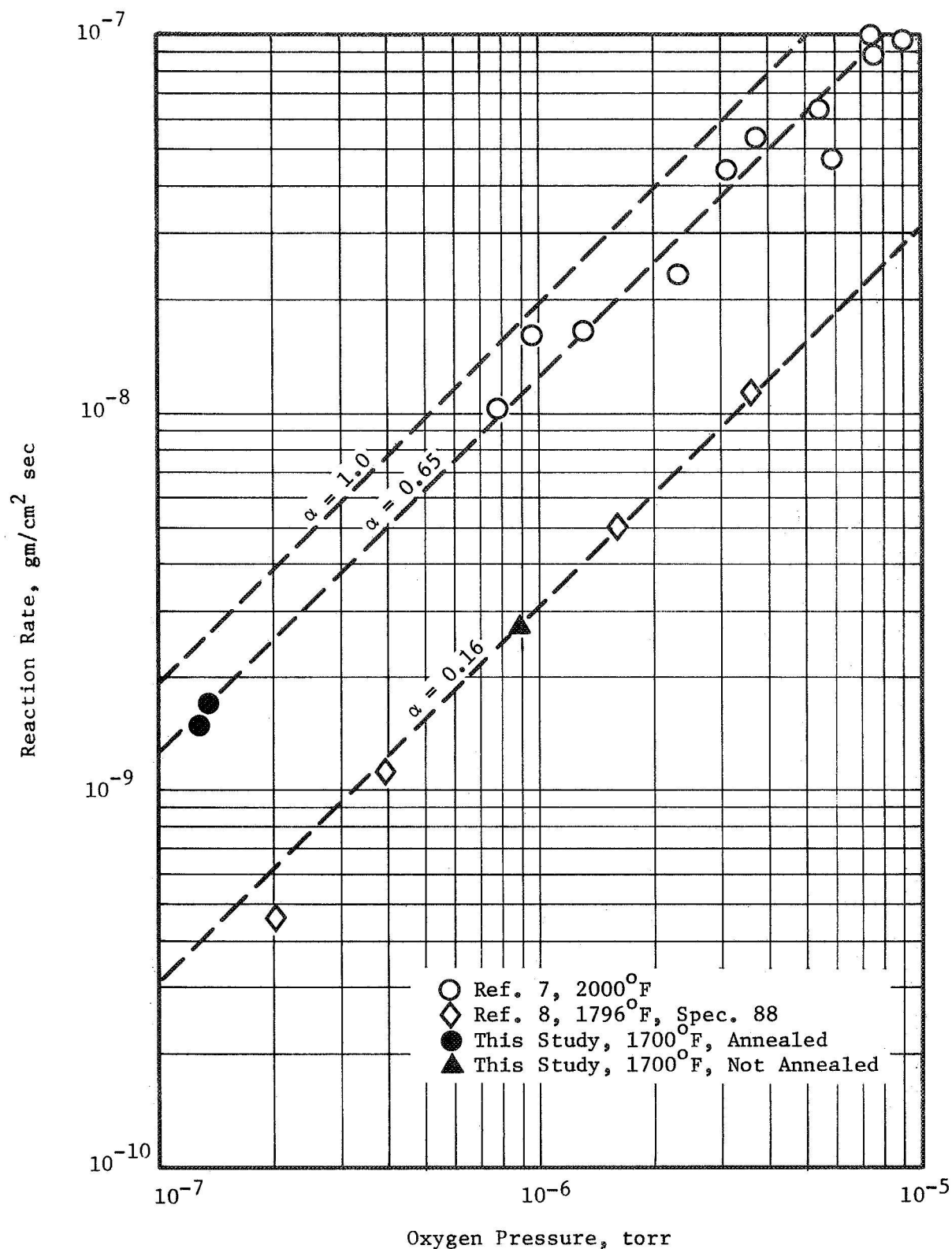
Figure 18. Comparison of Oxygen Reaction Rates From Several Studies. Rates for Annealed Specimens From This Study and the 2000°F Measurements of Reference 7 Correspond to Sticking Probability of 0.65. Rate for the Unannealed Specimen From This Study and 1796°F Measurements of Reference 8 Correspond to Sticking Probability of 0.16. All Measurements in "Cold Wall" System on Nominal Cb-1Zr.

The most reasonable explanation for this behavior is that a partially protective film exists on Cb-1Zr as a result of oxidation with ambient air, and this film persists at temperatures to at least 1800°F (982°C). The result is a relatively low reaction rate corresponding to a sticking probability of about 0.16. If oxidation rate measurements are made at 2000°F (1093°C) or higher, this surface film is removed by dissolution of oxygen in the base metal. Relatively rapid reaction of oxygen occurs on the bare metal surface with a sticking probability of about 0.65. The same higher reaction rate is obtained at lower temperatures (1700°F) if the protective film is initially removed, as for example, by annealing at 2200°F (1204°C). The postulation of such a mechanism thus gives a possible explanation for differences observed here between annealed and unannealed surfaces, and also for the apparent discrepancy between data of Hogan, et al.[7] and Barrett.[8] It should be noted that Barrett (his Table IV) lists the sticking probability on Cb-1Zr for the cold wall case at 2012°F (1100°C) as 0.161. However, this conclusion must have been drawn from his regression analyses, since no reaction rate data are listed for those conditions.

If the existence of a partially protective film is in fact the cause of the relatively low sticking probability observed on the unannealed specimens, then, during the course of the oxidation exposure, this film will probably increase in thickness. If it decreased in thickness, it would very likely disappear entirely since it is so thin (a few atomic layers in thickness) at the beginning of the exposure. The result would be an eventual increase in sticking probability. Since such an increase in sticking probability did not occur in these tests, it may be concluded that the film thickness increases at the oxidation rates employed here, and may be microscopically visible at high enough oxygen contents. Such surface film has, in fact, been observed as shown in Figure 19. Figure 19A shows the surface of specimen A of test No. 2 with 8460 ppm oxygen. This photograph clearly shows a surface layer of $Cb_2O_5 \cdot 6ZrO_2$ approximately 6×10^{-5} inches (1.4×10^{-4} cm) thick. This specimen was annealed but exposed to ambient air before the test exposure. As shown in Figure 19B, no such surface layer is visible on specimen A of test No. 3 which con-
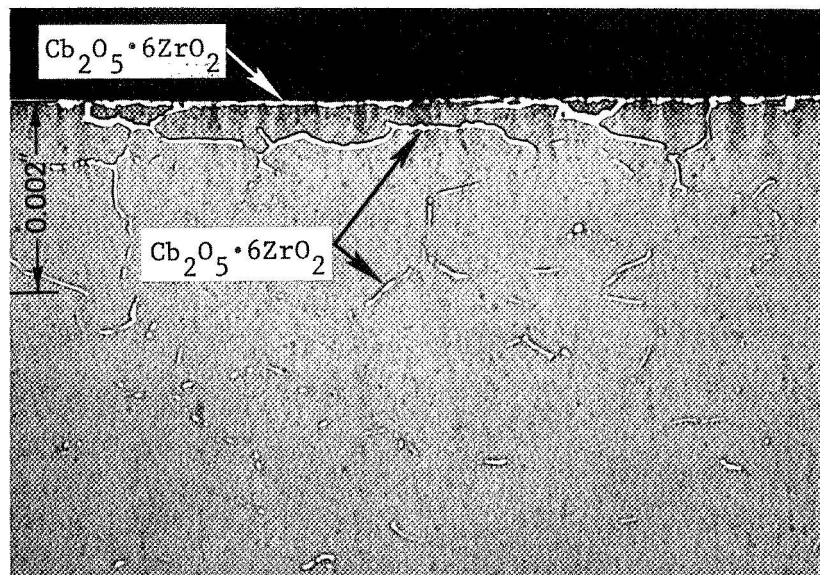
Electrolytic Stain Etch   H58011A

Figure 19A. Surface of Specimen A of Test No. 2 Showing Surface Layer of $Cb_2O_5 \cdot 6ZrO_2$ Approximately 6×10^{-5} in. $(1.4 \times 10^{-4}$ cm) Thick. Specimen Contains 8460 ppm Oxygen and was Annealed but Exposed to Ambient Air Before Test Exposure.
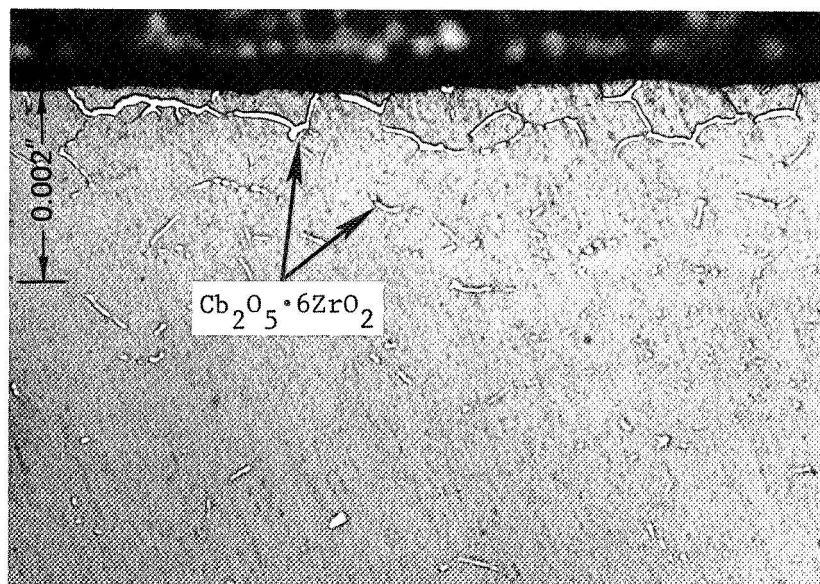
Electrolytic Stain Etch   H58021A

Figure 19B. Surface of Specimen A of Test No. 3 Shows no Surface Layer but Only Precipitated $Cb_2O_5 \cdot 6ZrO_2$. Specimen Contains 8130 ppm Oxygen and was Annealed Immediately Before the Test Exposure.

56

tains 8130 ppm oxygen and was annealed immediately before the test exposure. The oxide phase has been identified by X-ray diffraction techniques as explained in Section V of this report.

It is interesting to note that, in a study[9] of the welding of Cb-1Zr, it was reported that the microstructure of the weld metal, after annealing at 1700°F and 1800°F, showed little difference from that of the as-aged weld. However, upon annealing at 1900°F, a coherent network of intragranular precipitate just began to appear. This distribution of precipitate was quite different from that in the as-aged condition and ductile behavior resulted. This result demonstrates that, at temperatures of 1900°F (1073°C) and higher, the mobility of the constituents of the alloy is sufficiently high to enable this precipitation reaction to occur within a few hours. It is not unreasonable to expect that, at the same temperature, oxygen at the surface will diffuse into the bulk metal and precipitate as this intragranular phase. This is precisely what occurs according to the mechanism postulated to account for the observed differences in sticking probability.

In the measurements reported here, the increase of nitrogen was quite small for all specimens, being less than 50 ppm in each case. This observation indicates an extremely low average sticking factor for nitrogen under these conditions. This result is in general accord with the conclusion of Inouye[10] that, in the reaction of Cb-1Zr with nitrogen, the rate determining step for the reaction is the diffusion of nitrogen into the alloy after the initial reaction at the surface. This is in contrast to the oxygen reaction with Cb-1Zr where the rate controlling process is the impingement of oxygen molecules on the surface. The small increase in nitrogen content in these tests is thus explained by the extremely low diffusion coefficient which is calculated to be 3.5×10^{-13} cm^2 sec^{-1} at 1700°F (927°C) from the data of Reference 10.

[9] Franco-Ferreira, E. A. and Slaughter, G. M., Welding Research Supplement, pg. 18-S (January 1963).

[10] Inouye, H., "High-Temperature Sorption of Nitrogen by Nb-1%Zr in Ultrahigh Vacuum," ORNL-4403 (May 1969).

The increase in carbon content in these test exposures was surprisingly high. The increase in carbon for tests No. 3 and No. 4 was between 150 and 200 ppm for the exposures of 438 and 274 hours, respectively. These values correspond to a carbon reaction rate of about 5×10^{-11} gm per cm^2 per sec. The most obvious source of this carbon is backstreaming of diffusion pump oil, although the pumping system contained a liquid nitrogen-cooled baffle. It is estimated that hydrocarbon partial pressure is less than 10^{-9} torr. Accurate evaluation of the hydrocarbon partial pressures would require a knowledge of what species are present in the system and calibration of the mass spectrometer for these species.

The increase in nitrogen and carbon found in the present study is not inconsistent with data obtained at Oak Ridge National Laboratory.[11] In those tests, exposure of Cb-1Zr sheet specimens at 6.7×10^{-7} torr nitrogen partial pressure for 1000 hours caused a nitrogen increase of 55 ppm or less for temperatures between 618 and 1202°C. Exposure of 0.040-inch Cb-1Zr sheet at ORNL in a vacuum system (presumably oil diffusion pumped) with base pressure of 2.4×10^{-7} torr for 1000 hours caused carbon increase as high as 100 ppm.

It has been shown (see Figure 17) that definite differences in the maximum value of total hemispherical emittance were obtained depending on whether or not the specimens were annealed immediately before the test exposure. This observation can, at least qualitatively, be explained in terms of the postulated mechanism involving formation of a surface layer on oxidation of the specimens which were not annealed immediately before the test. For the unannealed specimens, or the specimens exposed to ambient air following annealing, (test No. 1 and test No. 2) the surface film is so thin that it is essentially transparent to the emitted radiation. This results in an initial emittance value which is the same as for the specimens without the surface film (test No. 3 and test No. 4). As the

[11] Thurber, W. C., et al., "Recent Studies on Columbium-1% Zirconium Alloy" in High-Temperature Refractory Metals (Metallurgical Society Conferences Vol. 34, Fountain, R. W., et al., Eds.) Gordon and Breach, New York (1966).

film thickness increases, the emittance correspondingly increases until, when the surface layer becomes opaque, a stable emittance value is reached which is characteristic of the oxide layer. For specimens of tests No. 3 and No. 4, in which no oxide layer is formed, the smaller increase in emittance must be due to some other change in the surface. This could be accounted for by an increase in surface nitrogen or carbon or perhaps by merely structural changes in the surface; that is, a purely thermal effect not related to the contamination.

Other studies[12] of the emittance of Cb-1Zr also showed changes in emittance which were not fully explained. The emittance was found to depend on the temperature to which the specimen was heated and was stable if that temperature was not exceeded on repeated heating. The measurements were made at pressure of 5×10^{-6} torr and, apparently, some surface reaction had occured since a thin white surface film was formed during the thermal treatment.

[12] McElroy, D. L., and Kollie, T. G., "Measurement of Thermal Radiation Properties of Solids, NASA SP-31 (Symposium at Dayton, Ohio, Sept. 5, 6, 7, 1962).

V. EVALUATION OF Cb-1Zr TEST SPECIMENS AFTER EXPOSURE

Evaluation of the Cb-1Zr test specimens included visual examination, chemical analyses, tensile tests, stress-rupture test, bend test, micro-hardness tests, X-ray diffraction, and metallographic examination. Of the seven test specimens exposed, mechanical tests were performed on five. The welded strip of test No. 3 was not completely evaluated since, with such high oxygen content (7080 ppm) it was expected to be extremely brittle, as judged from the results of mechanical tests of the welded specimen of test No. 4. Specimen A of test No. 3 (pickled and annealed) was not completely evaluated since it had essentially the same chemical composition as specimen A of test No. 2.

As has been discussed in previous sections, all specimens except specimen A of test No. 1 were annealed at 2200°F for 1 hour before the test exposure. The purpose of the annealing was to prevent embrittlement of welds by an aging reaction during the test exposure. It should be noted that some welding was performed on all specimens, although only two are denoted as "weld specimens." Other specimens contained a weld to join the longitudinal to the transverse sections.

Samples for evaluation were cut from each specimen only in the region in which uniform temperature was obtained during the exposure. No samples were taken within 2 inches of the end electrodes nor within one inch of the center weld, in the case of specimens with both longitudinal and trans-verse sections.

A. Visual Examination

Visual examination of each of the strips after the test exposure revealed nothing of an unusual nature. There were no surface discolora-tions, cracking, or apparent surface reactions resulting from exposures of the test strips at the various oxygen partial pressures.

B. Chemical Analyses

Posttest samples for chemical analyses were removed from each strip at various locations along the length. Samples were analyzed for oxygen, nitrogen, and hydrogen by the vacuum fusion method and for carbon by the combustion conductometric technique. The complete results of the chemical

analyses are presented in Table VI. These results indicate relatively uniform oxygen contamination throughout the base metal of the test specimens. The local oxygen concentration of the weld joining the longitudinal and transverse sections was found to be lower than the adjacent base metal. This is due to the increased thickness at the weld from addition of filler metal and subsequent dilution of contaminants during test exposure. The oxygen concentration of the weld metal of the specimen of test No. 1 was 3000 ppm compared to the base metal oxygen concentration of 5990 ppm. Analyses of weld metal of the grit-blasted strip of test No. 2 showed 6200 ppm oxygen as compared to the base metal oxygen concentration of 9670 ppm.

C. Tensile Tests

Room temperature tensile tests and tensile tests at $1700°F$ in vacuum were performed to determine the effects of oxygen contamination on the ultimate tensile strength, yield strength, and ductility of the metal. The results of the room temperature tensile tests are presented in Table VII. Generally, higher oxygen content causes an increase in strength and decrease in ductility. This is apparent in Figure 20 where ultimate tensile strength and elongation are plotted against oxygen content for the specimen with bare surface and orientation parallel to the rolling direction (longitudinal orientation). The ultimate tensile strength increases with oxygen concentration to about 6000 ppm where the strength is greater than the as-received value by nearly a factor of 3. The elongation decreases more gradually and, at 6000 ppm, is about half of the as-received value. At oxygen concentration greater than 6000 ppm, the ultimate tensile strength increases more gradually while the elongation falls rather rapidly until very little if any ductility remains above 8000 ppm.

The ultimate tensile strength of the grit-blasted strip with 9670 ppm oxygen is apparently less than that of the bare surface specimen containing 8460 ppm. However, the grit-blasted strip exhibited essentially zero elongation and the validity of tensile tests of such brittle material is questionable.

62

TABLE VI

CHEMICAL ANALYSES OF Cb-1Zr TEST SPECIMENS

Test No.	Test Specimen Pretreatment	Sample Location	Oxygen (ppm) Duplicates	Oxygen (ppm) Average	Nitrogen (ppm) Duplicates	Nitrogen (ppm) Average	Hydrogen (ppm) Duplicates	Hydrogen (ppm) Average	Carbon (ppm) Duplicates	Carbon (ppm) Average
	As-Received	-	50, 38	45	35, 6	22	2, 3	3	347, 338	342
1	A. Surface Pickled	Weld Metal	2900, 3100	3000	36, 52	44	3, 9	6	--	--
		1" Below Center Weld	6209, 6143	6176	77, 53	65	3, 3	3	--	--
		2" Below Top	6284, 6190	6237	81, 81	81	1, 2	2	--	--
		9" Below Top	5529, 5603	5566	67, 60	64	3, 1	2	--	--
		Posttest Contamination Average		5990 (Base metal only)		70		2		-
2	A. Pickled, Annealed	4.5" Below Top	8582, 8336	8460	36, 39	38	17, 2	10	--	--
2	B. Pickled, Grit-Blasted, Annealed	As Grit-Blasted	366, 360	363	23, 21	22	1, 2	2	322, 370	346
		Weld Metal	6250, 6150	6200	37, 39	38	11, 1	6	436	436
		4.5" Below Top	9692, 9669	9681	34, 37	36	1, 17	9	700, 739	720
		13.5" Below Top	9852, 9646	9649	39, 42	41½	1, 40	20	679, 810	745
		Posttest Contamination Average		9670 (Base metal only)		39		15		733
3	A. Pickled, Annealed	4.5" Below Top	8186, 8065	8130	27, 33	30	8, 1	5	587, 488	538
3	B. Weld Strip - Pickled, Annealed	As-Welded	21, 21	21	24, 27	26	< 1	< 1	313, 256	285
		4.5" Below Top	6947, 7203	7080	45, 48	47	6, 1	4	497, 372	435
4	A. Pickled, Annealed	4.5" Below Top	4308, 4599	4454	46, 45	46	1, 10	6	452, 566	509
		13.5" Below Top	4417, 4406	4412	51, 49	50	12, 2	7	532, 615	574
		Posttest Contamination Average		4430		48		7		542
4	B. Weld - Strip Pickled, Annealed	As-Welded	105, 167	136	21, 23	22	1, 1	1	314, 321	318
		4.5" Below Top	4058, 4356	4207	56, 52	54	5, 9	7	420, 393	407
		13.5" Below Top	4497, 3941	4219	45, 47	46	6, 5	6	521, 597	559
		Posttest Contamination Average		4210		50		7		483

63

TABLE VII

ROOM TEMPERATURE TENSILE TESTS OF Cb-1Zr TEST SPECIMENS

Test No.	Test Specimen Pretreatment	Sample Orientation	Oxygen Concentration (ppm)	U.T.S. (ksi)	0.02% Y.S. (ksi)	0.2% Y.S. (ksi)	Elongation (%)
	As-Received	Longitudinal	45	43.4	18.3	21.4	29.6
		Longitudinal	45	43.7	18.7	21.8	31.6
				43.6 Avg.	18.5 Avg.	21.6 Avg.	30.6 Avg.
		Transverse	45	49.8	17.6	24.0	28.6
		Transverse	45	49.5	20.5	25.0	32.4
				49.7 Avg.	19.1 Avg.	24.5 Avg.	30.5 Avg.
4	A. Pickled, Annealed	Longitudinal	4430	81.0	47.5	54.1	17.7
		Longitudinal	4430	81.0	47.2	55.3	20.6
				81.0 Avg.	47.3 Avg.	54.7 Avg.	19.2 Avg.
		Transverse	4430	74.1	45.7	54.4	9.3
		Transverse	4430	82.1	42.0	55.0	16.8
				78.1 Avg.	43.9 Avg.	54.7 Avg.	13.1 Avg.
1	A. Surface Pickled	Longitudinal	5990	122.0	78.0	87.5	15.4
		Longitudinal	5990	116.0	75.0	84.0	16.8
				119.0 Avg.	76.5 Avg.	85.8 Avg.	16.1 Avg.
		Transverse	5990	120.0	79.7	89.5	13.4
		Transverse	5990	115.0	72.2	85.5	14.0
				117.5 Avg.	76.0 Avg.	87.5 Avg.	13.7 Avg.
2	A. Pickled, Annealed	Longitudinal	8460	133.0	(a)	129.0	2.0
		Longitudinal	8460	133.0	(a)	123.0	1.0
				133.0 Avg.		126.0 Avg.	1.5 Avg.
2	B. Pickled, Grit-Blasted, Annealed	Longitudinal	9670	111.0(b)	(a)	(a)	-
		Longitudinal	9670	121.0	(a)	(a)	0.5
		Transverse	9670	117.0(b)	(a)	(a)	-
		Transverse	9670	84.7	(a)	(a)	-
4	B. Welded Strip - Pickled, Annealed	Longitudinal	4210	34.4	(a)	(a)	0.9
		Longitudinal	4210	46.1	34.9	46.1	1.4

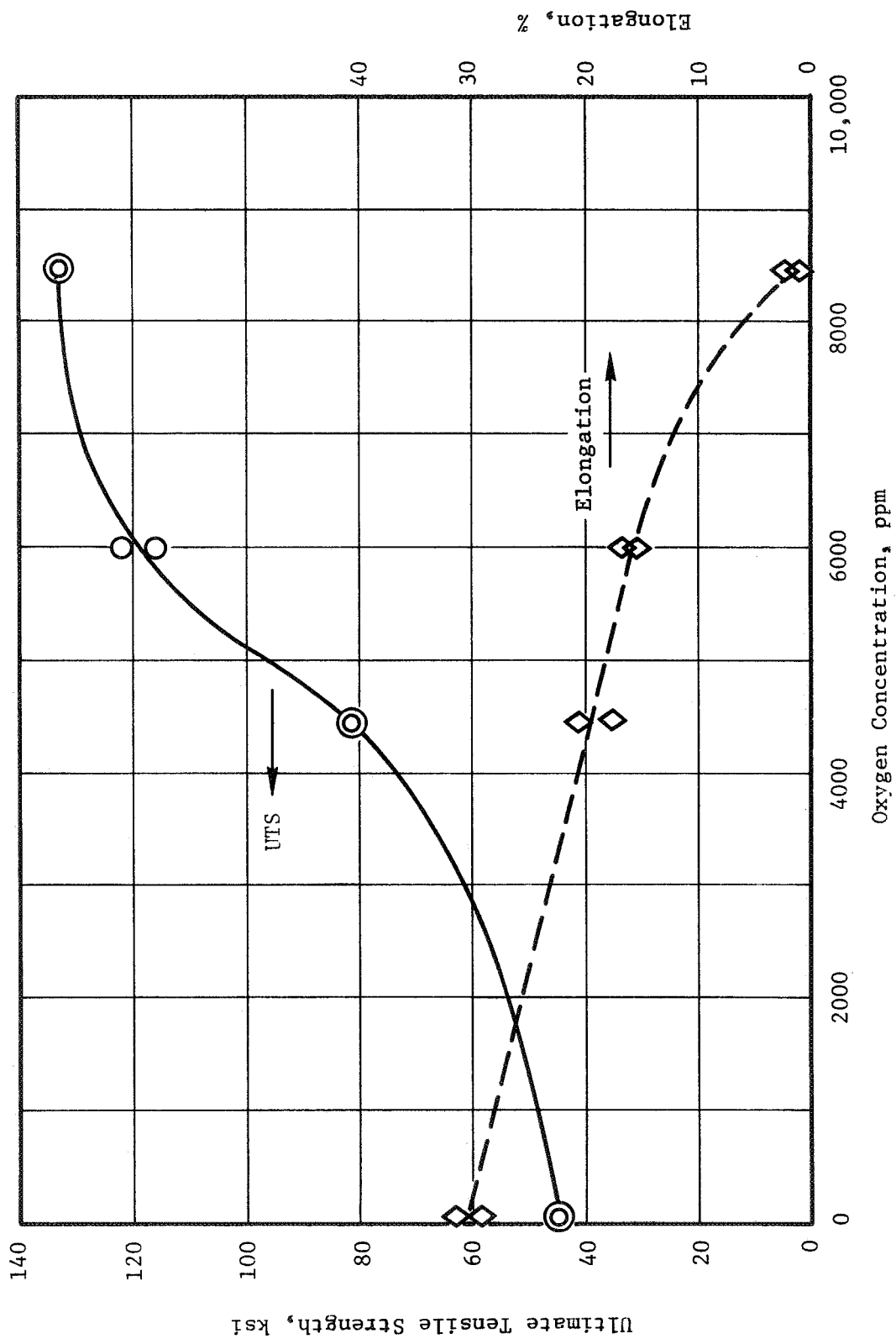(a) Failed before yield was obtained.

(b) Failed in pinhole.

64

Figure 20. Ultimate Tensile Strength and Elongation Versus Oxygen Concentration for Specimens With Bare Surface and Orientation Parallel to the Rolling Direction.

65

The longitudinally welded strip of test No. 4 containing 4210 ppm oxygen (weld metal concentration) was machined in such a way that the gauge section of the tensile specimen was entirely weld metal. This allowed for evaluation of the contaminated weld and for a comparison with the strength of the base metal which had been contaminated to the same level. The results indicated the strength of the weld metal to be slightly less than the strength of the as-received material and approximately equal to half the strength of the surface-pickled and annealed strip of the same test containing a similar oxygen concentration of 4430 ppm oxygen. The ductility of the weld metal is essentially nil as compared to the ductility of the bare strip containing a comparable amount of oxygen.

Comparison of room temperature tensile tests of samples of the same specimen shows little effect of specimen orientation on the ultimate tensile strength. There is, however, a somewhat smaller elongation obtained in the transverse direction than in the longitudinal direction.

Results of tensile tests in vacuum at 1700°F are shown in Table VIII. With increasing oxygen content there is a corresponding increase in strength at 1700°F up to about 6000 ppm oxygen. However, the specimen with grit-blasted surface and 9670 ppm oxygen had lower ultimate tensile strength at 1700°F than the bare surface specimen with 5990 ppm oxygen.

In contrast to the room temperature elongation, the tensile elongation at 1700°F for samples tested in the longitudinal direction was about the same for oxygen concentrations between 4430 and 9670 ppm.

D.   Stress-Rupture Testing of Welded Specimen

Stress-rupture tests were performed on the longitudinally welded and annealed specimen (test exposure No. 4) with 4210 ppm oxygen. The test specimens were machined in such a way that the gauge sections were entirely weld metal. The tests were performed at 1700°F and 10^{-6} torr total pressure. Rupture was not obtained in 15 hours at stress levels of 20 and 30 ksi with elongations of only 0.2 and 0.3 percent, respectively. Additional testing would be required in order to obtain more definitive data on stress-rupture properties.

TABLE VIII

1700°F VACUUM[a] TENSILE TESTS OF Cb-1Zr TEST SPECIMENS

Test No.	Test Specimen Pretreatment	Specimen Orientation	Oxygen Concentration (ppm)	U.T.S. (ksi)	0.02% Y.S. (ksi)	0.2% Y.S. (ksi)	Elongation (%)
4	A. Pickled, Annealed	Longitudinal	4430	56.4	45.9	51.2	12.5
		Longitudinal	4430	56.0	47.4	51.0	11.0
				56.2 Avg.	46.7 Avg.	51.1 Avg.	11.8 Avg.
		Transverse	4430	56.5	45.0	50.1	11.0
		Transverse	4430	55.4	43.7	50.1	12.5
				56.0 Avg.	44.3 Avg.	50.1 Avg.	11.8 Avg.
1	A. Surface Pickled	Longitudinal	5990	70.0	57.0	60.9	14.3
		Transverse	5990	65.7	50.2	57.5	6.7
2	B. Surface Grit-Blasted	Longitudinal	9670	61.0	46.0	52.9	11.4
		Longitudinal	9670	55.5	44.0	47.2	14.7
				58.3 Avg.	45.0 Avg.	50.1 Avg.	13.1 Avg.
		Transverse	9670	61.9	45.2	52.6	6.7
4	B. Welded Strip - Pickled, Annealed	Longitudinal	4210	48.9	41.3	45.4	4.8

(a) Tensile tests performed at 1 x 10^{-6} torr total pressure.

E. Bend Testing

A single bend test was performed on the specimen of test No. 1 after contamination to a level of 5990 ppm oxygen. A 0.031-inch x 1.0-inch x 2.0-inch sample was bent 90° at room temperature using a 2t radius and a load rate of 0.025 inch per minute. The specimen exhibited ductile behavior as shown in Figure 21. After the sample reached a bend angle of 90°, the load was removed and 20° spring-back was observed.

A series of bend tests at various temperatures was performed on the longitudinally welded specimen of test exposure No. 4 which contained 4210 ppm oxygen in an attempt to determine the ductile-brittle bend transition temperature. The test temperature was achieved by immersing the test sample mounted on the Vee block in a constant temperature bath. Temperature was measured using a copper-constantan thermocouple attached to the bend test Vee block. The samples were bent 90° with the weld face in tension and the bending axis perpendicular to the weld axis. A load rate of 0.2 inch per minute was used with an anvil of 1t (0.031-inch) radius. The bend test results for temperatures between 32° and 550°F are shown in Table IX and Figure 22. The test samples all cracked in the weld metal at very low bend angles. From these results, the bend transition temperature is estimated to be well above 550°F.

The bend test results are consistent with the tensile elongation measurements discussed above. The welded and annealed strip contaminated to 4210 ppm oxygen exhibits very little room temperature ductility.

After it was determined that the bend transition temperature for the welded specimen was about 550°F, a sample was vacuum annealed at 2200°F for one hour in an attempt to improve the ductility. This sample was subsequently bend tested at room temperature using the same parameters as in the previous tests. The weld metal again cracked on bending.

F. Metallographic Examination – X-Ray Diffraction

Metallographic examination of the contaminated specimens generally
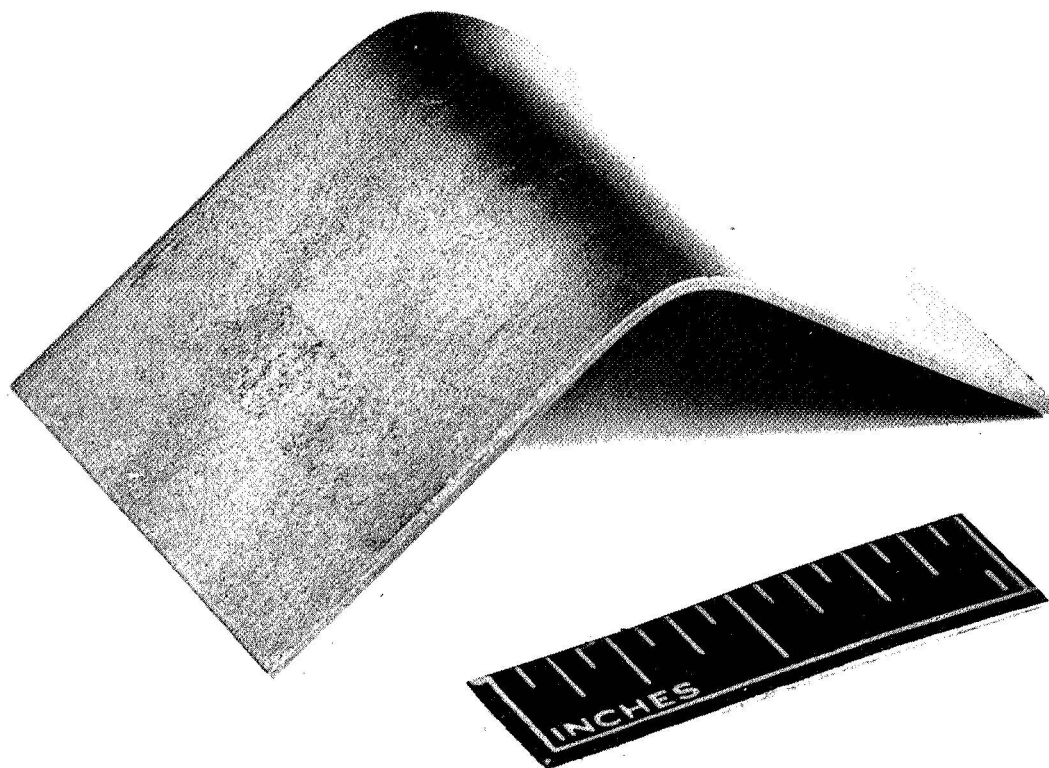
Figure 21. Room Temperature Bend Sample of Cb-1Zr Sheet Containing 5990 ppm Oxygen. Sample From Test Exposure No. 1. (P69-1-35B)

TABLE IX

BEND TESTS OF OXYGEN CONTAMINATED, LONGITUDINALLY WELDED TEST STRIP

Oxygen Concentration (ppm)	Test Temperature ($^\circ$F)	Heat Transfer Media	Ultimate Load (lbs)	Bend Test Results	Bend Angle (Degrees)
4210	32	Water	48.6	Cracked in Weld	7.2
4210	75	Air	46.3	Cracked in Weld	7.2
4210	75[a]	Air	42.6	Cracked in Weld	7.2
4210	200	F-50 Silicone Base Oil	49.2	Cracked in Weld	9.0
4210	500	F-50 Silicone Base Oil	56.0	Cracked in Weld	12.6
4210	550	F-50 Silicone Base Oil	45.2	Cracked in Weld	13.0

[a] Specimen heat treated 1 hour at 2200°F in vacuum after oxygen contamination and prior to bending.

70
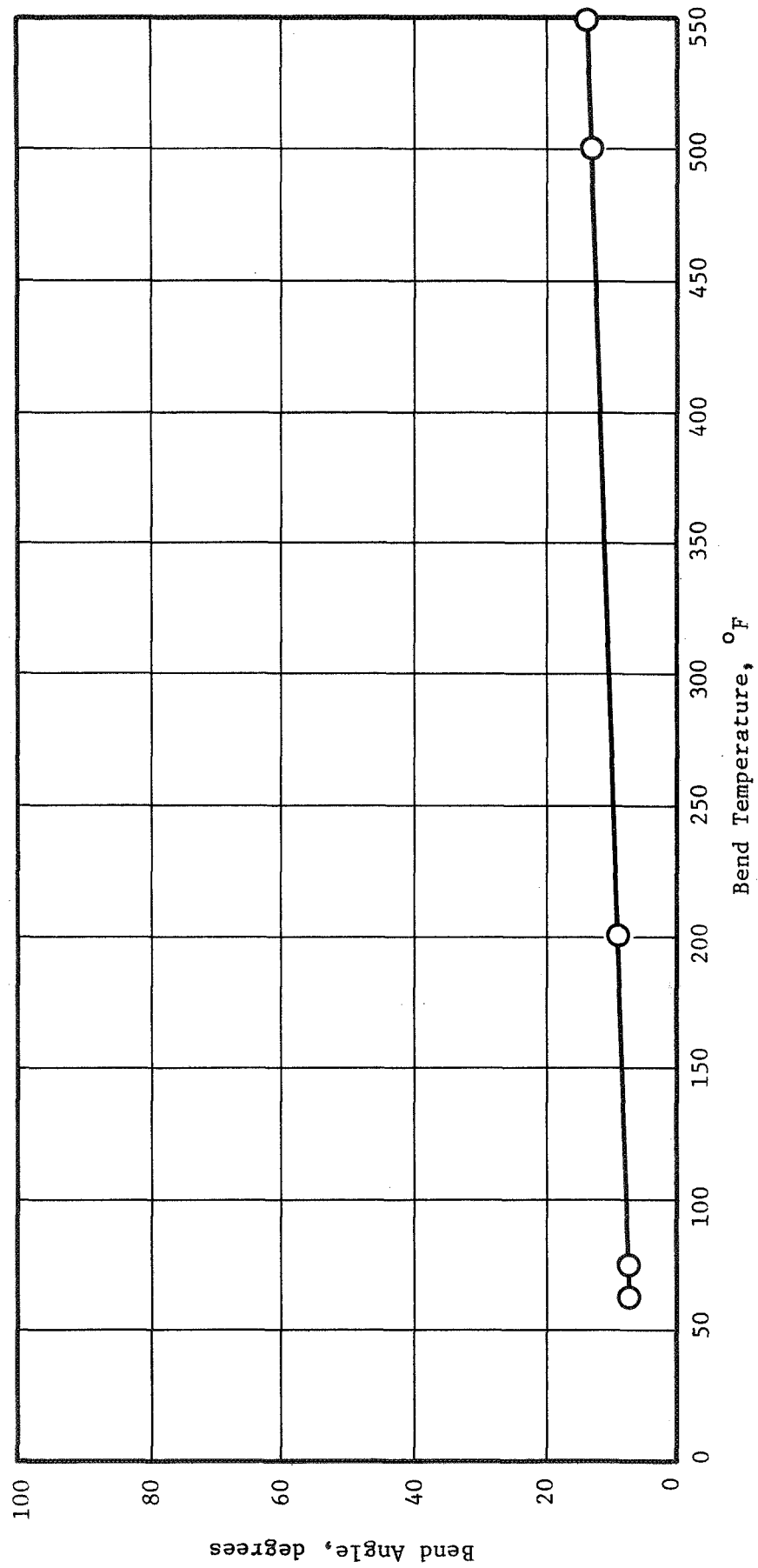
Figure 22. Results of Bend Tests Performed on Longitudinally Welded Strip Specimen of Test No. 4 Containing 4210 ppm Oxygen.

71

revealed relatively large amounts of intergranular precipitate. A method of anodic staining[13] was used to distinguish between the phases present within the sample. With this technique, different phases produce different interference colors depending upon the composition and structure. To identify the phases present, selected samples were obtained from the test specimens by bromine extraction techniques and examined by X-ray diffraction. Results of the phase identification by X-ray diffraction are given in Table X. In each sample, the major phase detected was $Cb_2O_5 \cdot 6ZrO_2$. A minor phase of Cb_2N and a trace of monoclinic ZrO_2 were also found. In the sample with highest oxygen concentration (9670 ppm) a submajor phase of CbO was also detected. Data from a typical X-ray diffraction spectrum is given in Table XI.

Figure 23 shows the microstructure of the contaminated parent metal with various oxygen concentrations. In each case, the major precipitated phase is $Cb_2O_5 \cdot 6ZrO_2$, which tends to concentrate in the grain boundaries. Relatively more precipitate may be noted at 5990 ppm than at 4430 ppm oxygen. In the specimen with 9670 ppm oxygen, CbO precipitate is also found in grain boundaries near the surface. A surface layer of $Cb_2O_5 \cdot 6ZrO_2$ may also be seen on this specimen. Note that this specimen was contaminated during the same test as the specimen shown in Figure 19B which also had a visible surface oxide film.

Figure 24 is a composite of the weld, heat-affected zone, and parent metal of the longitudinally welded strip of test No. 4 containing 4210 ppm oxygen. It may be noted that the intergranular precipitate of $Cb_2O_5 \cdot 6ZrO_2$ nearly completely covers the grain boundaries of the large grains in the weld. This may be seen more clearly in Figure 25 which shows the microstructure of the weld metal at higher magnification.

G. Microhardness

Microhardness surveys were made on those samples selected for metallographic examination in order to obtain some indication of the

---

[13] R. S. Crouse, *Identification of Carbides, Nitrides, and Oxides of Niobium and Niobium Alloys by Anodic Staining*, ORNL-3821 (July 1965).

72

TABLE X

PHASE IDENTIFICATION BY X-RAY DIFFRACTION OF EXTRACTED
SAMPLES FROM Cb-1Zr TEST SPECIMENS

Test Specimen	Oxygen Concentration (ppm)	Phases Detected	Relative Amount
Test #4 - Specimen B Weld Metal	4210	$Cb_2O_5 \cdot 6ZrO_2$	Major
		Cb_2N	Minor
		Monoclinic ZrO_2	Trace
Test #4 - Specimen A	4430	$Cb_2O_5 \cdot 6ZrO_2$	Major
		Cb_2N	Minor
		Monoclinic ZrO_2	Trace
Test #1 - Specimen A	5990	$Cb_2O_5 \cdot 6ZrO_2$	Major
		Cb_2N	Minor
		Monoclinic ZrO_2	Trace
Test #2 - Specimen B	9670	$Cb_2O_5 \cdot 6ZrO_2$	Major
		CbO	Sub-major
		Cb_2N	Minor
		Monoclinic ZrO_2	Trace

TABLE XI

TYPICAL X-RAY DIFFRACTION SPECTRUM -
SPECIMEN FROM TEST NO. 1 (5990 PPM OXYGEN)

d, $\mathring{A}$	Relative Intensity	hkl	Identification	Ortho ASTM Data
3.64	W	101	Ortho + Mono ZrO_2	3.61
3.15	W		Mono ZrO_2	
2.94	S	111	Ortho	2.95
2.85	W		Mono ZrO_2	
2.680	W*	100	Cb_2N	
2.62	VW	002	Ortho	2.64
2.53	MW	020	Ortho	2.56
2.475	MW*	002, 200	Cb_2N, Ortho	2.48
2.38	W	012	Ortho	2.35
2.36	S*	101	Cb_2N	
2.34	W	021	Ortho	2.31
2.08	VW	121	Ortho	2.09
1.82	MS	022	Ortho	1.838
1.80	M	102,202	Cb_2N, Ortho	1.809
1.79	MW	220	Ortho	1.782
1.710	VW	212	Ortho	1.706
1.649	W	103	Ortho	1.649
1.577	W	113	Ortho	1.579
1.563	W	110	Cb_2N	
1.529	M	131	Ortho	1.545
1.510	W	311	Ortho	1.511
1.477	W	222	Ortho	1.478
1.405	W*	103	Cb_2N	
1.322	VW*	112	Cb_2N	
1.314	VW	004	Ortho	1.321
1.294	W*	201	Cb_2N	

* These lines sharp, all others broad and diffuse.

Ortho = orthorhombic $Cb_2O_5 \cdot 6ZrO_2$ (ASTM Card 9-251).

74
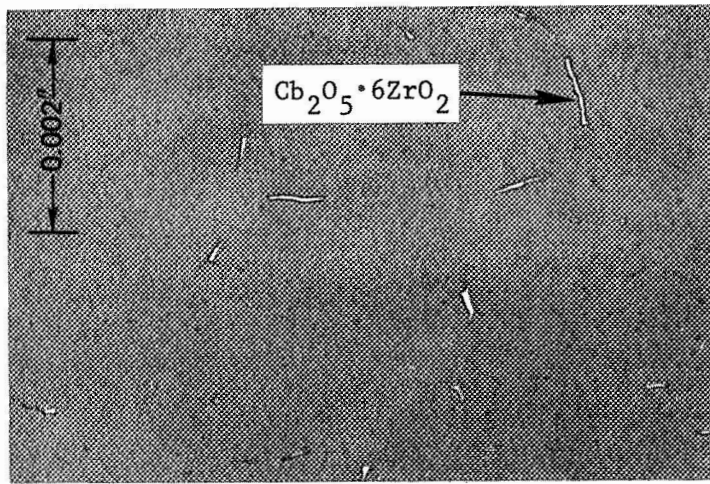
H27011B

Specimen A, Test No. 4.   4430 ppm Oxygen
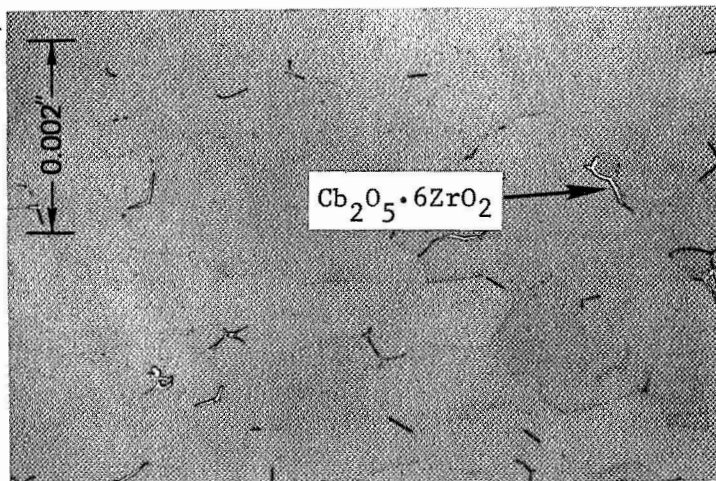
MB–567L

Specimen From Test No. 1.   5990 ppm Oxygen
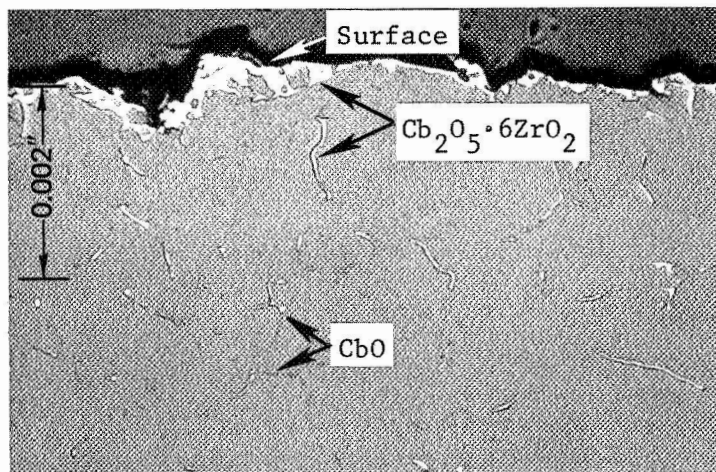
G95011E

Specimen B, Test No. 2.   9670 ppm Oxygen

Figure 23.   Parent Metal With Various Oxygen Concentrations.
Electrolytic Stain Etch.
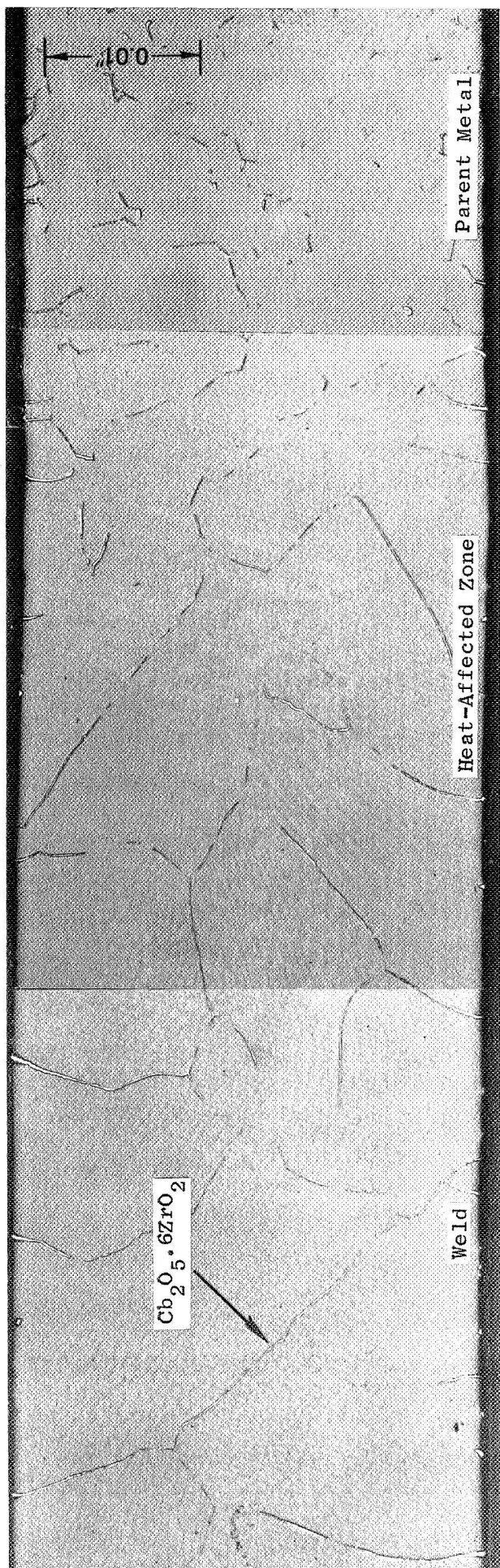
Figure 24. Composite of Weld, HAZ, and Parent Metal of Longitudinally Welded Strip of Test No. 4 Showing Intergranular Precipitate of $Cb_2O_5 \cdot 6ZrO_2$. Electrolytic Stain Etch.
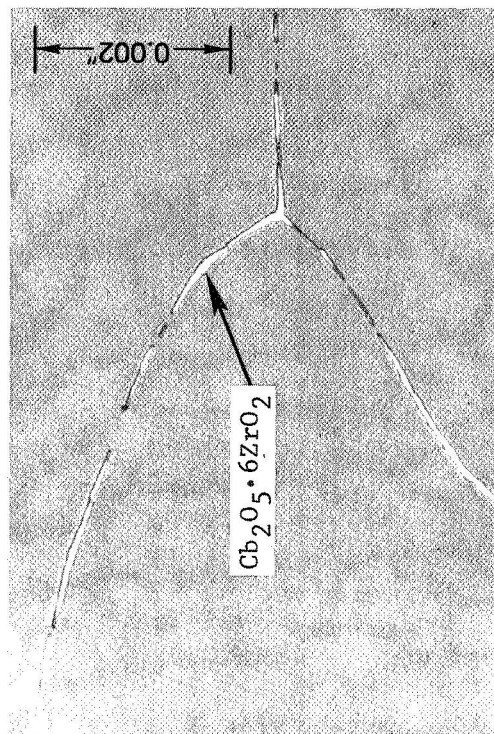
Figure 25. Section of Weld of Longitudinally Welded Strip of Test No. 2 Showing Massive Intergranular Precipitate of $Cb_2O_5 \cdot 6ZrO_2$. Electrolytic Stain Etch.

76

uniformity of the oxygen concentration thoughout the specimen thickness. Results of microhardness traverses taken from the surface of the specimen through the half-thickness are shown in Figure 26. These data indicate a relatively uniform hardness except for the specimen from test No. 1 (5990 ppm oxygen) in which a hardness gradient extends to a depth of about 8 mils. The uniform hardness throughout the thickness indicates uniform oxygen concentration. It is thus concluded that, under conditions of these test exposures, the oxygen diffusion rate through Cb-1Zr is greater than the surface reaction rate.

The increase in hardness with oxygen concentration is shown in Figure 27 where the central (or half-thickness) hardness is plotted against oxygen concentration.

H.   Discussion of Evaluation Results

With homogeneous addition of oxygen to Cb-1Zr at 1700°F (927°C) there is a concurrent increase in ultimate and yield strengths and a decrease in ductility. These property changes are consistent with the observed changes in microstructure and hardness. It should be noted that these effects are similar to the well-documented[9,14,15] age hardening effects in the Cb-1Zr alloys even though the microstructural changes are quite different. As-cast or as-welded Cb-1Zr is subject to embrittlement upon high-temperature aging in the temperature range 1500° to 1800°F (816° to 982°C) for periods of the order of 100 hours. This embrittlement is caused by a finely dispersed intragranular oxide precipitate which may be submicroscopic. Annealing in the temperature range from 1900° to 2200°F (1038° to 1204°C) results in formation of larger precipitated particles (overaging) which minimizes embrittlement upon subsequent heating at lower temperatures.

[14] Hobson, D. O., "Aging Phenomena in Columbium-Base Alloys" in High-Temperature Materials II (Metallurgical Society Conferences Vol. 18, Ault, G. M., et al., Eds.) Gordon and Breach, New York (1963).

[15] Stewart, J. R., Liberman, W., and Rowe, G. H., "Recovery and Recrystallization of Columbium-1.0% Zirconium Alloy" in Columbium Metallurgy (Metallurgical Society Conferences Vol. 10, Douglas and Kung, Eds.) Interscience, New York (1961).
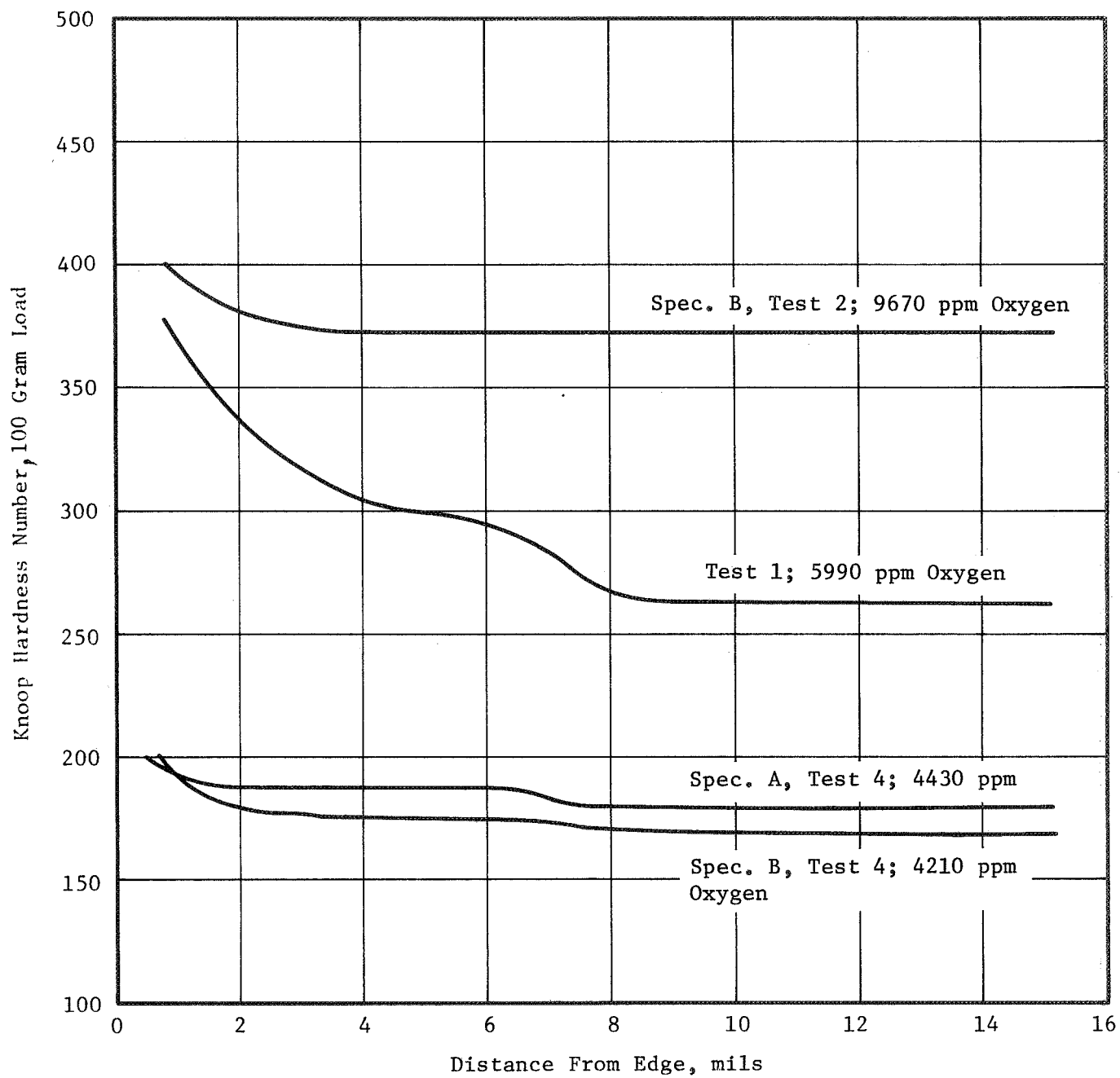
Figure 26. Hardness Traverses of Contaminated Test Specimens.

The chart shows Knoop Hardness Number, 100 Gram Load (y-axis, 100 to 500) versus Distance From Edge, mils (x-axis, 0 to 16). Curves are labeled:
- Spec. B, Test 2; 9670 ppm Oxygen
- Test 1; 5990 ppm Oxygen
- Spec. A, Test 4; 4430 ppm
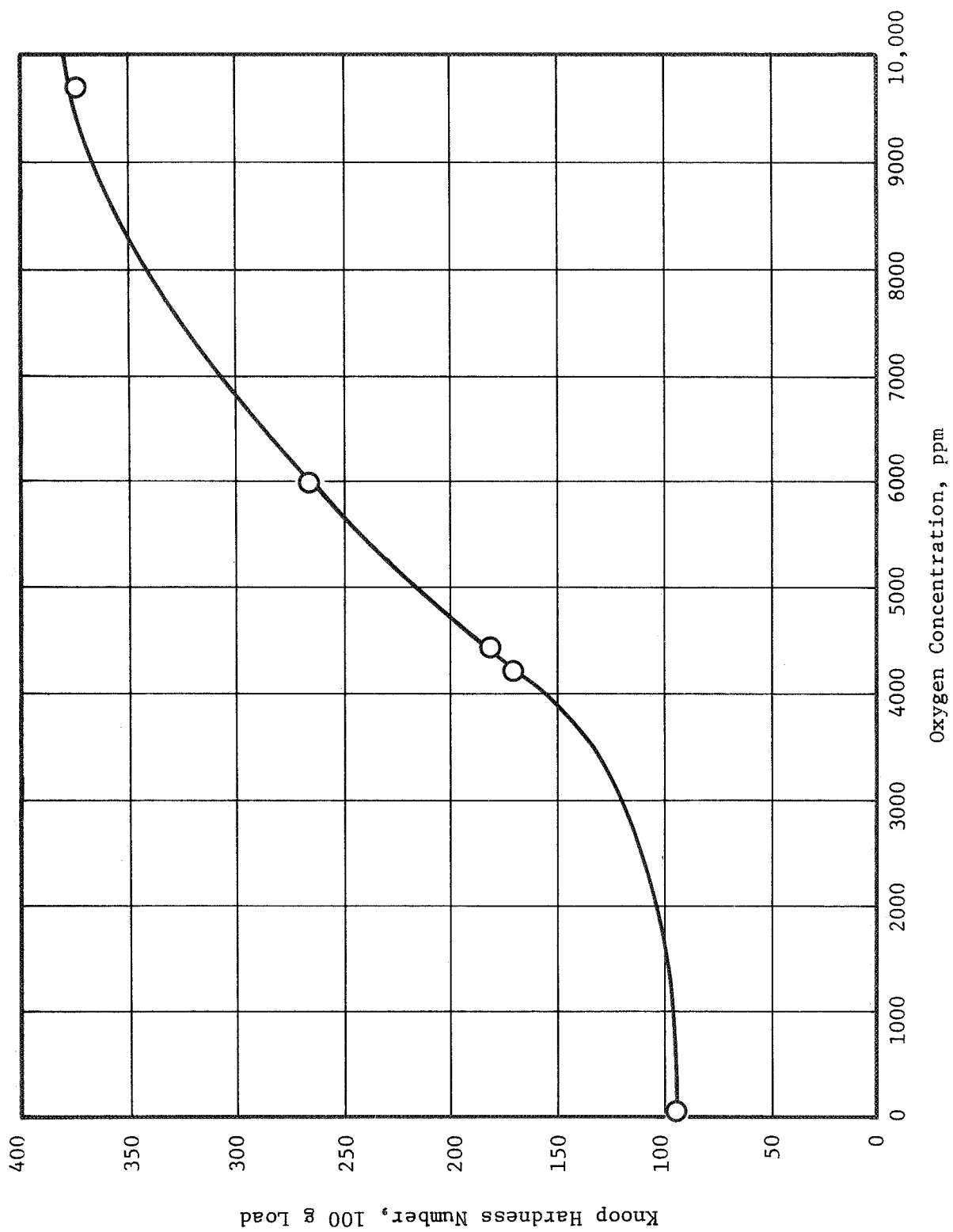- Spec. B, Test 4; 4210 ppm Oxygen

Figure 27. Hardness Increase of Contaminated Test Specimens as a Function of Oxygen Concentration.

79

In contrast to this behavior, the relatively high level of oxygen contamination in the present study caused embrittlement by massive precipitation of oxides in the grain boundaries, rather than by the fine intragranular precipitate found in the aging reactions. In addition, all test specimens in this study (except the specimen of test No. 1) were annealed in order to prevent embrittlement of the material by an aging reaction which might have occurred during the course of the contamination exposures.

Cb-1Zr, welded and annealed, is considerably more sensitive to oxygen concentration than is the parent metal. At 4300 ppm oxygen the weld metal is brittle, while at 6000 ppm oxygen the parent metal is still quite ductile. The reason for this seems to be simply a matter of grain size. Since the grains in the weld are so large, a relatively smaller amount of oxygen creates sufficient oxide precipitate to nearly completely cover the grain boundaries resulting in brittle behavior. This may be seen quite clearly in Figure 25. At an equivalent oxygen concentration, the oxide is more dispersed in the smaller grains of the parent metal as can be seen in Figure 24. Since the embrittlement of the weld metal is due basically to the comparatively large grain size, it might be expected that postweld annealing would have little if any effect on this process, since annealing does not appreciably change the grain size.

It was also found that ductility of the longitudinally welded and contaminated specimen (specimen B of test No. 4) could not be restored by the usual annealing treatment of 2200°F for one hour. This indicates that the massive oxide precipitate formed by the intentional oxidation cannot be readily redistributed by subsequent heat treatment so as to produce a ductile structure. In the welding study[9] previously referred to, it was found that contaminated Cb-1Zr with 4200 ppm is brittle as welded but regained good ductility after annealing. It thus appears that this sequence of oxygen addition, welding, and annealing produces a different distribution of oxide precipitate and hence better ductility than does the sequence of welding, annealing, oxygen addition, and re-annealing which was employed in the present study.

It is interesting to note that the major precipitated oxide phase found in the contaminated specimens of the present study was the complex oxide,

80

$Cb_2O_5 \cdot 6ZrO_2$, with a minor phase of monoclinic ZrO_2. Apparently, this is the first time that this complex oxide has been identified in the precipitate from Cb-Zr alloys. Hogan, et al.[7] identified monoclinic ZrO_2 by electron diffraction of extracted particles from their contaminated specimens. Several crystalline forms of ZrO_2 as well as unindentified phases were found in as-cast Cb-1Zr by Stewart, et al.[15] using electron diffraction analyses. Barber and Morton,[16] in their study of the Cb-Zr-O system, found ZrO_2 in their specimens by X-ray diffraction techniques.

It should first be recognized that interpretation of patterns from the extracted residue is quite difficult, especially when multiple phases of similar structure are present. There is thus the possibility of misinterpretation of the patterns on the part of any of the investigators, the present study included. On the other hand, there is equal possibility that the compositions, time, and temperature of the present study are such as to allow the equilibration of the complex oxide phase while such conditions were not imposed in the other investigations cited.

The existence of the compound, $Cb_2O_5 \cdot 6ZrO_2$ was firmly established by work of Roth and Coughanour[17] who investigated phase relations in the Cb_2O_5-ZrO_2 system. The structure of this compound is orthorhombic and it melts incongruently at about 3040°F (1670°C). There seems to be no fundamental reason why it could not precipitate as a result of oxidation of Cb-1Zr.

(16) Barber, A. C. and Morton, P. H., "A Study of the Niobium-Zirconium-Carbon and Niobium-Zirconium Oxygen Systems" in High-Temperature Refractory Metals Part 2 (Metallurgical Society Conferences Vol. 34, Gordon and Breach, New York (1966).

(17) Roth, R. S. and Coughanour, L. W., Jour. Res., National Bureau of Standards 55, 209 (1955).

VI. SUMMARY AND CONCLUSIONS

Flat sheet specimens of Cb-1Zr were exposed at 1700°F (927°C) in a vacuum chamber at various levels of total pressure in the 10^{-6} torr range. Pressure levels were maintained by controlled in-leakage of air. Oxygen reacts rapidly with Cb-1Zr under these conditions, and exposure times were adjusted to give various final oxygen content of the specimens between 4000 and 9000 ppm. It was shown that the relative gas composition depends on the parameter $\frac{\alpha A}{S}$ where α is the oxygen sticking probability, A the exposed area of the specimen, and S is the pumping speed of the vacuum system. Thus by measurement of the relative gas composition and the system pumping speed, α could be calculated at various times during the test exposure. The values of α, averaged over the test exposure time, were in good agreement with the overall effective value of α calculated from the final oxygen content of the specimen.

Evaluation of the contaminated specimens included chemical, metallographic, and X-ray diffraction analyses, along with tensile, stress rupture, and bend transition temperature determinations on selected specimens.

A summary of the significant test parameters and evaluation criteria for the seven test specimens is as follows:

Specimen Pretreatment

1. Pickling - sheet material was pickled before specimen fabrication;
2. Annealing - a) one specimen not annealed;
   b) two specimens annealed but exposed to ambient air before test exposure;
   c) four specimens annealed immediately before test exposure;
3. Surface Roughness - one specimen grit blasted before exposure;
4. Welding - two specimens contained full-length GTA welds;
5. Orientation to Rolling Direction - five specimens contained both longitudinal and transverse sections.

Specimen Exposure Conditions

1. Temperature - 1700°F (927°C);
2. Oxygen Partial Pressure - 10^{-7} torr range;

3. Exposure Time- 200 to 500 hours.

Evaluation Criteria

1. Oxygen Content after Exposure - 4000 to 9000 ppm;

2. Oxygen Reaction Rate - approximately 2×10^{-9} gm/cm^2 sec;

3. Microstructure and identity of precipitated phases;

4. Ductility;

5. Strength;

6. Hardness.

From the results of these tests, the following significant conclusions are obtained:

1. Under the conditions of these tests, the rate of reaction of Cb-1Zr with oxygen is significantly reduced by the presence of a normally undetectable oxide film which is present on the surface as a result of oxidation with ambient air. At temperatures above about 1900°F (1038°C) the film is removed by dissolution of the oxygen in the bulk material. The result is a much higher reaction rate corresponding to a sticking probability of about 0.65. If the oxide film is initially present, it will increase in thickness at oxygen partial pressures in the 10^{-7} torr range and temperatures of 1700°F (927°C). A surface layer of $Cb_2O_5 \cdot 6ZrO_2$ becomes microscopically visible after oxidation to about 8000 ppm oxygen.

2. The reaction of nitrogen with Cb-1Zr is diffusion rate limited at 1700°F (927°C) and nitrogen partial pressures in the 10^{-6} torr range. For all tests, the total nitrogen increase was less than 50 ppm.

3. An increase in carbon content of about 200 ppm was generally observed. This is presumably due to reaction with backstreaming oil from the diffusion pump.

4. Under the conditions of these tests, an increase in total hemispherical emittance occurs over the initial 100 hours of test exposure. For specimens with the surface oxide film, a maximum emittance of about 0.34 is obtained. For specimens without the oxide layer, a maximum emittance of about 0.24 is obtained.

5. The rate of oxidation of the base metal surface is about 14 percent higher than the rate on the welded (fusion zone) material. The rate of oxidation of a grit-blasted surface is about 11 percent higher than the rate on the base metal surface.

6. Cb-1Zr alloy is considerably strengthened by addition of oxygen up to an oxygen content of about 6000 ppm, while still maintaining reasonably good room temperature ductility. At higher oxygen contents, serious loss of ductility occurs with little additional strengthening.

7. Cb-1Zr alloy, welded and annealed, is considerably more sensitive to oxygen content than the base metal. After addition of 4300 ppm oxygen, the weld metal is brittle at room temperature, and the bend transition temperature appears to be above $550°F$ ($290°C$).

8. Prolonged exposure of Cb-1Zr to air at a total pressure in the 10^{-6} torr range results in massive grain boundary precipitation of $Cb_2O_5 \cdot 6ZrO_2$. Minor phases of Cb_2N and ZrO_2 can also be detected. At oxygen concentration greater than 9000 ppm, a CbO phase is also observed near the surface.

9. The increase in strength and reduction in ductility with increasing oxygen content is not the result of aging in either the weld metal or base metal, but is rather the result of the formation of a brittle oxide phase along the grain boundaries.

APPENDIX

CAPSULE HEATING SYSTEM

The original contract required the testing of two bellows capsules, filled with lithium fluoride, and coated with iron titanate. These capsules were 3.25 inch OD with a convoluted portion 10 inches long. An inner tube, 1.25-inch OD, passes completely through the capsule. The lithium fluoride was contained within the space between the inner tube and the convoluted portion. In order to maintain the proper freezing pattern of the LiF, heat is rejected on the interior of the inner tube by radiation to an air cooling tube, sealed from the vacuum system. The capsule was required to be cycled from 1500°F (816°C) to 1700°F (927°C) in 60 minutes and back to 1500°F in 36 minutes. This cycle was to have been repeated over the test duration of 1000 hours. A complete description of the lithium fluoride filled capsules and their thermal behavior during temperature cycling is given elsewhere.[18]

The test exposure conditions placed severe restrictions on the capsule heating system. Since the capsule had to be exposed to the chamber environment, no thermal shielding could be employed to restrict radiant heat loss from the capsule. In order to maintain the proper melting and freezing pattern in the lithium fluoride, the heat had to be supplied on the exterior (convoluted) surface. The heat source itself could not be located in close proximity to the capsule, since this too would interfere with impingement of environmental gases on the capsule surface. Finally, the materials of construction had to be compatible with operation both in air and in high vacuum. The only feasible heating system seemed to be one in which a radiant heat source was located some distance from the capsule surface, and the heat energy was directed at the capsule by means of a suitable system of reflectors.

---

[18] Harrison, R. W. and Hendrixson, W. H., "Corrosion Tests of Lithium Fluoride in Contact with Columbium Alloys, Topical Report II," NASA Contract NAS 3-8523, GESP-436, January 1970.

A.   Total Heat Flux Requirements

The very complicated geometry of the capsule and proposed heating system prevented a rigorous thermal analysis of the system. The maximum total heat flux to the capsule was thus calculated using several simplifying assumptions. The total incident heat flux must be sufficient to supply the following heat losses:

1.   Radiant loss from the capsule;

2.   Power required to raise the temperature of the LiF charge from 1500° to 1700°F in one hour;

3.   Heat loss to the cooling air;

4.   Radiant power reflected from the capsule.

The radiant loss from the capsule is assumed to be equivalent to that from a cylinder 3.25 inches OD and 10 inches long, surrounded by a completely absorbing surface. The total hemispherical emittance was taken to be 0.86. The radiant loss from the capsule, with these assumptions, is 4510 watts at 1500°F (816°C) and 6660 watts at 1700°F (927°C).

The power required to increase the temperature of the LiF from 1500° to 1700°F in one hour was calculated assuming a charge of 1040 gm and that the power to the LiF was constant during the period. The result was 380 watts.

The heat loss to the cooling air was estimated from previous bellows capsule tests performed at GE-NSP.[18] Steady state temperature measurements with and without cooling air gave 426 watts heat loss at 1500°F and an estimated 1000 watts heat loss at 1700°F.

The radiant power reflected from the capsule is obtained by assuming a total absorptivity of 0.86; that is, 14 percent of the total incident power is reflected. The total incident radiant power required is the summation of the four losses calculated as described above. These calculated values are shown in Figure 28 along with the total incident power required between 1500° and 1700°F. It should be noted that the value for the power required to raise the LiF temperature from 1500°F to 1700°F is not actually a heat loss but is regained as the capsule temperature is lowered.

Based on the calculated total heat flux requirements and the additional

requirement that the heating system be inert with respect to the chamber atmosphere, a GE-NSP Engineering Specification was prepared (Spec. No. 02-0209-00-A, "Tungsten Quartz Lamp Heater Assembly for Ultrahigh-Vacuum Service").

B.   Fabrication and Acceptance Test of Capsule Heating System

The entire heater assembly to meet the requirements of Specification No. 02-0209-00-A was designed, fabricated, and tested at Heat Technology Laboratory, Inc., Huntsville, Alabama. The heater assembly is shown in Figure 29. The system consists of fifteen GE Model 1600T3/VB quartz lamps held in the vertical position to form a cylindrical array around the test capsule. Each lamp has an individual reflector that can be adjusted to direct the radiant energy from the lamp toward the lithium fluoride capsule. The lamp reflectors are made of extruded aluminum with a highly polished, hand-buffed reflective surface. The reflector shape is a modified parabola especially designed for this application by Heat Technology Laboratory. The lamp sockets, mounting bracket, screws, and other parts of the lamp reflector are fabricated from aluminum. All electrical connectors are nickel-plated copper and all electrical insulators are 99.5 percent alumina. The type 304 stainless steel frame is made in three equal sections to allow the entire unit to be assembled around the test capsule for ease in instrumentation and inspection of the test specimen. Four mounting lugs are attached to the frame for mounting the heater assembly in the vacuum chamber.

The heater assembly is designed to deliver a total net power of 10 kw, incident upon the capsule, with a uniform axial heat flux that does not vary by more than 10 percent of the average incident flux along the length of the capsule. The maximum total rated power to the lamps is 24 kw.

After fabrication of the capsule heating system, initial tests of the system were performed by the vendor. Due to the lack of adequate vacuum facilities, the tests were made in ambient air. The purpose of the tests was to determine the uniformity of heat flux from the quartz lamp heater assembly both along the vertical axis and in several radial directions, and to determine the total heat flux at rated lamp power.
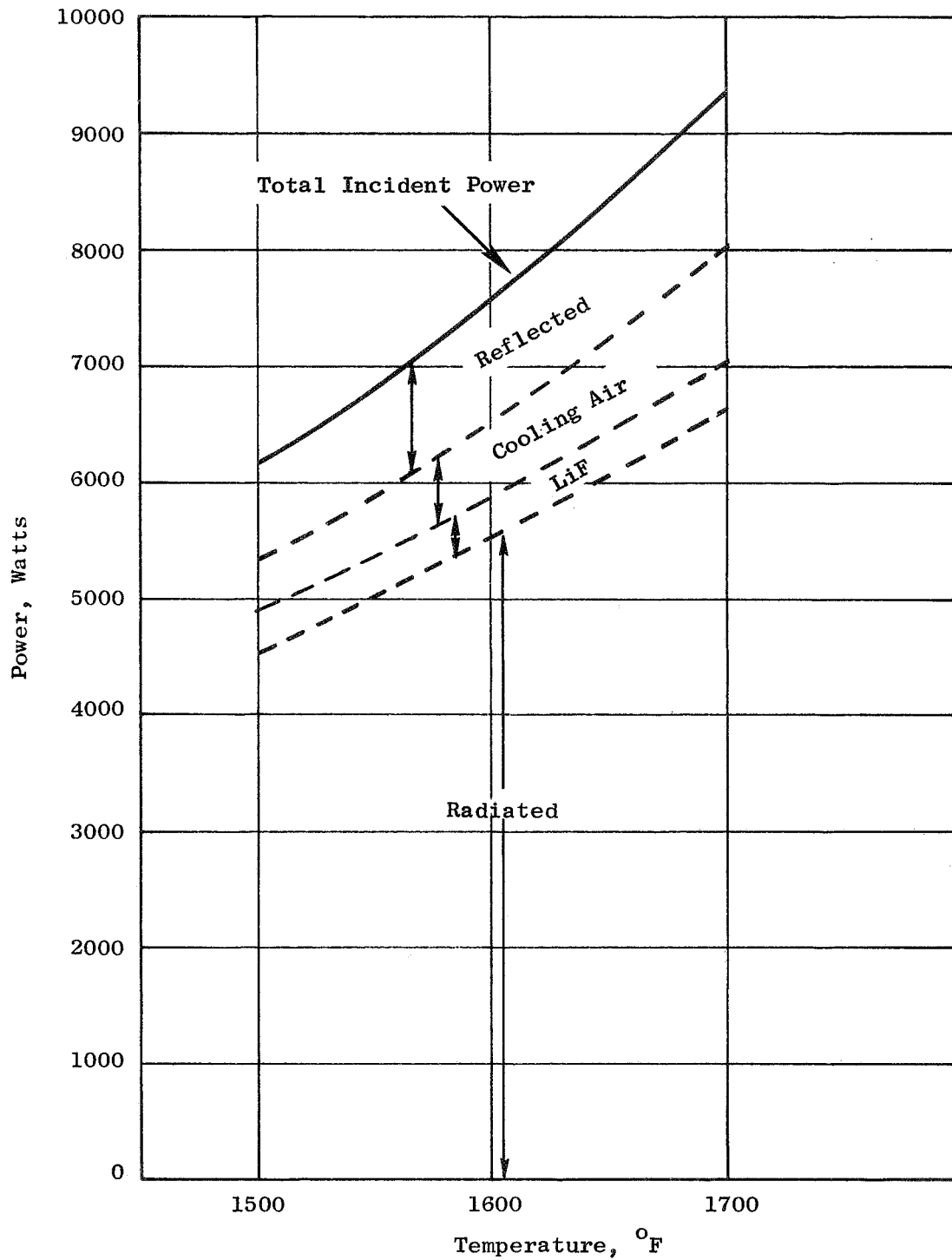
Figure 28. Calculated Total Incident Power Required to Heat Bellows Capsule From 1500 to 1700°F in One Hour.
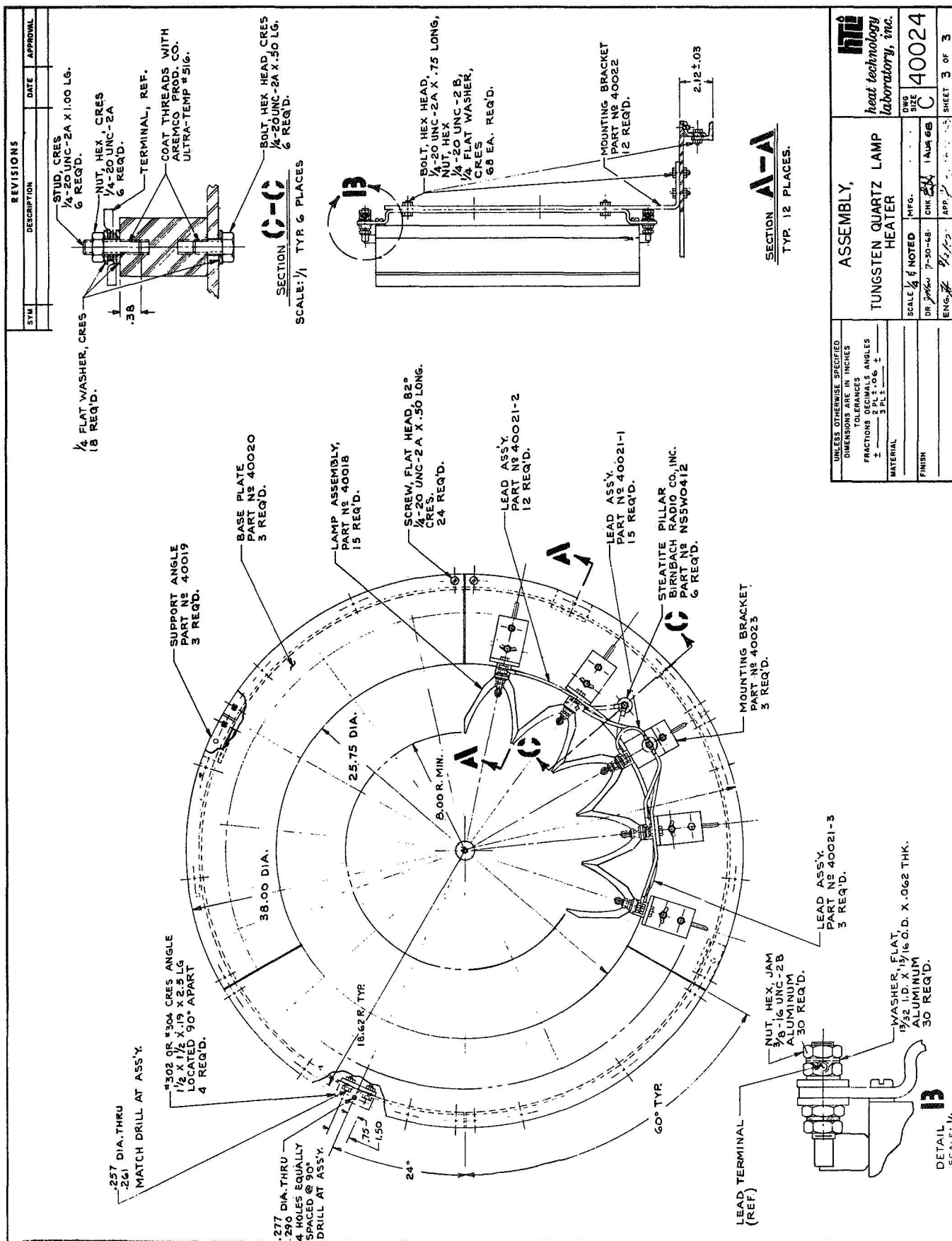
Figure 29. Tungsten Quartz Lamp Heater Assembly for Heating the Lithium Fluoride-Filled Bellows Capsule.

Measurements were made with an HTL Model GT80 heat flux transducer with accuracy of $\pm$ 3 percent at 80 Btu per ft^2-sec. The transducer was positioned horizontally and flush with the outer surface of a 1.25-inch-OD copper tube. The transducer and tube were cooled by water flow of 0.7 gallon per minute.

The tube and transducer were mounted so that they could be moved to different vertical positions within 5 inches of the center line of the lamp assembly, and also rotated to face in different radial directions. Heat flux measurements were made at five different locations along the axis of the assembly as shown in Figure 30, and at four different radial directions as shown in Figure 31 for a total of twenty test points.

The measurements were made with the lamps operated at rated voltage (240 volts). Results of the tests are shown in Table XII. These data show excellent uniformity in both the radial and axial direction with the minimum measured flux being 3.8 percent lower than the average value and the maximum being 5.8 percent higher than the average.

Assuming uniform heat flux at the average value of Table XII, the incident heat flux on a cylindrical surface 3.25 inches OD and 10 inches long would be 6.56 Btu per second or 6.92 kw. This is about 75 percent of the estimated required value at 1700°F. Due to the possibility that additional heat flux would be required, measurements were made at HTL up to twice the rated voltage of the lamps. Results of these tests are shown in Figure 32 where the heat flux is plotted against applied voltage between 150 and 440 volts. These data show that the estimated required value (9.3 kw) of heat flux incident on a cylinder, 3.25 inches OD and 10 inches long, can be obtained with 300 volts applied to the lamps.

C. Power Control Equipment for Capsule Heating System

The power control circuit was designed to provide for either manual variation of electric power to the lamps, or for automatic cyclic control in accordance with the required variation in capsule temperature. Power to the system was varied by means of three saturable reactors, one in each phase of the 440-volt line. Power control was provided by a cam-operated, program-type set point unit operating off a control thermocouple
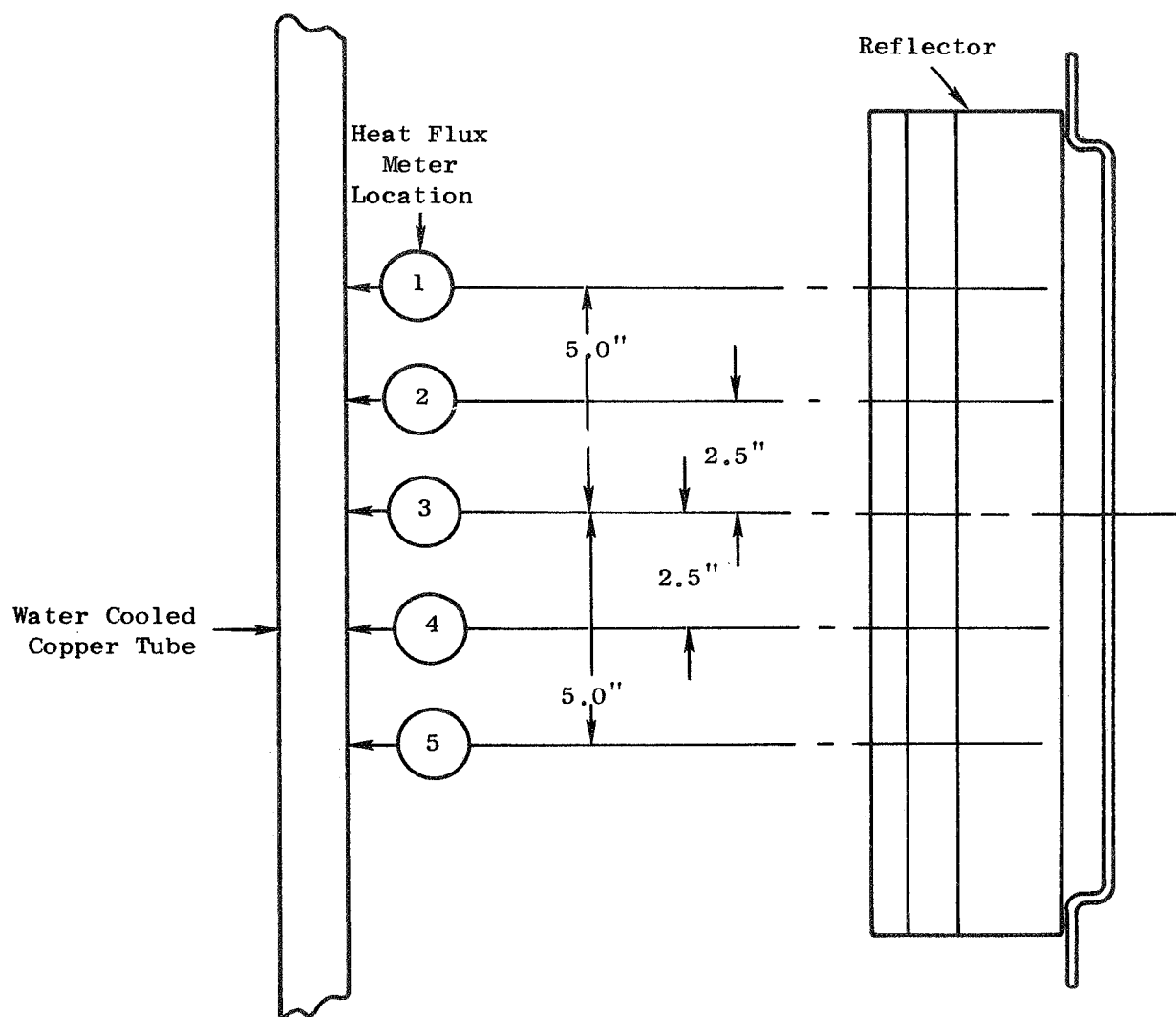
Figure 30. Vertical Locations of Heat Flux Measurements for Quartz Lamp Heating System.
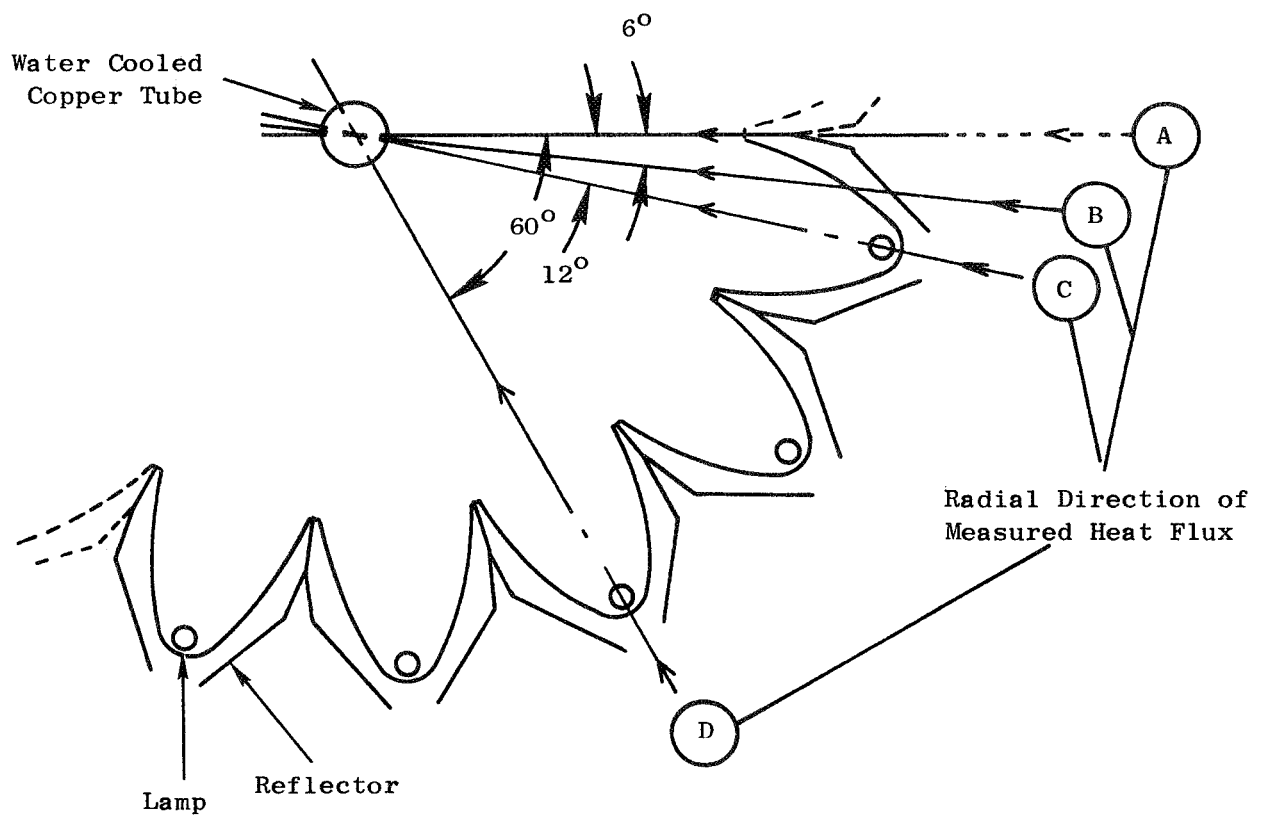
Figure 31. Radial Locations of Heat Flux Measurements for Quartz Lamp
Heating System.

TABLE XII

HEAT FLUX MEASUREMENTS AT VARIOUS AXIAL AND RADIAL POSITIONS FOR TUNGSTEN QUARTZ LAMP HEATER ASSEMBLY

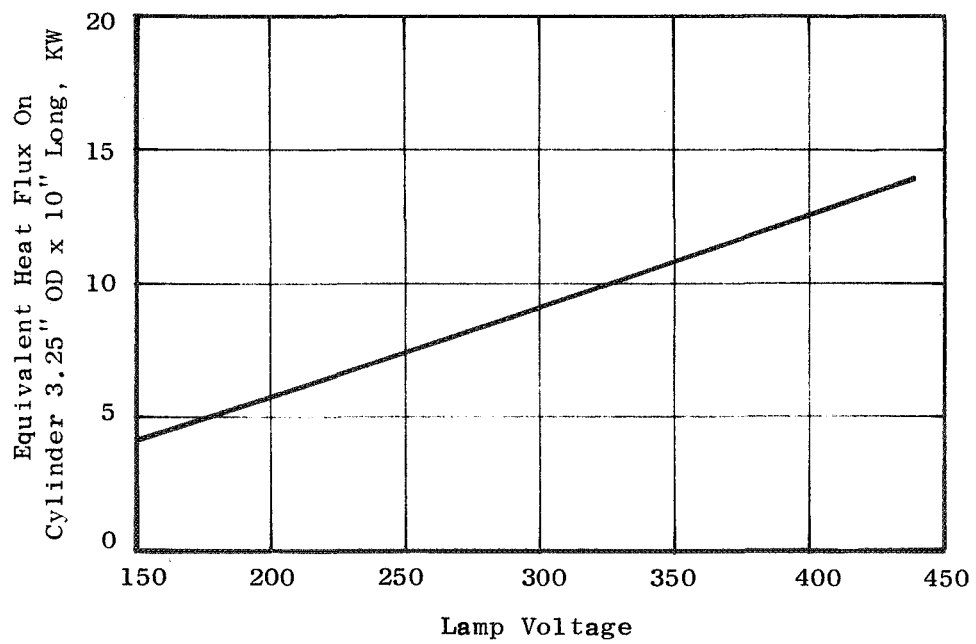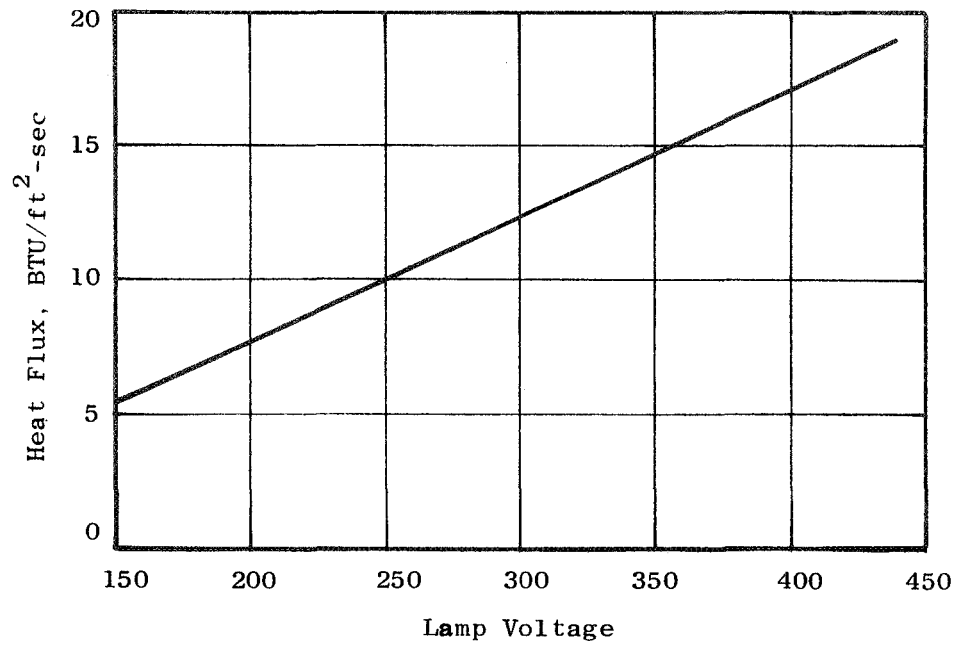| Radial Position (Ref. Figure 31)	Axial Position (Ref. Figure 30)					Average	
	1	2	3	4	5		
A	8.90	9.32	9.65	9.35	8.90	9.224	Btu/ft^2-sec
B	9.02	9.32	9.65	9.35	8.90	9.248	Btu/ft^2-sec
C	9.03	9.32	9.75	9.44	8.90	9.288	Btu/ft^2-sec
D	8.90	9.32	9.80	9.35	9.00	9.274	Btu/ft^2-sec
Average	8.962	9.320	9.712	9.372	8.925		

Average 20 test points = 9.258 Btu/ft^2-sec.

Figure 32. Heat Flux Versus Applied Voltage for Quartz Lamp Heating System.

on the apex of the center convolution on the capsule. The basic elements of the power control circuit are shown in Figure 33. This system is capable of providing 430 volts at approximately 80 amps to the lamps in the vacuum chamber. Control of the lamp power may be manual or automatic. In the automatic mode the 4-20 ma dc control current to the magnetic amplifier is generated in a program-type set point unit (West Instrument Corp. Model JSBGF-S79). This device generates an output signal proportional to the difference between the set point temperature and a temperature derived from a thermocouple attached to the test specimen. The set point is varied automatically by means of a cam which can be cut to give the desired time-temperature relationship. The cam makes one complete rotation each 96 minutes. Both automatic and manual control signals pass through a current limit circuit which can be adjusted to limit the maximum output of the saturable reactor without turning off the power or causing any step change in power level. Meters for monitoring phase voltages and currents are provided. Meters are also provided to indicate control circuit voltages and currents.

D. Initial Operation of Capsule Heating System in Vacuum

The capsule was installed and instrumented in the vacuum system and the quartz lamp heating system placed in position surrounding the capsule. Twenty thermocouples (W-3Re/W-25Re) were spot welded to the capsule surface. Figure 34 shows the instrumented bellows capsule with one section (five lamps) of the heating system in position. The supporting tubulation on the capsule is insulated with Cb-1Zr foil. The exit line for the capsule cooling air is visible at the top of the photograph. Thermocouples were also attached to the aluminum reflectors.

In the initial vacuum operation of the capsule heating system, it was found that, with the capsule temperature at 1200°F, the temperature of the reflectors exceeded the maximum recommended level of 800°F. The apparent total power to the lamps was 9.2 kw. The fact that the reflectors apparently did not reach such high temperatures in the acceptance tests, even though the lamps were operated in excess of rated power (24 kw), is due to convective cooling by ambient air during the acceptance tests. In addition,
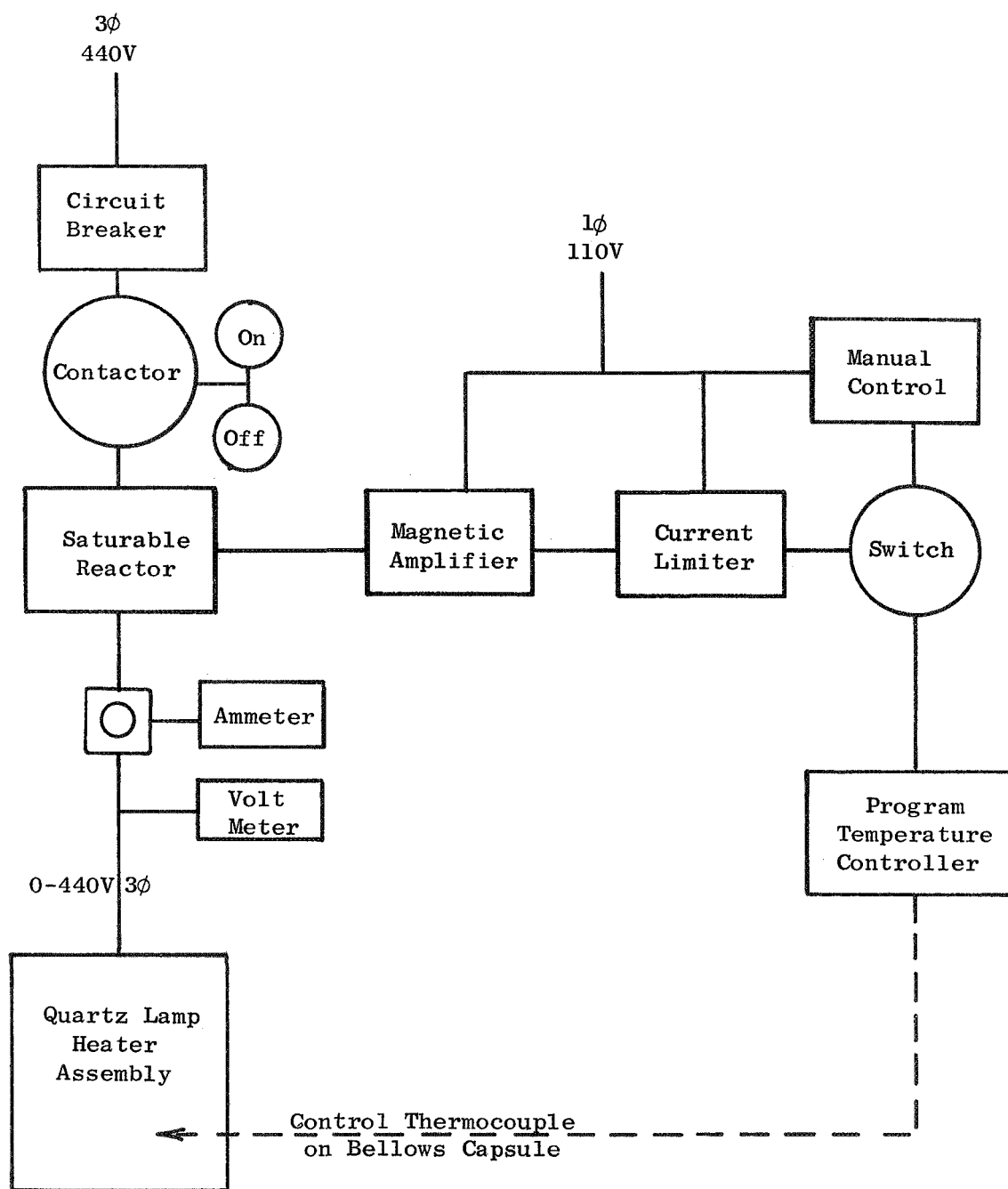
97

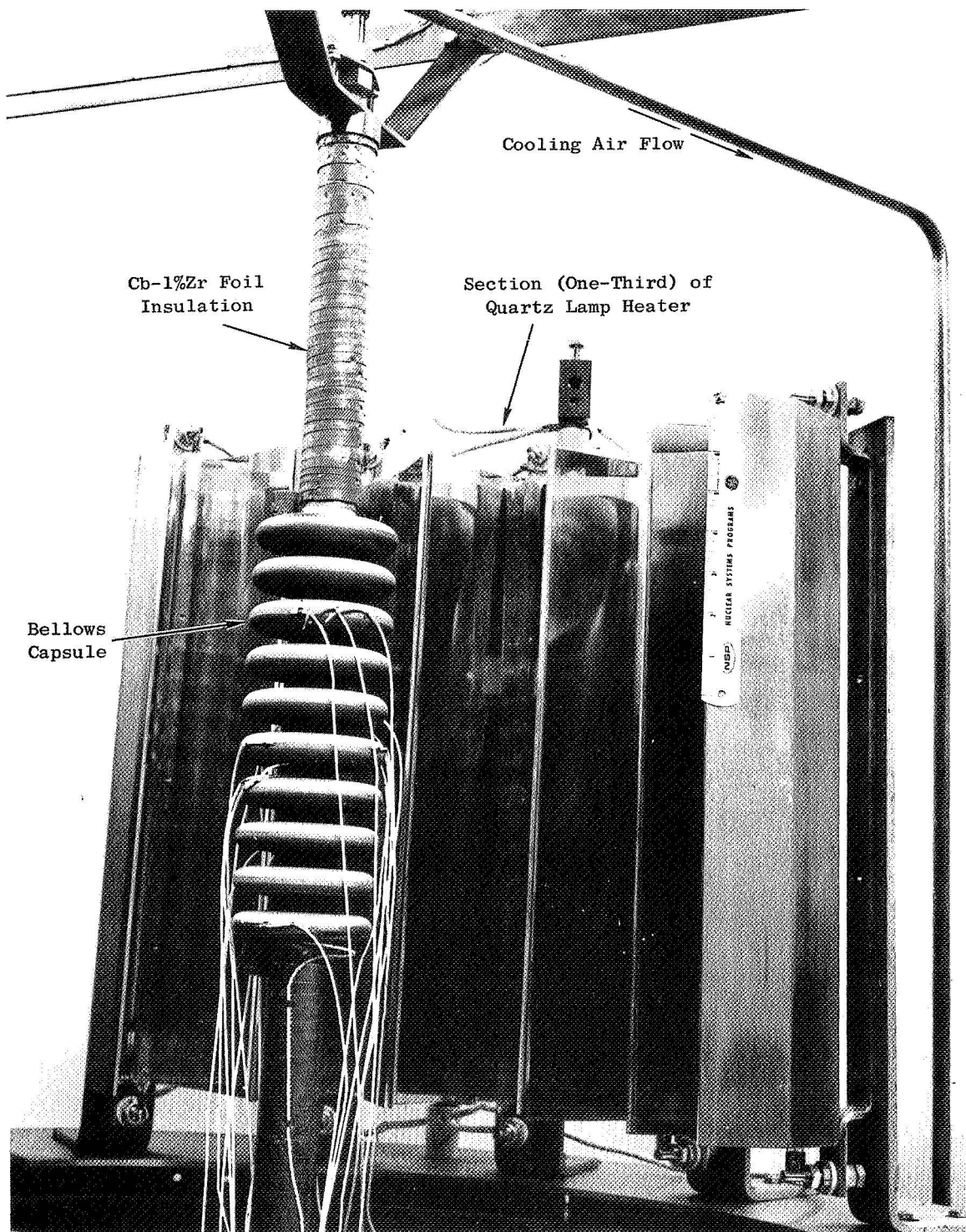Figure 33. Bellows Capsule Power and Control Circuit.

Figure 34. Instrumented Bellows Capsule with One Section (Five Lamps) of Quartz Lamp Heating System. (P69-1-25A)

99

during the vacuum tests, the bellows capsule operating at high temperature was an additional heat source to the reflectors, where, during the acceptance tests, the reflectors faced a water-cooled tube.

It was thus apparent that some means of cooling the reflectors had to be employed for vacuum operation of the heating system at power levels exceeding 9 kw. Several methods of cooling the reflectors were investigated, including direct water cooling and radiative cooling by application of high-emittance coatings to the back of the reflectors and to the vacuum chamber walls. Water cooling was finally selected as the most positive solution to the problem.

E. Modification of Capsule Heating System

Several methods of attachment of the water cooling tubes to the reflectors were investigated. These methods included attachment by mechanical fasteners, brazing, and welding. Welding was selected as the best means of providing good thermal contact. Careful design of the weld joint was essential to prevent excessive distortion of the reflector contour. Aluminum tubes (3003-H14 alloy), 0.50-inch-OD with 0.065-inch-wall, were recessed in circular grooves, 0.19-inch-deep, machined in each side of each reflector. Machined grooves, one on each side of each tube, provided a projection which was gas tungsten arc welded to the tube wall. The aluminum tubes on adjacent reflectors were interconnected by stainless steel tubing loops with Swagelok fittings. Figure 35 shows the completed water-cooled heater assembly mounted in the vacuum chamber with the instrumented bellows capsule in position.

Initial vacuum thermal tests with the water-cooled reflector system were made by measuring the capsule temperatures obtained with various values of apparent electrical power input to the lamp system. In Figure 36, the total lamp system power input is plotted against the fourth power of the capsule temperature. This temperature is measured at the apex of the convolution near the center of the capsule. Extrapolating these data to the maximum required capsule temperature of 1700°F (927°C), the lamp system power required would be about 37 kw or approximately 1.5 times the rated value (24 kw) of the system. Similar data obtained
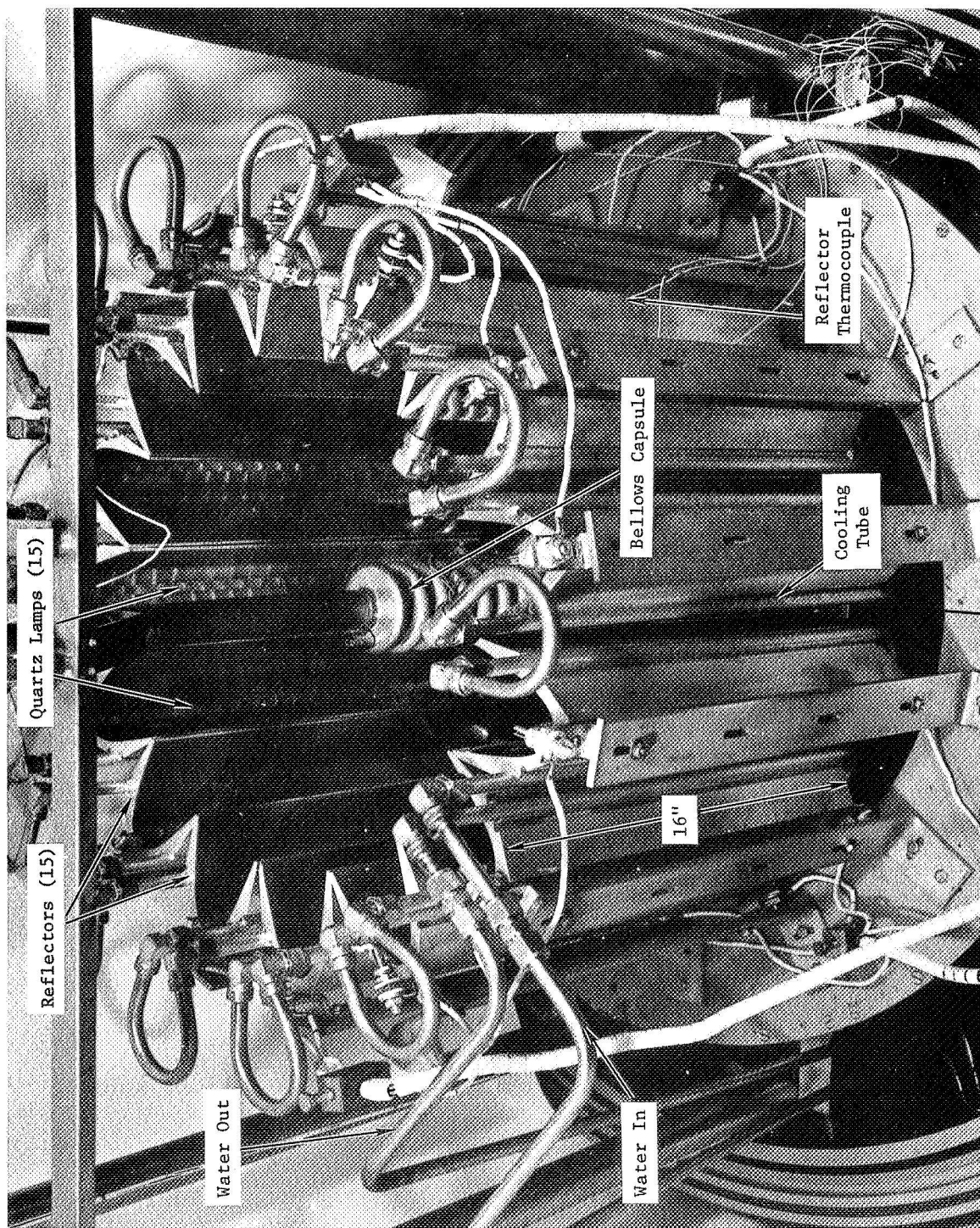
100

Figure 35. Instrumented Bellows Capsule with Water-Cooled Quartz Lamp Heating System. (P69-6-7B)
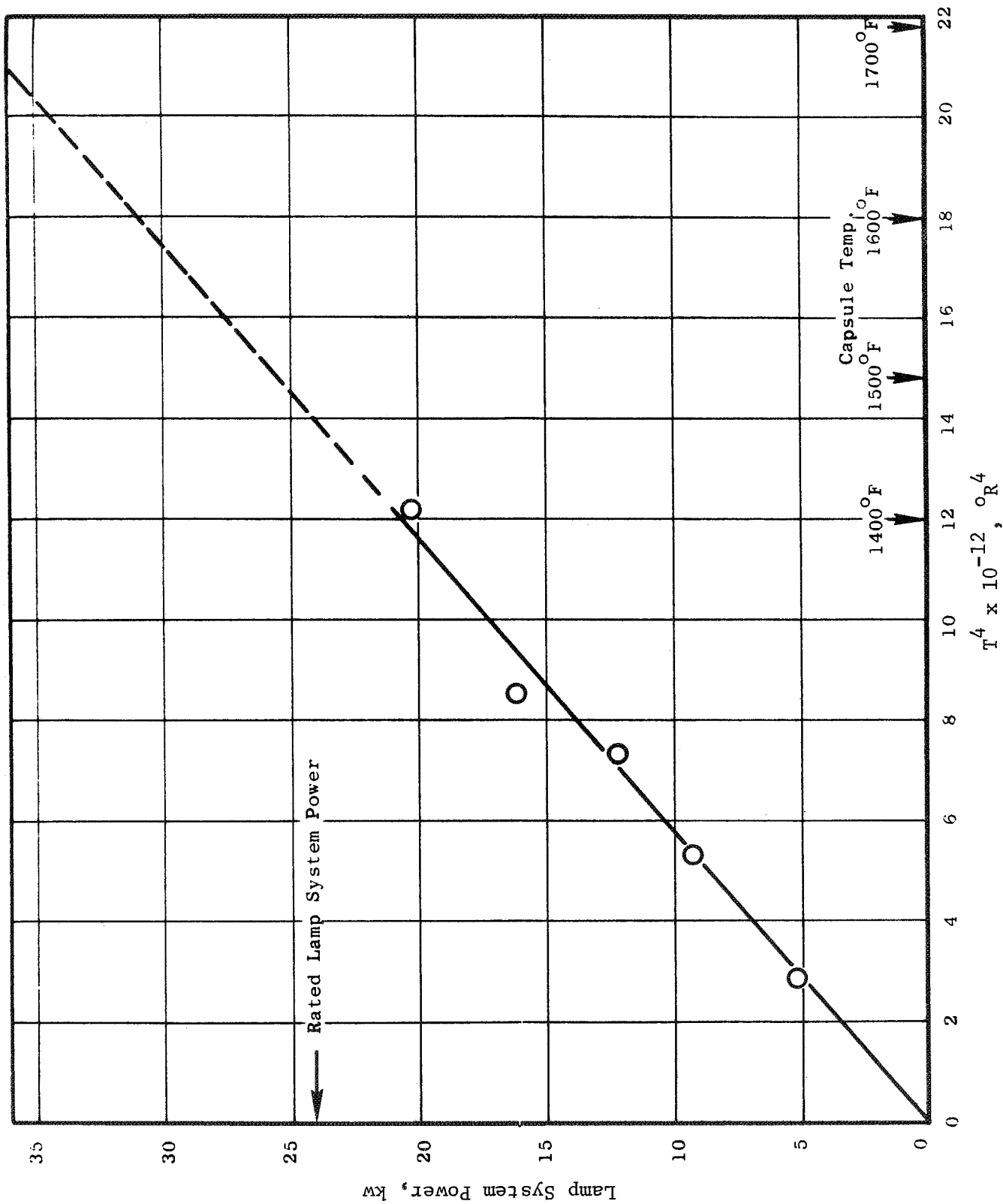
Figure 36. Lamp System Electrical Power Input Versus Fourth Power of the Capsule Temperature. The Capsule Temperature is that Measured at the Apex of the Convolution Near the Center of the Capsule. Reflectors are Water Cooled.

during the tests with uncooled reflectors indicated that 1700°F (927°C) could be obtained with 24 kw applied to the lamps. It is thus apparent that, with uncooled reflectors, a significant portion of the total heat flux to the capsule resulted from direct radiation from the hot reflectors to the capsule. This energy was not available when the reflector temperature was reduced by water cooling.

It was expected that the life of the lamps would be significantly reduced by operating at power levels much above the rated value. Several attempts were thus made to increase the fraction of emitted heat flux that was incident on the capsule. This involved placement of additional reflecting surfaces in such positions as to direct the radiation toward the capsule. These attempts generally resulted in no appreciable increase in heat flux.

After it had been determined that no significant increase in total heat flux could be obtained by simple geometrical changes or by insertion of additional reflecting surfaces, the capsule was temperature-cycled several times using the programmed temperature control circuit, and permitting lamp voltage considerably in excess of the rated value. For these tests, the programmer was adjusted to provide a linear temperature increase from 1500°F (816°C) to 1700°F (927°C) in 60 minutes followed by a linear temperature decrease from 1700° to 1500°F in 36 minutes. The current limiting circuit was adjusted to limit the power to the lamps to the value required to reach a capsule temperature of 1700°F. Under these conditions, temperature variations such as that shown in Figure 37 were obtained. The corresponding lamp voltage as a function of time during the cycle is also shown in Figure 37. The capsule temperature is obtained from a thermocouple located on the apex of one of the center convolutions on the capsule. The capsule temperature and lamp voltage increase steadily at the beginning of the cycle until the lithium fluoride begins to melt. At this point (about 12 minutes into the cycle) the capsule temperature falls below the programmed value but additional power is not supplied to the lamps since the maximum voltage is limited in the control circuit. The lamp voltage is thus held at its maximum value until the heatup
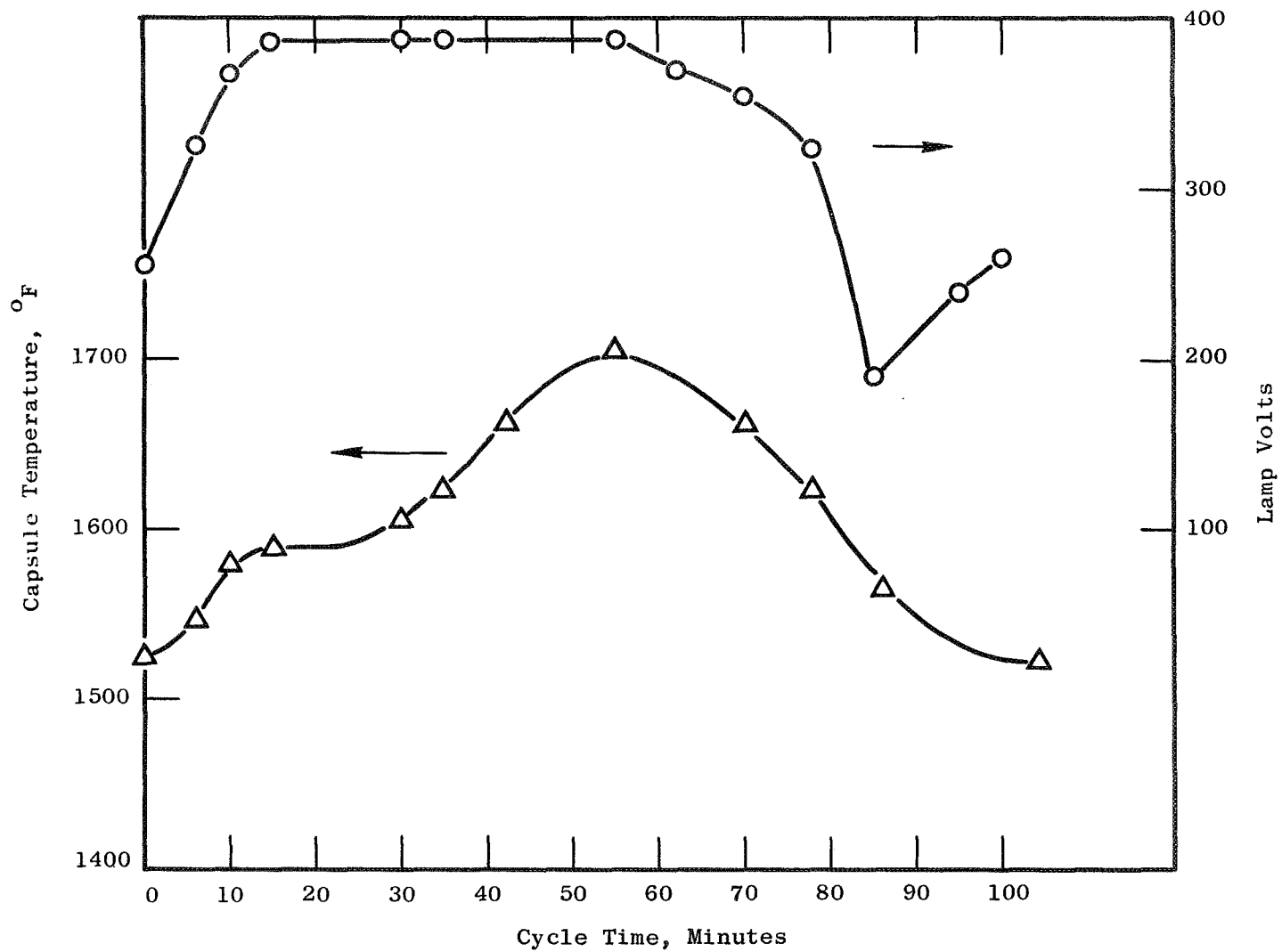
103

Figure 37. Typical Temperature and Voltage Profile During Thermal Cycling
Test of the Lithium Fluoride Filled Bellows Capsule.

portion of the cycle is completed. On the decreasing portion of the cycle, the capsule temperature and lamp voltage steadily decrease until the lithium fluoride begins to freeze. At this point (about 80 minutes into the cycle) the programmed temperature tends to be lower than the capsule temperature and the lamp voltage required drops rapidly until freezing is complete. At this point the lamp voltage increases somewhat in order to maintain the required cooling rate. The capsule temperature was cycled several times to determine that adequate temperature control was maintained by the automatic control circuit. During this period , indications of malfunction in the heating system were observed.

Following these tests, the chamber was opened in order to determine the cause of the apparent malfunction. One quartz lamp envelope was found completely shattered. Rather severe distortion of all lamp envelopes was noted. Several of the lamps are shown in Figure 38 along with a new lamp for comparison purposes. The mica spacers which center and support the filament may be noted on the broken lamp. The envelope has a tendency to melt through in the vicinity of these spacers.

It was obvious from the results of these tests that operation of the lamps at 380 volts in vacuum caused softening of the quartz and distortion of the envelope and that lamp failure could be expected after but a few hours of operation. No test of any significant duration could thus be performed under these conditions.

In conjunction with NASA Project Management, a plan was formulated whereby the bellows capsule would have been contaminated in this facility utilizing the capsule heating system under isothermal conditions at about 1500°F (816°C) with the lamps operating near their rated voltage. The contaminated capsule would have then been cycled in a separate facility utilizing a different heating system. This plan was not, however, pursued due to a shift of emphasis on the Solar Heat Receiver Program.
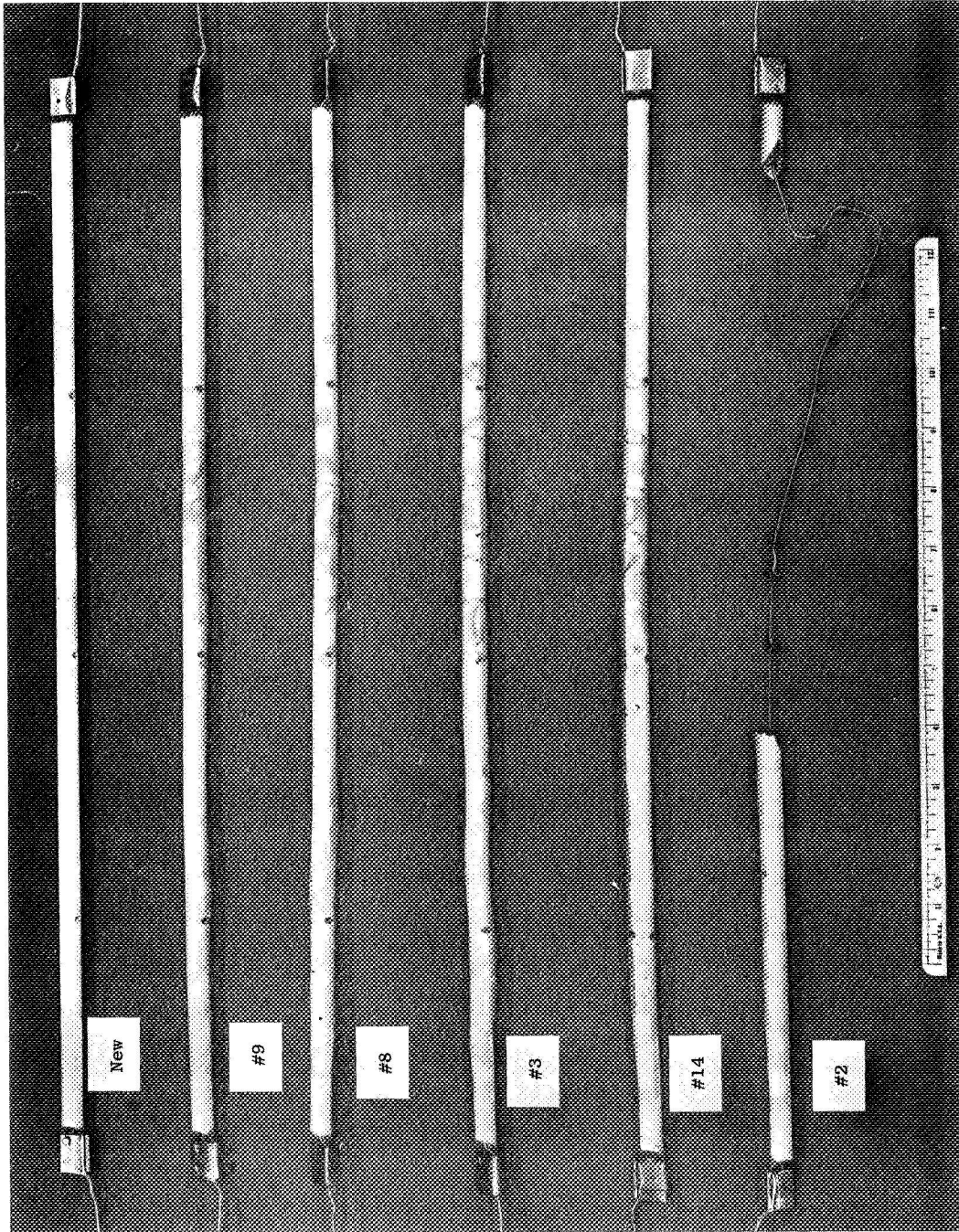
105

Figure 38. Quartz Lamps After Thermal Cycle Test Compared with New Lamp. (P69-9-14C)

NASA-Headquarters
Washington, D. C. 20546
Attn: George C. Deutsch (RW)
        James J. Lynch (RNP)
        James J. Gangler (RWM)
        R. R. Miller (SG)
        Librarian

NASA
Scientific and Technical
  Information Facility
P. O. Box 33
College Park, Maryland 20740
Attn: Acquisitions Branch (SQT-34054)
                            (2 + repro.)

NASA
Goddard Space Flight Center
Greenbelt, Maryland 20771
Attn: Librarian

NASA
Langley Research Center
Hampton, Virginia 23365
Attn: Librarian

NASA
Lewis Research Center
21000 Brookpark Road
Cleveland, Ohio 44135
Attn: Librarian, MS 60-3
        G. M. Ault, MS 3-13
        R. L. Davies, MS 106-1
        L. W. Schopen (2), MS 77-3
        M. Sabala, MS 3-19
        N. T. Saunders, MS 105-1
        C. Scheuerman, MS 106-1
        Report Control Office, MS 5-5
        W. Hlavin, MS 3-10
        W. T. Wintucky, MS 500-201
        R. English, MS 500-201
        J. A. Milko (5), MS 106-1
        R. W. Hall, MS 105-1

NASA
George C. Marshall Space Flight Center
Huntsville, Alabama 38512
Attn: Librarian

NASA
Lewis Research Center
Plum Brook Station
Sandusky, Ohio 44870
Attn: Space Power Facility Division
        Librarian

Jet Propulsion Laboratory
California Institute of Technology
4800 Oak Grove Drive
Pasadena, California 91103
Attn: Librarian

National Bureau of Standards
Washington, D. C. 20225
Attn: Librarian

Army Ordnance Frankford Arsenal
Bridesburg Station
Philadelphia, Pennsylvania 19137

Bureau of Mines
Albany, Oregon
Attn: Librarian

Bureau of Ships
Department of the Navy
Washington, D. C. 20225
Attn: Librarian

Bureau of Weapons
Research and Engineering
Materials Division
Washington, D. C. 20225
Attn: Librarian

U. S. Atomic Energy Commission
Germantown, Maryland 20767
Attn: C. Johnson
        R. Anderson
        G. Newby
        Technical Reports Library

U. S. Atomic Energy Commission
Technical Information Service
  Extension
P. O. Box 62
Oak Ridge, Tennessee 37831 (3)

Office of Naval Research
Power Division
Washington, D. C. 20225
Attn: Librarian

U. S. Naval Research Laboratory
Washington, D. C. 20225
Attn: Librarian

Aerojet-General Corporation
P. O. Box 209
Azusa, California 91702
Attn: Librarian

AiResearch Manufacturing Company
Sky Harbor Airport
402 South 36th Street
Phoenix, Arizona 85034
Attn: Librarian

AiResearch Manufacturing Company
9851-9951 Sepulveda Boulevard
Los Angeles, California 90045
Attn: Librarian

Atomics International
8900 DeSoto Avenue
Canoga Park, California 91303
Attn: H. Pearlman
      T. A. Moss

Avco
Research and Advanced Development
  Department
201 Lowell Street
Wilmington, Massachusetts 01800
Attn: Librarian

Battelle Memorial Institute
505 King Avenue
Columbus, Ohio 43201
Attn: Librarian
      E. M. Simmons

Battelle-Northwest Laboratories
P. O. Box 999
Richland, Washington 99352

The Bendix Corporation
Research Laboratories Division
Southfield, Michigan
Attn: Librarian

The Boeing Company
Seattle, Washington 98100
Attn: Librarian

Brookhaven National Laboratory
Upton, Long Island, New York 11973
Attn: Librarian

Chance Vought Aircraft, Inc.
P. O. Box 5907
Dallas, Texas 75222
Attn: Librarian

Clevite Corporation
Mechanical Research Division
540 East 105th Street
Cleveland, Ohio 44108
Attn: N. C. Beerli
         Project Administrator

Convair Astronautics
5001 Kerrny Villa Road
San Diego, California 92111
Attn: Librarian

Curtiss-Wright Corporation
Wright-Aeronautical Division
Woodridge, New Jersey 07075
Attn: S. Lombardo

Ford Motor Company
Aeroneutronics
Newport Beach, California 92660
Attn: Librarian

General Atomic
John Jay Hopkins Laboratory
P. O. Box 608
San Diego, California 92112
Attn: Ling Yang
         Librarian

General Electric Company
Atomic Power Equipment Division
P. O. Box 1131
San Jose, California

General Electric Company
Missile and Space Division
P. O. Box 8555
Philadelphia, Pennsylvania 19114
Attn: Librarian

General Electric Company
Vallecitos Atomic Laboratory
Pleasanton, California 94566
Attn: Librarian

General Dynamics/Fort Worth
P. O. Box 748
Fort Worth, Texas 76100
Attn: Librarian

General Motors Corporation
Allison Division
Indianapolis, Indiana 46206
Attn: Librarian

Hamilton Standard
Division of United Aircraft Corpor-
   ation
Windsor Locks, Connecticut
Attn: Librarian

Hughes Aircraft Company
Engineering Division
Culver City, California 90230-2
Attn: Librarian

IIT Research Institute
10 West 35th Street
Chicago, Illinois 60616
Attn: Librarian

Lockheed Missiles and Space Division
Lockheed Aircraft Corporation
Sunnyvale, California
Attn: Librarian

Marquardt Aircraft Company
P. O. Box 2013
Van Nuys, California
Attn: Librarian

Teledyne Isotopes
Nuclear Systems Division
110 West Timonium Road
Timonium, Maryland 21093

Martin Marietta Corporation
Metals Technology Laboratory
Wheeling, Illinois
Attn: Librarian

Materials Research and Development
ManLabs, Inc.
21 Erie Street
Cambridge, Massachusetts 02139

Materials Research Corporation
Orangeburg, New York
Attn: Librarian

McDonnel Aircraft
St. Louis, Missouri 63100
Attn: Librarian

Union Carbide Metals
Niagara Falls, New York 14300
Attn: Librarian

United Aircraft Corporation
Pratt and Whitney Division
400 West Main Street
Hartford, Connecticut 06108
Attn: R. E. Cleary
         Librarian

United Nuclear Corporation
Research and Engineering Center
Grassland Road
Elmsford, New York 10523
Attn: Librarian

Union Carbide Corporation
Parma Research Center
P. O. Box 6115
Cleveland, Ohio 44101

Wah Chang Corporation
Albany, Oregon
Attn: Librarian
         M. McNabb

Westinghouse Electric Corporation
Astronuclear Laboratory
P. O. Box 10864
Pittsburgh, Pennsylvania 15236
Attn: Librarian
         R. W. Buckman

Westinghouse Electric Corporation
Materials Manufacturing Division
RD No. 2, Box 25
Blairsville, Pennsylvania
Attn: Librarian

Westinghouse Electric Corporation
Research and Development Center
Pittsburgh, Pennsylvania 15235
Attn: Librarian
         R. T. Begley

Grumman Aircraft
Bethpage, New York
Attn: Librarian

Lawrence Radiation Laboratory
Livermore, California
Attn: Librarian (2)
        J. Hadley

Allison-General Motors
Energy Conversion Division
Indianapolis, Indiana
Attn: Librarian

North American Aviation, Inc.
Atomics International Division
P. O. Box 309
Canoga Park, California 91304
Attn: Director, Liquid Metals
        Information Center

Douglas Aircraft Company, Inc.
Missile and Space Systems Division
3000 Ocean Park Boulevard
Santa Monica, California
Attn: Librarian

Climax Molybdenum Company of Michigan
1600 Huron Parkway
Ann Arbor, Michigan 48105
Attn: Librarian
        M. Semchyshen

MSA Research Corporation
Callery, Pennsylvania 16024
Attn: Librarian

North American Aviation
Los Angeles Division
Los Angeles, California 90009
Attn: Librarian

Oak Ridge National Laboratory
P. O. Box X
Oak Ridge, Tennessee 37831
Attn: W. H. Cook
        W. O. Harms
        Librarian
        J. H. DeVan
        H. Inouye

Engineering Library
Fairchild Hiller
Republic Aviation Corporation
Farmingdale, Long Island, New York
Attn: Librarian

Rocketdyne
Canoga Park, California 91303
Attn: Librarian

Solar
2200 Pacific Highway
San Diego, California 92112
Attn: Librarian

Southwest Research Institute
8500 Culebra Road
San Antonio, Texas 78206
Attn: Librarian

Superior Tube Company
Norristown, Pennsylvania
Attn: Librarian

Sylvania Electrics Products, Inc.
Chemical and Metallurgical
Towanda, Pennsylvania
Attn: Librarian

TRW, Inc.
Caldwell Research Center
23555 Euclid Avenue
Cleveland, Ohio 44117
Attn: Librarian
        K. Shettler

Cabot Corporation
Stellite Division
Kokomo, Indiana
Attn: Librarian
        T. K. Roche

Fansteel Metallurgical Corporation
North Chicago, Illinois
Attn: Librarian

National Research Corporation
405 Industrial Place
Newton, Massachusetts
Attn: Librarian

Varian Associates
Vacuum Products Division
611 Hansen Way
Palo Alto, California
Attn: Librarian

NASA
Manned Spacecraft Center
Houston, Texas 77001
Attn: Librarian

Los Alamos Scientific Laboratory
University of California
Los Alamos, New Mexico
Attn: Librarian

TRW, Inc.
TRW Systems Group
One Space Park
Redondo Beach, California 90278
Attn: H. P. Silverman

Sandia Corporation
Aerospace Nuclear Safety Division
Sandia Base
Albuquerque, New Mexico 87115
Attn: A. J. Clark (3)
       Librarian
       J. Jacob

NASA
Ames Research Center
Moffett Field, California 94035
Attn: Librarian